

Investigation into the Discrepancies Between Computational Fluid Dynamic Lift Predictions and Experimental Results

by

Randall S. Fairman

DISTRIBUTION STATEMENT A

Approved for Public Release
Distribution Unlimited

B.S.M.E., University of Washington (1991)
M.S.M.E., Massachusetts Institute of Technology (2000)
Naval Engineer, Massachusetts Institute of Technology (2000)

Submitted to the Department of Ocean Engineering
in partial fulfillment of the requirements for the degree of

Doctor of Philosophy

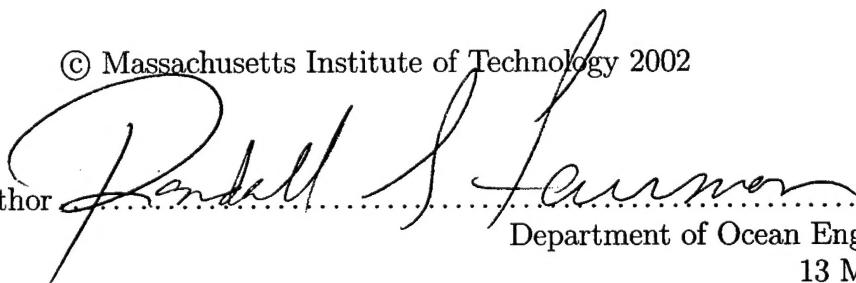
at the

MASSACHUSETTS INSTITUTE OF TECHNOLOGY

June 2002

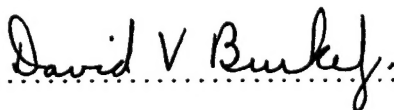
© Massachusetts Institute of Technology 2002

Signature of Author



Department of Ocean Engineering
13 May 2002

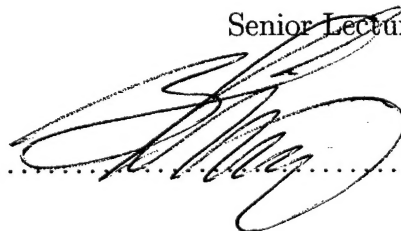
Certified by



David Burke

Senior Lecturer, Department of Ocean Engineering
Thesis Supervisor

Accepted by



Henrik Schmidt

Professor of Ocean Engineering
Chairperson, Department Committee on Graduate Students

20020822 006

Investigation into the Discrepancies Between Computational Fluid Dynamic Lift Predictions and Experimental Results

by

Randall S. Fairman

Submitted to the Department of Ocean Engineering
on 13 May 2002, in partial fulfillment of the
requirements for the degree of
Doctor of Philosophy

Abstract

An analysis of current computational fluid dynamics capabilities in predicting mean lift forces for two dimensional foils is conducted. It is shown that both integral boundary layer theory and Reynolds Averaged Navier Stokes algorithms provide the same over-prediction of lift forces when properly converged. It is also shown that the over-prediction is insensitive to turbulence model details.

Experimentation and computational fluid dynamics modeling show that discrete vortices are shed with significant sizes and distinct frequencies. These vortices are shown to result in significant cfd prediction errors when they are asymmetric in size or shape. Inaccuracies in flow predictions in the near wake appear to result in an effective change in the Kutta Condition due to pressure biasing associated with vortex asymmetry. The net result is a consistent overprediction of mean lift.

Based on an analysis of over 1000 historical experiments an empirical model is developed to allow the error in predicted lift coefficient to be anticipated based on the local flow conditions at the trailing edge of the foil. A series of experiments are conducted and reported to test the accuracy of the empirical model. The result is a significant improvement in mean lift prediction and pressure profile for both RANS and IBLT.

Thesis Supervisor: David Burke

Title: Senior Lecturer, Department of Ocean Engineering

Contents

1	Introduction	9
1.1	History	9
1.1.1	Efforts Prior to Computer Modeling	9
1.1.2	Exploring Capabilities in Computer Modeling	10
1.1.3	Efforts to Reconcile Experiments and Computations	11
1.2	Organization	13
1.2.1	Overview	13
1.2.2	Chapter 2	13
1.2.3	Chapter 3	13
1.2.4	Chapter 4	13
1.2.5	Chapter 5	13
1.2.6	Chapter 6	14
1.2.7	Chapter 7	14
1.2.8	Chapter 8	14
2	Overview of Turbulence Modeling for Computational Fluid Dynamics	15
2.1	Integral Boundary Layer Models	15
2.2	Eddy-Viscosity Models (EVM)	16
2.3	Other approaches	18
2.4	Turbulence Model Limitations	18

3	Integral Boundary Layer Theory Predictions Compared to NACA 6-Series	21
	Experimental Data	21
3.1	NACA FOIL DESIGN	22
3.1.1	Thickness Distribution	22
3.1.2	Cambered Foil Design	24
3.2	IBLT Convergence Study	26
3.3	Parametric Modeling of Viscous Lift Prediction Errors	26
3.4	Conclusions	29
4	Experimental Validation	31
4.1	Experimental Facilities	31
4.2	Experimental Procedures	32
4.3	HRA Series of Foils	33
4.3.1	HRA Baseline Foil	34
4.3.2	HRA Blunt Foil	35
4.3.3	HRA Beveled Foil	36
4.4	B1 Series of Foils	37
4.4.1	B1 Blunt Foil	37
4.4.2	B1 Anti-singing Foil	38
4.4.3	B1 Cupped Foil	39
4.5	Conclusions	40
4.5.1	It is demonstrated:	40
4.5.2	Questions for further exploration:	41
5	Integral Boundary Layer Theory Compared to RANS	42
5.1	Grid Topology	43
5.2	Boundary Conditions	44
5.3	Iterative Convergence	46
5.4	Grid Density	47
5.4.1	Y Plus Convergence	47
5.4.2	Grid Spacing	48

5.4.3	Turbulence Models	49
5.5	Foil Comparisons	49
5.6	RANS Solution with Walls	51
5.7	Conclusions	51
6	Analysis of Assumptions	54
6.1	Navier-Stokes Equations	54
6.2	Reynolds Averaged Navier-Stokes Equations	56
6.3	Turbulence Modeling	57
6.4	Conclusions	58
7	Unsteady Analysis	61
7.1	Observed Vortex Shedding	61
7.1.1	HRA Fine Trailing Edge Foil Vortex Shedding	62
7.1.2	B1 Cupped Trailing Edge Foil Vortex Shedding	63
7.2	Asymmetric Vortex Shedding Analysis	64
7.3	Unsteady RANS Analysis	66
7.4	Conclusions	69
8	Recommendations	70
8.1	Long Term Solution	70
8.2	Short Term Solution	70
A	Coupled Integral Boundary Layer Theory Convergence Study	72
A.1	Foil Geometry	73
A.2	Grid Convergence	73
A.3	Domain Size	75
A.4	Mach Number	75
B	HRA Fine Trailing Edge Foil Experimental Data	78
C	HRA Blunt Trailing Edge Foil Experimental Data	83

D HRA Beveled Trailing Edge Foil Experimental Data	88
E B1 Blunt Trailing Edge Foil Experimental Data	94
F B1 Antisinging Trailing Edge Foil Experimental Data	100
G B1 Cupped Trailing Edge Foil Experimental Data	107
H Decaying Vortex Tracking Program	113

List of Figures

1-1	Vortex Shedding Patterns Behind Several Foils at High Reynolds Number	12
3-1	6-Series Thickness Sections	23
3-2	NACA Foils Analysis Overview	27
3-3	Computed and Measured Lift Curve Slopes	28
3-4	Comparisons of Experimental and Computational Lift Curve Slopes	30
4-1	HRA Fine Trailing Edge Foil Data	34
4-2	HRA Blunt Trailing Edge Foil	35
4-3	HRA Beveled Trailing Edge Foil	36
4-4	B1 Blunt Trailing Edge Foil	38
4-5	B1 Antisinging Trailing Edge Foil	39
4-6	B1 Cupped Trailing Edge Foil	40
5-1	Leading Edge Grid Topology	44
5-2	Trailing Edge Grid Topology	45
5-3	Iterative Convergence History	46
5-4	Y Plus Convergence for B1 Blunt Foil	47
5-5	Bulk Grid Area Maximum Spacing	48
5-6	B1 Cupped Foil Geometry	49
5-7	Solution Comparisons for the B1 Cupped Trailing Edge Foil	50
5-8	Comparison of Slip and No-Slip Solutions for Cupped Foil	52
6-1	Cupped Foil Near Wake Turbulence Characteristics	59

7-1	Blunt and Beveled Foil Unsteadiness	62
7-2	Wake Observation for the HRA Fine Trailing Edge Foil	62
7-3	Wake Observation for the B1 Cupped Trailing Edge Foil	63
7-4	Time Averaged vs Time Accurate Representations of Symmetric Vortices	65
7-5	Time Accurate and Time Averaged Effects of Core Size Asymmetry	66
7-6	Time Accurate and Time Averaged Effects of Vortex Origination Point	67
7-7	Steady and Unsteady RANS Analysis for B1 Cupped Foil	68
7-8	Unsteady Rans Non-Isotropic Turbulence	69
A-1	NACA 66021 Foil Geometry	73
A-2	MSIS Grid Convergence Summary	74
A-3	Predicted Lift Coefficient vs MSIS Domain Length	75
A-4	Predicted Lift Coefficient vs MSIS Domain Height	76
A-5	Predicted Lift Coefficient vs Mach Number	77

Chapter 1

Introduction

The thrust produced by a marine propeller is a result of a propeller blade “wing” section oriented such that the relative motion caused by rotation produces “lift” forces in the direction of ship motion. It is for this reason that much attention has been given by the marine industry to analysis and prediction of two dimensional foil section performance.

1.1 History

1.1.1 Efforts Prior to Computer Modeling

A great deal of effort has been given to wing section development by the aircraft industry. The early stages are described in Reference [1]. The quote here is from 1949.

“Until recently the development of wing sections has been almost entirely empirical. Very early tests indicated the desirability of a rounded leading edge and of a sharp trailing edge. The demand for improved wings for early airplanes and the lack of any generally accepted wing theory led to tests of large numbers of wings with shapes gradually improving as the result of experience. The Eiffel and early RAF series were outstanding examples of this approach to the problem.

The gradual development of wing theory tended to isolate the wing-section problem from the effects of plan form and led to a more systematic experimental approach. The tests made at Gottingen during the First World War contributed much to the

development of modern types of wing sections. Up to about the Second World War, most wing sections in common use were derived from more or less direct extensions of the work at Gottingen. During this period, many families of wing sections were tested in the laboratories of various countries, but the work of the NACA was outstanding. The NACA investigations were further systematized by the separation of the effects of camber and thickness distribution, and the experimental work was performed at higher Reynolds numbers than were generally obtained elsewhere. The wing sections now in common use are either NACA sections or have been strongly influenced by the NACA investigations."

The wing theory discussed in this quote is strictly inviscid. The results of these investigations are very well documented and freely available. In the process of conducting this research I have considered many experimental data points and the characteristics of several facilities. After having reviewed the experimental procedures, opinions of others, and the facilities utilized, it is my opinion that the most accurate experimental two dimensional wing section characteristics available are those conducted in the NACA two-dimensional low-turbulence pressure tunnel. The majority of the wings tested in this facility are presented in Reference [1] and a few more are presented in NACA Technical Notes and Technical Reports published after this reference.

1.1.2 Exploring Capabilities in Computer Modeling

As computer speed and software progress the viscous effects are increasingly being considered in a general way. The time averaged effects of viscosity can be accounted for by modifying the local boundary conditions at the edges of the inviscid domain according to the integrated effect of the boundary layer or by turbulence modeling throughout the domain. A couple examples where the former method has been successful are PBD [17] and XFOIL [8]. The latter method is typically associated with RANS solvers such as DTNS [13], UNCLE [3] and CFDSHIP [23].

Because of the circumferential non-uniformity a marine propeller typically operates in, a study was conducted at MIT concerning the need for modifications to the Kutta Condition and other flow models in the presence of unsteady inflow conditions [22]. Experiments were

conducted and blind predictions performed by the authors of a number of flow codes. The panel of experts who modeled this experiment in the computational flow domain found a mixture of encouraging and discouraging results. They found that in general, it was possible to model the unsteady behavior and achieve results consistent with the variations observed in the experiment. On the other hand, they found that the zeroth harmonic (or mean behavior) showed significant deviation when typical turbulence models were used. One of the publications following this project put it this way: [23]

The zeroth harmonic, which was the same as steady flow calculations, displayed typical foil response and showed that turbulence model corrections for pressure gradient were necessary for accurate solution.

and

...This level of agreement, which required pressure-gradient modifications to the turbulence model, appears to be a general assessment of the current capabilities of isotropic turbulence models since it is consistent with the other participants in the FFX workshop and overall results found in the literature.

1.1.3 Efforts to Reconcile Experiments and Computations

As a result of these inconsistencies a study of the steady behavior of two dimensional foils and the associated computations was undertaken at the MIT water tunnel. A foil with a more drastic cup than typical for the type of anti-singing trailing edge in the flapping foil experiment was designed and experimentally evaluated. Blind tests were conducted by the authors of the same computational fluid dynamics codes. In an engineer's thesis by John Dannecker [7] the results of the different flow codes were shown to have major variations between flow codes. Also, each of the codes over-predicted the experimental results by between 25% and 100% for an experimental lift coefficient of about 0.5.

The radical errors and consistent over prediction by the flow codes motivated a more extensive validation of the experiment. The questions about the experiment and associated steady predictions were the sole topic of a masters thesis by Jergen Jorde [15]. He concluded that the original experiment was correct and the most probable cause for the discrepancy was incorrect



Figure 1-1: Vortex Shedding Patterns Behind Several Foils at High Reynolds Number

modeling of tunnel walls, but there was no final closure on the differences between the codes and the over prediction of lift forces.

In parallel with the work of Jorde, Kimball and Shearer conducted a study of foil trailing edge details as it pertains to cavitation performance improvement [19]. Their study was focused on cavitation performance design and experimental validation, so the lift predictions were not explicitly compared to the experiment. A part of this experiment included high speed photography which revealed the wake structure shown in Figure 1-1. It was interesting to note that for the blunt and beveled trailing edge foils there was a distinct repeated organization to the vortex shedding in the wake. It appears that there is significant viscous-inviscid interaction at a frequency that would make accurate predictions with any sort of time averaged flow code questionable.

Following these efforts Fairman [11] conducted a survey of the experimental and computational efforts on various foil sections evaluated in the MIT water tunnel. He updated both experimental and computational efforts for the foils discussed in the previous history at MIT. It was shown that the three dimensional effects at the tunnel walls do not effect the ability of the foil to represent a two-dimensional space near the mid-span. He also updated the computational results to fully include the effects of the upper and lower tunnel walls.

1.2 Organization

1.2.1 Overview

The current research attempts to bring to closure many of the issues surrounding the work on two dimensional hydrofoils at the MIT Water Tunnel. The following summary of each chapter is provided to allow the reader to navigate to the section of personal interest:

1.2.2 Chapter 2

A brief review of the physics associated with the various forms of computational fluid dynamics in use today is conducted. The governing equations and methods of implementation are briefly discussed with references given for further evaluation.

1.2.3 Chapter 3

A comparison between experiments performed by other facilities and computational predictions by the integral boundary layer theory code MSES is performed. The quality of the historical experiments is evaluated and appropriate references given to allow further evaluation. A parametric evaluation is conducted and a simple parametric model is proposed to account for differences between experimental and computational lift.

1.2.4 Chapter 4

An experimental validation of the parametric model suggested in Chapter 3 is performed. It is shown that the full viscous solution combined with the parametric fit provides consistently outstanding results.

1.2.5 Chapter 5

It is shown that Integral Boundary Layer Theory and Reynolds Averaged Navier Stokes (RANS) codes provide the same over prediction in lift coefficient when fully converged. It is shown that several RANS turbulence models also provide the same over prediction of lift coefficient.

1.2.6 Chapter 6

Possible assumptions common to these codes that could potentially be in error are considered. It is shown that the most likely erroneous assumptions can be related to known coherent vortex shedding at the foil trailing edge.

1.2.7 Chapter 7

An analysis of the effects of vortex shedding and unsteadiness on time average lift coefficient is provided. It is shown that it is possible to provide a complete time accurate calculation of the flow domain using unsteady RANS. The average of the time accurate calculation results in lift predictions which are consistent with time average measurements. The conclusion is drawn that the need for a parametric adjustment to the full viscous solution is caused by the fact that the vortex shedding patterns represent an unmodeled physical phenomenon relevant to determining time averaged lift.

1.2.8 Chapter 8

A brief summary of the conclusions and how they can be practically utilized is presented.

Chapter 2

Overview of Turbulence Modeling for Computational Fluid Dynamics

Vast quantities of books and papers are available on the topic of turbulence modeling. When this research is presented it is common that the response of the turbulence modeling expert is to wonder if the new turbulence model that they are working on will solve the entire problem. Certainly this may someday be true, but for the time being this research is using turbulence models which are widely available for engineering applications. Clearly much progress has been made in turbulence modeling and many types of flows seem to have been mastered.

The Reynolds number at which marine propellers typically operate is very large; therefore, there is clearly a need for turbulence modeling. The manner in which turbulence models determine the Reynolds-stresses varies, but all of them essentially use a model for turbulence behavior coupled with experimentally determined constants. Reference [14] is a total of 34 pages and is an excellent summary of turbulence models in current use.

2.1 Integral Boundary Layer Models

The integral momentum equation (Equation 2.1) was first derived by Kármán (1921) and is taken here from White. [29]

$$\frac{d\theta}{dx} + (2 + H) \frac{\theta}{U_e} \frac{dU_e}{dx} = \frac{\tau_w}{\rho U_e^2} = \frac{C_f}{2} \quad (2.1)$$

$$\theta = \text{momentum thickness} = \int_0^\infty \frac{\bar{u}}{U_e} (1 - \frac{\bar{u}}{U_e}) dy$$

$$H = \text{momentum shape factor} = \frac{\delta^*}{\theta}$$

$$\delta^* = \text{displacement thickness} = \int_0^\infty (1 - \frac{\bar{u}}{U_e}) dy$$

This is the most simple and robust type of turbulence model. This method does not explicitly consider the changing conditions across the boundary, but makes use of the shape factors and integral quantities to represent turbulence quantities. This allows the partial differential equations needed to explicitly solve the entire flow domain to be replaced by a set of ordinary differential equations representing the integrated quantities.

This type of turbulence model can then be coupled with an Euler Solver (as in MSES [10]) or a Vortex Lattice Method (as in PBD [17] and XFOIL [9]) to provide very fast and stable solutions. It is shown in this research, that in the case of two-dimensional foils, these models are every bit as accurate as more general eddy viscosity models and require a small fraction of the time and effort to compute a flow solution. (Chapter ??)

2.2 Eddy-Viscosity Models (EVM)

This type of turbulence model assumes a single scalar quantity (eddy viscosity) coupled with velocity gradients can be used to adequately represent the Reynolds-stresses throughout a flow field (Equation 2.2). Within this concept is the notion that turbulent transport and molecular transport contain an analogy useful for solving the flow properties, but eddy viscosity is NOT a fluid property and varies a great deal throughout the flow domain. Most modern Reynolds Averaged Navier Stokes (RANS) codes use this type of turbulence model.

$$-\overline{u'_i v'_j} = \nu_t \left(\frac{\partial u_i}{\partial x_j} + \frac{\partial u_j}{\partial x_i} \right) - \frac{2}{3} k \delta_{ij} \quad (2.2)$$

$$\overline{u'_i v'_j} = \text{Reynolds stress}$$

$$\nu_t = \text{eddy viscosity}$$

$$k = \text{turbulent kinetic energy}$$

The manner in which turbulence models in this category determine the eddy viscosity to be used is varied. In essence, the dimensions of eddy viscosity and understanding of the turbulence problem lead to the following non-dimensionalization found in many references such as [20]:

$$\nu_t = f(x, y) \times V \times L \quad (2.3)$$

$$f(x, y) = \text{dimensionless spatially varying function}$$

$$V = \text{turbulent velocity scale}$$

$$L = \text{turbulent length scale}$$

The following is a summary of how many modern turbulence models estimate the parameters involved in the eddy viscosity turbulence models.

- algebraic models

These models use purely algebraic relationships to define all three of the constants in equation 2.3. Examples of these types of models are:

- mixing length model
- Cebeci & Smith model
- Baldwin & Lomax model

- one-equation models

These models use one differential equation to model some characteristic property of the turbulence (typically eddy viscosity or turbulent kinetic energy) and then supplement

with algebraic equations for the remainder of the constants. Examples of this type of model include:

- Spalart and Allmaris
- k-l model of Bradshaw et al
- two-equation models

These models use two full sets of differential equations including some sort of production, loss and diffusion of eddy viscosity to model the eddy viscosity throughout the domain. Examples of this type of model include:

- k- ϵ Model (Differential equations are solved for turbulent kinetic energy and dissipation.)
- k- ω Model (Differential equations are solved for turbulent kinetic energy and turbulence dissipation rate.)

2.3 Other approaches

Differential Reynolds Stress Models (DRSM) solve a complete set of differential equations for each component of the Reynolds Stress Tensor. In two dimensions this approach requires three sets of differential equations. In three dimensions six sets of differential equations are required.

Large-Eddy Simulations (LES) model only small scale turbulent structures and large scale structures are calculated based on an unsteady time integration.

Direct Numerical Simulations solve the unsteady Navier-Stokes equations without applying a turbulence model. Very small time steps and extremely fine grids are required for this approach.

2.4 Turbulence Model Limitations

The turbulence models that are readily available for marine propulsion application utilize either the integral boundary layer or eddy viscosity approach. The following limitations exist for

Flow feature that can lead to inaccurate prediction[14]	Potential Implication for Predicting Two Dimensional Lift
flows with abrupt changes in the velocity field	trailing edge pressure side where extremely thin boundary layer exists
flow along strongly curved surfaces	trailing edge of a foil with separation
flow along strongly curved surfaces	trailing edge of a foil with blunt trailing edge
flow along strongly curved surfaces	leading edge of a foil
stagnant flow regions	leading edge and trailing edge
low frequency unsteadiness	trailing edge in the presence of vortex shedding

Table 2.1: Turbulence Model Weaknesses

existing one equation and two equation eddy viscosity models and integral boundary layer turbulence models:

- The turbulent viscosity is assumed to be a scalar quantity.
- Turbulence anisotropy is not explicitly taken into account.
- A linear relation exists between the Reynolds stresses and the gradient of the mean velocity field.

Many sources, such as [14] and [4] discuss some of the particular weaknesses of these types of turbulence modeling. In particular, these restrictions can lead to inaccurate prediction of flows in regions which exhibit specific types of flow characteristics. In the first column of Table 2.1 is a list of flow features Henkes [14] specifically states result in the potential for inaccurate predictions. In the second column of Table 2.1 is an analysis of how this type of flow might effect the prediction of lift on a two-dimensional foil.

These weaknesses are combatted using wall functions and other creative turbulence model modifications. Often these modifications are specific to an application or a location in the domain. Many publications and books have sought to provide closure to these issues in a myriad of ways. An expert in turbulence modeling, Henkes summarizes his view of the status of turbulence modeling in a book published as recently as 1998 [14]:

As the Reynolds number for the flow around the aerofoils and fuselage of aircraft is usually very large, most of the boundary-layer flow along the surface will be turbulent. It is not possible to compute all the details of the turbulent motion within a reasonable turn-around time (say several hours); therefore for all practical computations the use of turbulence models is mandatory.

Up to now most designers and developers of aerofoils compute turbulent flows with older generation models, like the algebraic models of Cebeci-Smith, Baldwin-Lomax or Johnson-King. More recently some industries and research institutes (like NLR) have also applied two-equation models. All these models assume the existence of a single turbulent velocity and length scale, which is only approximately right for so-called equilibrium flows, such as attached boundary layers in a zero or moderate streamwise pressure gradient. Indeed those models have shown to be rather inaccurate for non-equilibrium flows, like separating boundary layers occurring in high-lift configurations; examples of such configurations are aerofoils under high angle of attack, and multi-element aerofoils. Therefore all these models are only accurate in a limited number of flow types, and they do not meet the high-accuracy requirements for a wide range of configurations. As a result of this, experiments in wind tunnels still serve as the major source of design information.

Chapter 3

Integral Boundary Layer Theory Predictions Compared to NACA 6-Series Experimental Data

The experiments referenced here are fully reported in the Theory of Wing Sections, Reference [28]. Numerical values are taken from the tabulation of these experiments reported in Aerofoil Sections, Reference [25]. Computational geometries for the wing sections are constructed based on governing equations and then verified to be accurate by comparison with measured data points in Appendix 1 of Reference [28]. The “rough” experimental results at a Reynolds Number of 6×10^6 are considered. These foils are tested in the NACA two-dimensional low-turbulence pressure tunnel. This tunnel is specifically designed to provide an environment for testing relatively large wing sections in a two-dimensional environment at turbulence levels so low they approach the turbulence level of the atmosphere. This tunnel is further described in Reference [28].

The foils are constructed with great care to produce smooth surfaces which avoid prematurely tripping the boundary layer near the leading edge. It is found in the testing that even the slightest roughness near the leading edge causes a transition to turbulence. After testing foils with a smooth surface, various forms of surface treatment are considered. Experiments are conducted using “turbulence stimulating strips” at various points along the chord. It is found

that their impact increases as they move forward on the foil. Experiments are also conducted with a sparse field of grains over the leading 8% of the chord surface. The grain density is such that about 5 to 10 percent of the leading edge area is coated. Grains of differing sizes are tested and it is shown that the initial placement of grains of any size cause the largest change then there is a continuing reduction in foil performance at a slower rate with increasing grain size. Eventually, a grain size of 0.011 inches (0.05% of the chord) is selected based on the idea that there is little further change in wing performance and this is still a smaller imperfection than would be expected by an actual wing in service. More information on the roughness selection process and analysis is documented in Reference [2].

The chord length of the foils experimentally evaluated is 2 feet. The tunnel throat is rectangular with a 7.5 foot height and 3 foot width. The lift coefficient is determined based on measured pressure distribution along the top and bottom of the tunnel. In order to evaluate whether or not the tunnel environment truly provided the equivalent of a two dimensional environment, several wing sections are selected to be evaluated at different chord lengths. Chord lengths of 1, 2 and 4 feet are evaluated and the lift curve versus angle of attack characteristics are found to be consistent. In order to ensure that the zero angle of attack reference point is correct, lift curve versus angle of attack characteristics are measured right side up and upside down.

3.1 NACA FOIL DESIGN

3.1.1 Thickness Distribution

The NACA 6-series thickness sections are used for this portion of the analysis. The experimental work demonstrates the lift curve slope to be virtually independent of the section camber design and highly dependent on the section thickness distribution. The design of these sections attempts to delay transition to a turbulent boundary layer by maintaining a favorable pressure gradient to a specified chord-wise location. For example, the 63012 foil section can be broken down as follows:

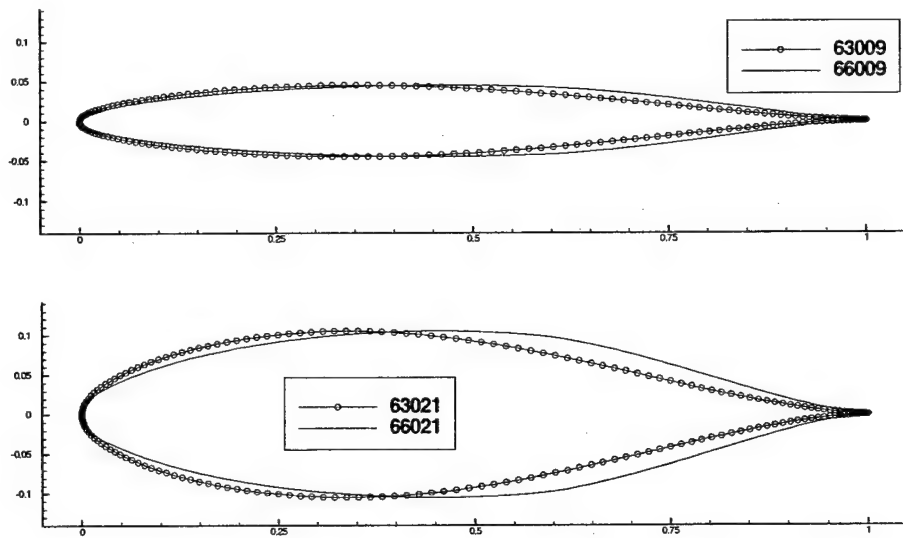


Figure 3-1: 6-Series Thickness Sections

63012

6 = foil series designation

3 = the location of minimum pressure due to thickness is at $\frac{3}{10}$ Chord

0 = ideal lift coefficient is 0.0 at AOA = 0.0

12 = maximum foil thickness is 12% of the chord length

The basic shape of these foils is shown in Figure 3-1. As shown in this figure, the 66XXX foils have a significantly fuller aft section for the same thickness. In the comparisons which follow, it is observed that this change in shape results in a far more significant change in the experimentally measured lift coefficient than it does in the computational lift coefficient. In subsequent chapters of this research it is important to remember that the same experimental procedure is used for both of these sections, yet the deviation between experiment and computations grows significantly.

3.1.2 Cambered Foil Design

The camber loading of the foils in the 6-series family arises from efforts to reduce the effect of the "compressibility burble" on airplane wings as their speed approaches the speed of sound. Compressibility effects are observed more as a function of peak loading on the foil than average loading. The strategy used to reduce compressibility effects is to minimize the peak to average loading ratio by creating a constant loading over the chord of the foil. A series of foils referred to as the "16-series" was developed based on this premise and experimentally evaluated. The development and testing of these foils is reported in Reference [26]. These tests are conducted with an aspect ratio of six in a circular wind tunnel and extrapolated to an equivalent two dimensional behavior. The results show a somewhat greater over prediction than those tested in the NACA Langley Two Dimensional Pressure Tunnel, but have not been used for comparison here due to the lack of certainty of the true 2-dimensional behavior and lack of knowledge about whether or not the boundary layer is transitioned.

At the time these foils were developed the understanding of the effects of viscosity on two-dimensional foil theory was in its infancy. The thin foil theory was applied to give a completely flat loading all the way from the leading edge to the trailing edge. This loading is referred to as the " $a = 1$ " loading and is used as the default camber line for the extensive testing accomplished. It is not actually possible in a fluid with finite viscosity to maintain loading all the way to the trailing edge, so separation occurs and the fluid unloads the trailing edge. An alternative strategy used for a few of the foils was to linearly unload the foil trailing edge from a specified chord-wise position to the trailing edge. For example, the " $a = 0.8$ " line has become a popular camber distribution for marine propellers. This camber distribution maintains a flat loading to the 80% chord-wise position and then linearly reduces the loading to zero at the trailing edge. The following is the complete designation of the 6-series family of foils:

66409 $a = 0.8$

6 = foil series designation

6 = the location of minimum pressure due to thickness is at $\frac{6}{10}$ Chord

4 = ideal lift coefficient is 0.4 at AOA = 0.0

09 = maximum foil thickness is 9% of the chord length

$a = 0.8$

foil is linearly unloaded from 80% chord position to trailing edge

if no designation, foil design remains fully loaded to trailing edge

Delaying of the "compressibility burble" for an aircraft wing has as a direct analogy in delaying cavitation in a hydrofoil. In a fluid with sufficient gas nuclei, cavitation occurs when the local pressure falls below the vapor pressure of the fluid in which the foil is operating. In the potential region of the flow around a foil, the pressure is inversely proportional to the square of the velocity. If the maximum velocity is minimized for a given lift coefficient, the result will be delaying the onset of cavitation to the maximum extent possible.

It is based on these concepts that Brockett [6] proposed the NACA 66 modified thickness section coupled with the $a=0.8$ mean line for use in propeller design. A discussion with one of the engineers involved in the decision to use the $a=0.8$ mean line instead of the $a=1.0$ mean line indicates that the $a=0.8$ mean line is chosen because at the time they were not able to predict the behavior of the $a=1.0$ mean line. It turns out that the viscous effect and potential flow thickness effect for an $a=0.8$ mean line nearly cancel one another. The result is that the $a=0.8$ mean line produces lift very near the value predicted by inviscid theory. On the other hand, it is impossible to maintain loading to the trailing edge of the foil in a viscous fluid so the camber loading on a foil with $a=1.0$ mean line produces only about 75% of the effect predicted by inviscid theory.

3.2 IBLT Convergence Study

MSES [10] is designed to allow analysis of multiple airfoil elements in an unrestricted domain or in a tunnel with walls. These capabilities make MSES particularly well suited for the analyses conducted in this research.

MSES is a streamline-based Euler discretization with a two-equation integral boundary layer formulation. The components are coupled through displacement thickness and solved via a full Newton method.

Solutions provided in this research are converged with respect to the grid geometry, grid density and run time parameters. Appendix A provides the details of a convergence study using the coupled integral boundary layer solver MSES.

Note: The calculations here were performed with MSIS, which is an MSES version which assumes strictly isentropic flow outside the boundary layers. This allows considerably faster execution. The results were verified to be consistent with the slightly slower MSES solution.

3.3 Parametric Modeling of Viscous Lift Prediction Errors

In the course of analyzing the NACA foil sections it is found that there is a pattern of over-prediction of lift. The question arises whether or not something about the foil geometry or the flow conditions can adequately anticipate the extent to which the over prediction exists.

In order to further explore this possibility over a thousand NACA experiments are simulated using MSES. A database is created that contains the experimental lift, the computed lift and a wide variety of boundary layer parameters near the trailing edge. This database is analyzed to determine whether or not the error in lift prediction can be anticipated.

In the course of evaluating the information in this database a wide variety of parameter combinations are considered. It is found that in general, the size and degree of asymmetry in the boundary layer parameters near the trailing edge tends to result in larger lift prediction errors. The parameter set chosen for anticipating the error in the full viscous lift prediction is based on a regression analysis of the database constructed, Equation 3.1. This equation can be used to predict the adjustment in computational angle of attack that will be required to cause

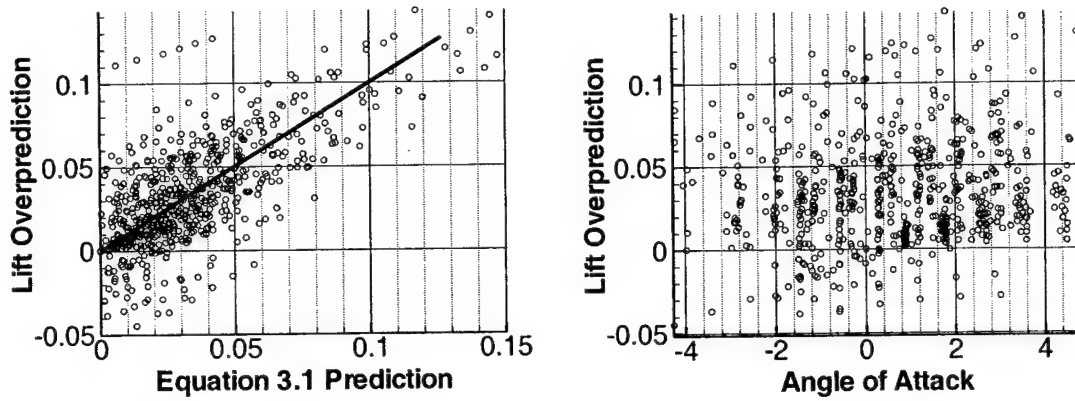


Figure 3-2: NACA Foils Analysis Overview

the full viscous computed lift to agree with the experimentally measured lift.

$$\Delta\alpha_{error} = -\frac{[\delta_{top}^* - \delta_{bottom}^*]}{chord} \quad (3.1)$$

$\Delta\alpha_{error}$ = Recommended change in angle of attack in radians

δ_{top}^* = Displacement thickness on upper foil surface at the trailing edge

δ_{bottom}^* = Displacement thickness on lower foil surface at the trailing edge

$chord$ = Foil chord length

Figure 3-2 shows examples of both incoherent and organized parameter selections for comparison. On the right set of axes is the near random distribution of over prediction with a positive mean when compared to experimental angle of attack. On the left set of axes a plot is made of lift over prediction compared to the Equation 3.1 predicted lift over prediction for the entire database. In essence, if Equation 3.1 is superimposed onto the full viscous prediction the result is a significant net reduction in lift prediction errors.

Figure 3-3 demonstrates the implications of Equation 3.1. The experimental evidence indicates that current viscous calculations do not adequately account for the reduction in lift due to viscous effects. In fact, the best fit for the data indicates that the correction is only about half of what it needs to be. The accuracy of this assessment and its physical cause is

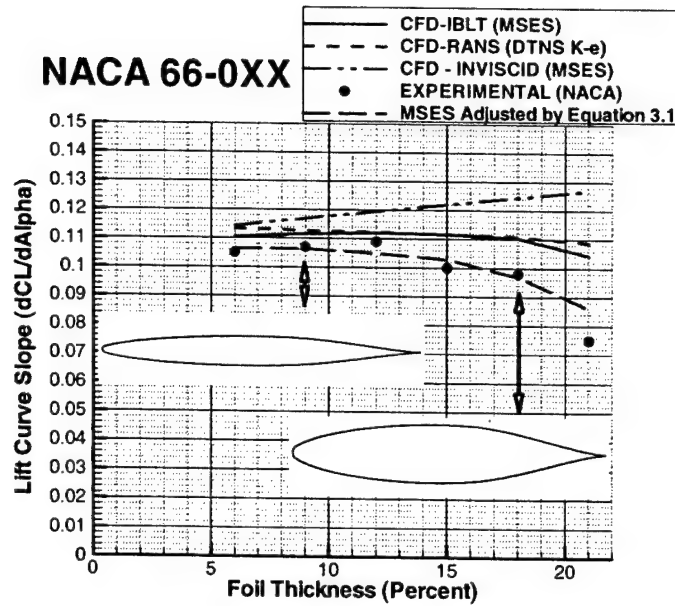


Figure 3-3: Computed and Measured Lift Curve Slopes

the basic foundation of the remainder of this research.

Figure 3-4 shows a comparison of calculated versus experimental lift curve slopes for the family of 6-series thickness sections. This set of curves is similar to Figure 3-3, but represents four different thickness forms while Figure 3-3 represents only one. The lift for these foils is computed at several angles of attack around zero, verified to be a linear relation and the slope is determined based on these results. Then the angle of attack is adjusted in accordance with Equation 3.1 and the lift curve slope is computed again. The experimental lift curve slope is taken from Table 11.1 of Reference [25].

The top set of axes in Figure 3-4 represents the lift curve slope computed and measured for the 6-series foils with minimum pressure at 30% of the chord length from a thickness of 6% on the left to 21% on the right. The other three sets of axes represent the 6-series foils with minimum pressure at 40%, 50% and 60%.

It is interesting to note that the effect of increasing thickness or moving the minimum pressure back on the foil has the effect of increasing the trailing edge wedge angle. It is noted by Hoerner [5] and other "conventional wisdom" that increasing the trailing edge wedge angle

can result in foil behavior which is difficult to predict.

3.4 Conclusions

The analyses conducted in this Chapter suggest that there is a systematic difference between computed results and experimental measurements. The results indicate that the differences between integral boundary layer theory and NACA experiments are predictable and simple. Some questions which are further explored in this thesis are:

1. "What is the physical reason for these systematic over predictions in lift?"
2. "Does the empirical fix derived based on the NACA 6-Series foils perform adequately for other geometries which include trailing edge thickness and other trailing edge treatments?"
3. "Does the empirical modification to the coupled integral boundary layer theory result in accurate local velocities as well as improved global solutions?"

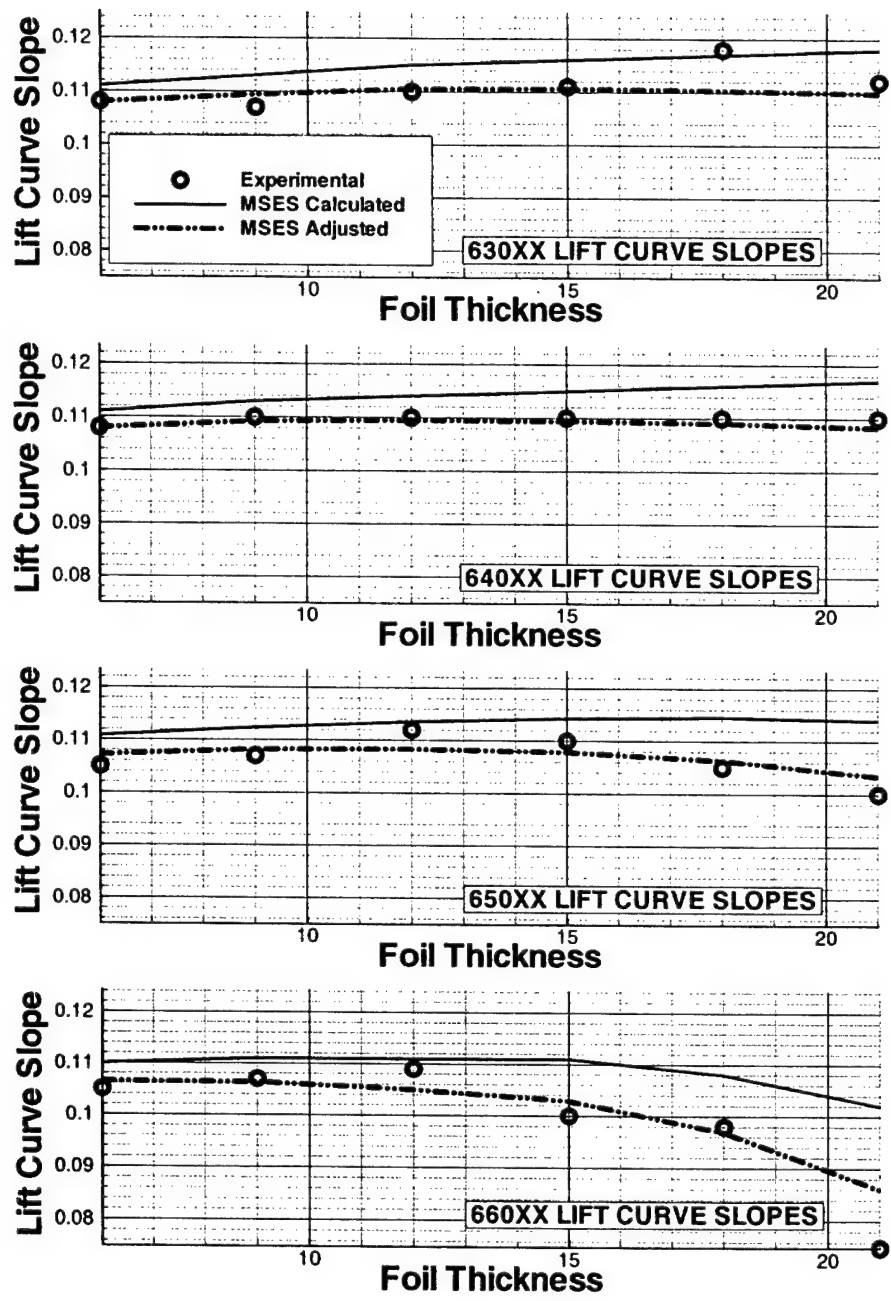


Figure 3-4: Comparisons of Experimental and Computational Lift Curve Slopes

Chapter 4

Experimental Validation

In Chapter 3 it is shown that MSES predicts a lift force higher than that which is experimentally measured by NACA. In order to allow a more detailed comparison between flow codes and the actual flow field, measured flow velocities at strategic locations in the fluid domain are desired. In this chapter a set of measurements are reported and comparisons with the flow code are made.

The geometries considered here have a range of features that make them of interest in propeller design including different forms of trailing edge modifications. They are quite different from the NACA geometries upon which Equation 3.1 is based, but the resulting improvement in flow field prediction is striking.

4.1 Experimental Facilities

The water tunnel at MIT is a variable pressure water tunnel described in Reference [16]. It is a closed-loop tunnel driven by a single 75 horsepower motor. The test section of the tunnel is twenty inches square and approximately four feet long. The maximum achievable test section velocity is $30 \frac{ft}{sec}$. Upstream of the test section is a five to one contraction fitted with fine honeycomb mesh and a wake screen to promote flow uniformity.

The test section has removable plexiglass walls on all four sides for ease of access and to allow fluid velocity measurements via laser Doppler velocimetry. For this experimental technique the velocity is inferred based on the Doppler shift in light frequency scattered by a neutrally

buoyant seed particle in the fluid. Detailed error analyses are conducted in Reference [21].

The flow conditions at the mid-span of the test section is demonstrated to be a two dimensional flow environment in the following ways:

1. In the NACA low turbulence wind tunnel a test section with a width of 3 feet is used to perform experiments on foils with a chord length of two feet. These experiments are shown to provide equivalent two dimensional performance at the mid-span based on the fact that the lift versus angle of attack curves are consistent for experiments conducted on foils with a chord of six inches, one foot and two feet [28]. The ratio of the foil chord length to tunnel span is similar for the NACA experiments and those conducted at the MIT variable pressure water tunnel.
2. In a thesis by Jergen Jorde [15], fluid velocities are measured across the span of the tunnel and are shown to be constant outside of the front and back side boundary layers which are less than one inch thick. It is demonstrated that the circulation as a function of span is constant outside of the tunnel wall boundary layers.
3. In a thesis by Randall Fairman [11] it is demonstrated that boundary layer migration from the tunnel walls does not effect the flow field at the center of the tunnel. This is accomplished using a number of fence designs to prevent three dimensional boundary layer migration.

4.2 Experimental Procedures

Seven hydrofoil geometries are tested. The hydrofoils tested range from fourteen inches to eighteen inches in chord and span the entire width of the tunnel. The Reynolds Number for these foils are 1.4×10^6 to 2.0×10^6 respectively. The boundary layer on the foils is tripped at the $\frac{1}{10}$ chord position. The development of these foils and turbulence strips is found in Reference [24] and Reference [18].

Each foil is mounted at the midpoint of the test section on a shaft which allows the foil to rotate about its axis. Each foil is also supported near the trailing edge to provide rigidity. For each geometry given, the axis of rotation is at (0,0) and the axis located vertically in the center

of the tunnel. The foil geometries in the Appendices are given at a zero angle of attack.

The actual position of the surface of the foil is measured via laser crossing at each experimental angle of attack. In general, the laser positioning device is capable of resolving position within 0.01 mm. The foil surface is rotated in the computational domain until the computational and experimental non-dimensional foil surface positions agree. This procedure for measuring angle of attack is found to be repeatable within 0.05 degrees. Lift curve versus angle of attack is measured both right side up and upside down for the "HRA Blunt" foil. These measurements demonstrate that the error in angle of attack is less than 0.1 degrees.

The tunnel velocity is held constant within 0.1% of free stream velocity. With a sample size of 2,500 valid velocity data points at each spatial location it is found that the velocity measurements are repeatable to within $0.01 \frac{m}{sec}$. The flow is non-dimensionalized by the measured inflow velocity for the given experiment which is typically about $5 \frac{m}{sec}$. The resulting error band for measured pressure coefficient is ± 0.004 (Equation 4.1).

$$C_p = 0.5 - \frac{U_{local}^2 + V_{local}^2}{2U_{\infty}^2} \quad (4.1)$$

where

C_p = pressure coefficient

U_{local} = horizontal velocity measured at x,y

V_{local} = vertical velocity measured at x,y

U_{∞} = average horizontal velocity at inlet side of control volume

4.3 HRA Series of Foils

The HRA series of foils are designed in conjunction with research seeking to improve cavitation performance in marine propellers. They are designed to obtain a flat pressure distribution over the majority of the foil with reduced loading near the leading and trailing edges. The reduced loading near the leading edge is intended to allow improved cavitation performance at off design angle of attack conditions. The details of the design and analysis of these foils can be found in Reference [18].

4.3.1 HRA Baseline Foil

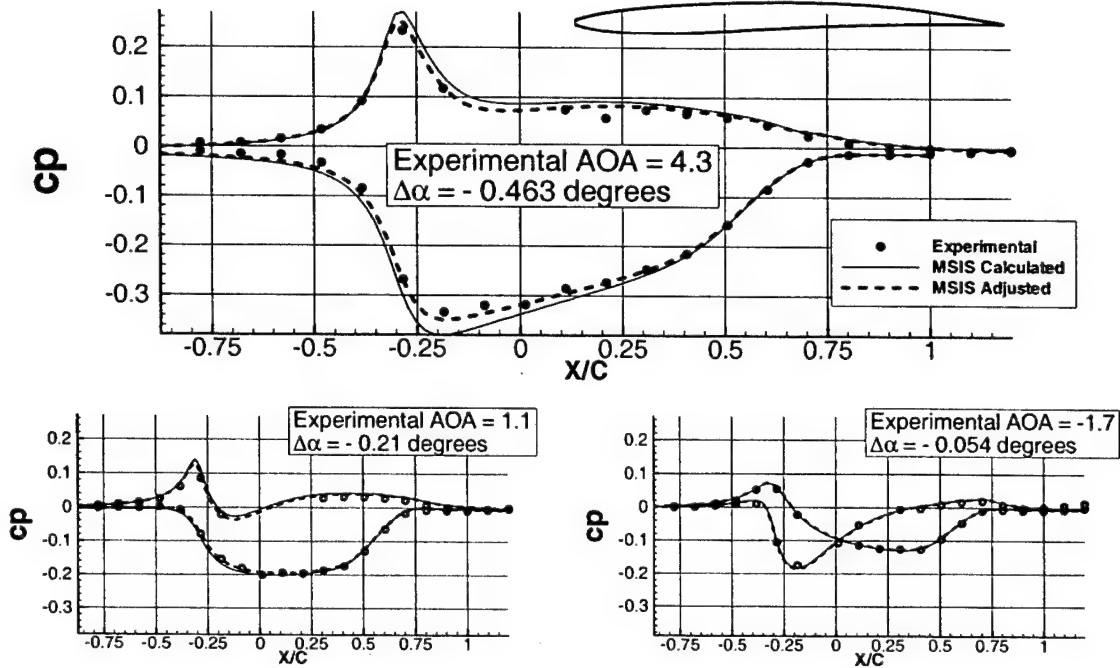


Figure 4-1: HRA Fine Trailing Edge Foil Data

The HRA baseline foil has a fine streamlined trailing edge. The foil geometry and tabulated experimental results are found in Appendix B. The foil has a chord length of 16 inches which yields a non-dimensional tunnel height of 1.25 chord lengths.

The fluid domain is analyzed using MSES as shipped and with the change in infinite angle of attack implied by Equation 3.1. The tunnel walls are modeled as a slip surface. In a subsequent section it is shown using the RANS program CFDHIP that the difference in calculated velocities between a slip tunnel wall and a no-slip tunnel wall is insignificant compared to variations under consideration here. Results are plotted as "Experimental", "MSES calculated" and "MSES adjusted" respectively. In this case the foil drag is relatively low and the resulting displacement thicknesses are relatively small.

Some noteworthy observations from Figure 4-1:

1. At all three experimental angles of attack the calculations as modified by Equation 3.1

provide superior results.

2. The implied error in lift coefficient at the highest angle of attack is $\approx 5\%$ for the "MSES calculated" results and less than 1% for the "MSES adjusted" results.
3. The adjustment in infinite angle of attack improves not only the global force prediction, but also the local velocity predictions.

4.3.2 HRA Blunt Foil

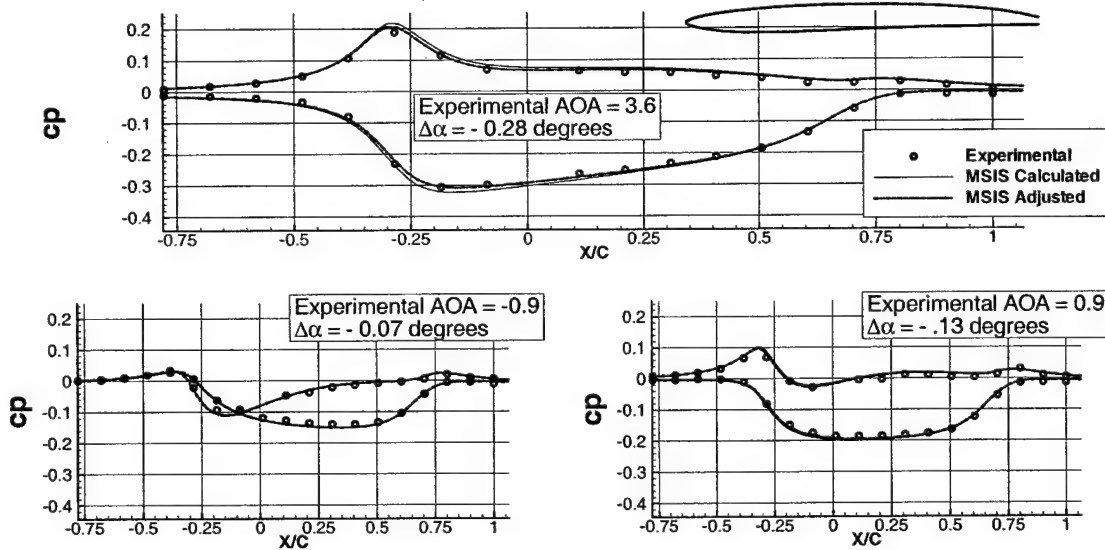


Figure 4-2: HRA Blunt Trailing Edge Foil

The HRA Blunt Foil is designed to have the same pressure profile as the HRA fine trailing edge foil but features a 2% thick trailing edge. The foil geometry and tabulated experimental results are found in Appendix C. The foil has a chord length of 16 inches which yields a non-dimensional tunnel height of 1.25 chord lengths. Figure 4-2 shows the computations and measurements for this foil.

Observations:

1. The presence of a large trailing edge thickness does not effect the magnitude of the over prediction.

2. As the trailing edge boundary layer approaches the symmetric condition the raw calculation, adjusted calculation and experimental results converge.

4.3.3 HRA Beveled Foil

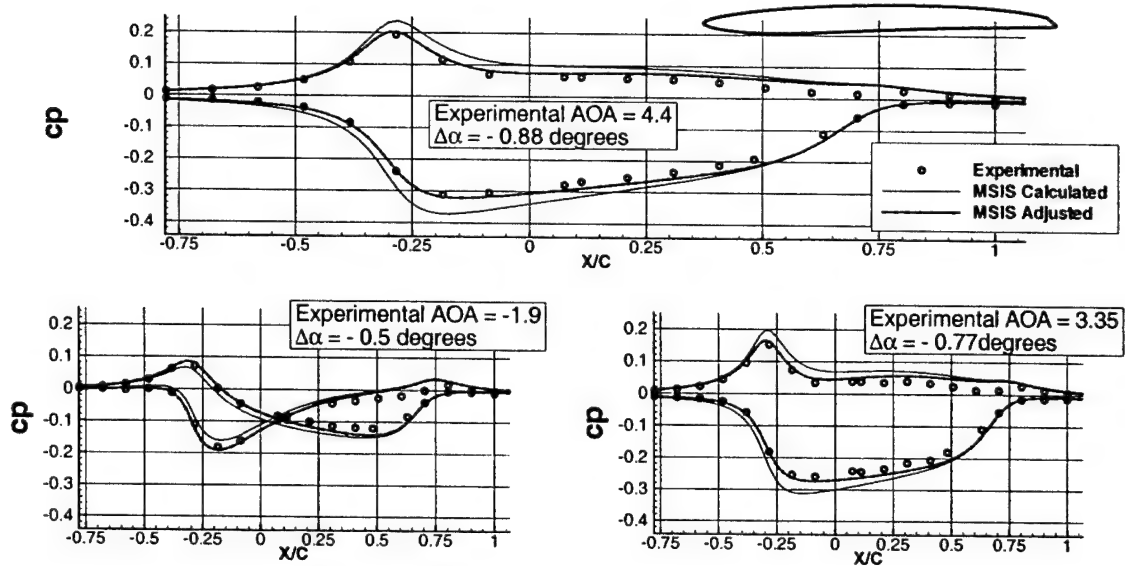


Figure 4-3: HRA Beveled Trailing Edge Foil

The HRA beveled trailing edge foil is identical to the HRA blunt trailing edge foil with the exception of a beveled suction side over the last 2.5%. This feature is shown to cause the vortex shedding pattern to become significantly asymmetric in Figure 1-1. Figure 4-3 is a summary of the data for this foil and the results are presented in tabular form in Appendix D.

Observations:

1. The presence of the beveled section near the trailing edge results in virtually no change in experimentally measured lift, yet yields a significant increase in the predicted lift.
2. The change in infinite angle of attack suggested by Equation 3.1 results in a significant improvement in prediction performance.
3. Even after adjusting the infinite angle of attack there remains a slight over-prediction in lift coefficient primarily caused by inaccuracies near the trailing edge.

4. In the MSES adjusted solution there is a slightly lower than actual loading near the leading edge and a slightly higher than actual loading near the trailing edge. When the MSES adjustment in accordance with Equation 3.1 is in error, this seems to be the nature of the error. It appears this error is amplified by flow curvature near the trailing edge. In each case here it seems that the overall lift force is still well predicted by Equation 3.1. The local loading could be more adequately predicted by coupling a more slight change in angle of attack with a modification to the "Kutta Condition" near the trailing edge. It is suspected that asymmetric vortex shedding results in pressure biasing which cannot be captured by an isotropic turbulence model. These issues will be further addressed in subsequent sections.
5. At the largest angle of attack the implied error in lift coefficient is about 0.16 ($\approx 20\%$) for the basic MSES calculation.

4.4 B1 Series of Foils

The B1 series of foils are constructed based on the Brockett [6] modification to the NACA 66 thickness section. These foils are commonly used in propellers so the experimental characteristics are of particular interest to the Naval Architect. The details of the design and analysis of these foils can be found in Reference [24].

4.4.1 B1 Blunt Foil

The B1 Blunt foil has a modestly blunted trailing edge ($\approx 0.75\%$) used for analysis as an alternative to the standard anti-singing design. Figure 4-4 is a summary of the data presented for this foil in tabular form in Appendix E along with the MSES calculations.

Observations

1. As in the case of the HRA Blunt foil, the performance of Equation 3.1 in predicting the computational error is good.
2. The implied error in lift coefficient for the basic MSES calculations is $\approx 10\%$.

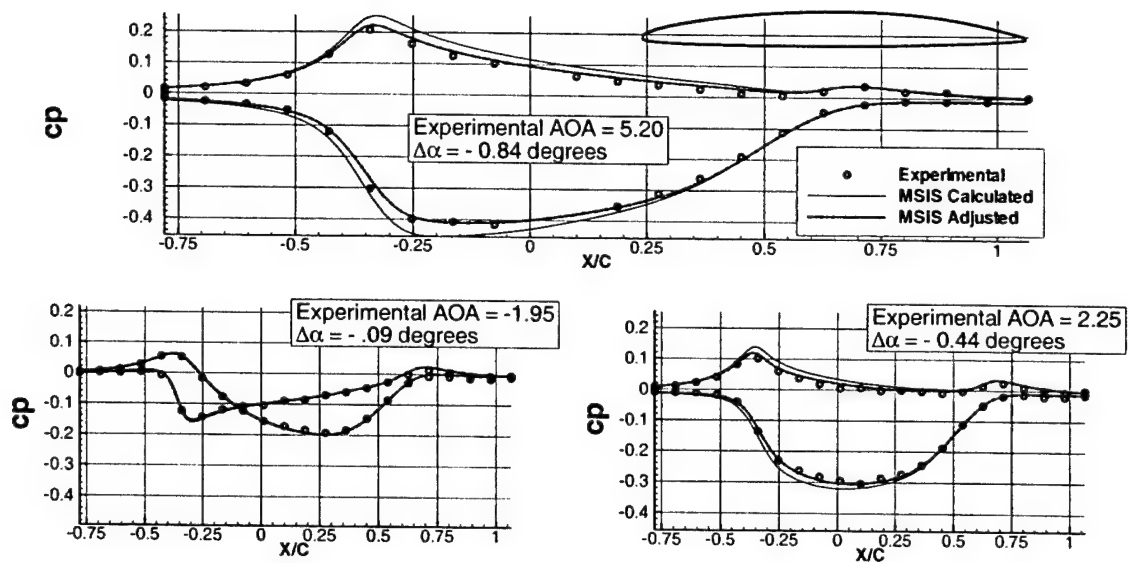


Figure 4-4: B1 Blunt Trailing Edge Foil

4.4.2 B1 Anti-singing Foil

This foil has a trailing edge which is modified in accordance with industry best practices used to prevent propeller “singing”. Figure 4-5 is a summary of the data presented for this foil in tabular form in Appendix F along with the MSES calculations.

Observations

1. This foil has slightly greater flow curvature near the trailing edge than the B1 Blunt foil and less than the HRA Beveled trailing edge foil. It also has a slightly greater over prediction of differential pressure at the trailing edge than the B1 Blunt foil and less over prediction of trailing edge differential pressure than the HRA Blunt foil.
2. At times the similarity in profile shapes between the computations and the measurements can cause one to doubt the importance of the differences. Consider:
 - (a) This foil is designed in accordance with typical best practices for military propeller blade shapes.
 - (b) The experiment operating at an angle of 2.25 degrees is well within the expected

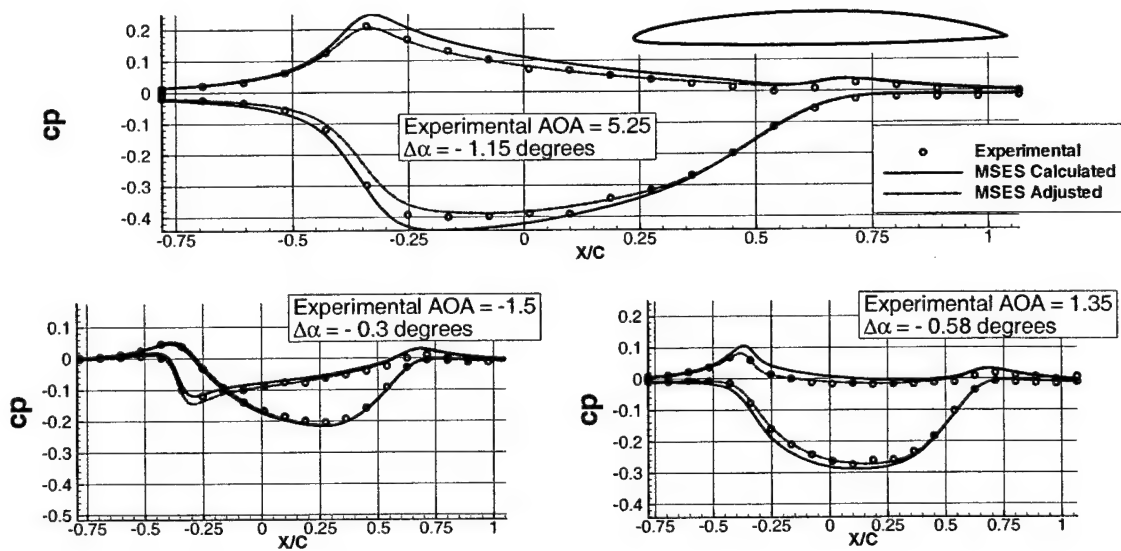


Figure 4-5: B1 Antisinging Trailing Edge Foil

operating region.

(c) The magnitude of the over prediction in lift at this angle is over 10%.

4.4.3 B1 Cupped Foil

This foil has a radically cupped trailing edge used to evaluate the capabilities of computational fluid dynamics in capturing the effects of trailing edge details on the global flow field. Figure 4-6 is a summary of the data presented for this foil in tabular form in Appendix G along with MSES calculations.

Observations

1. This foil was originally designed to highlight the weaknesses of computational fluid dynamics. The difficulties in evaluating the mean lift on this foil drove the investigation into other experimental efforts throughout the world and at MIT. The investigations of other experiments and computations led to Equation 3.1 which is now applied back to this foil. The result is an accurate lift prediction for this foil.
2. In terms of velocity distributions, this foil has greater trailing edge curvature and a greater

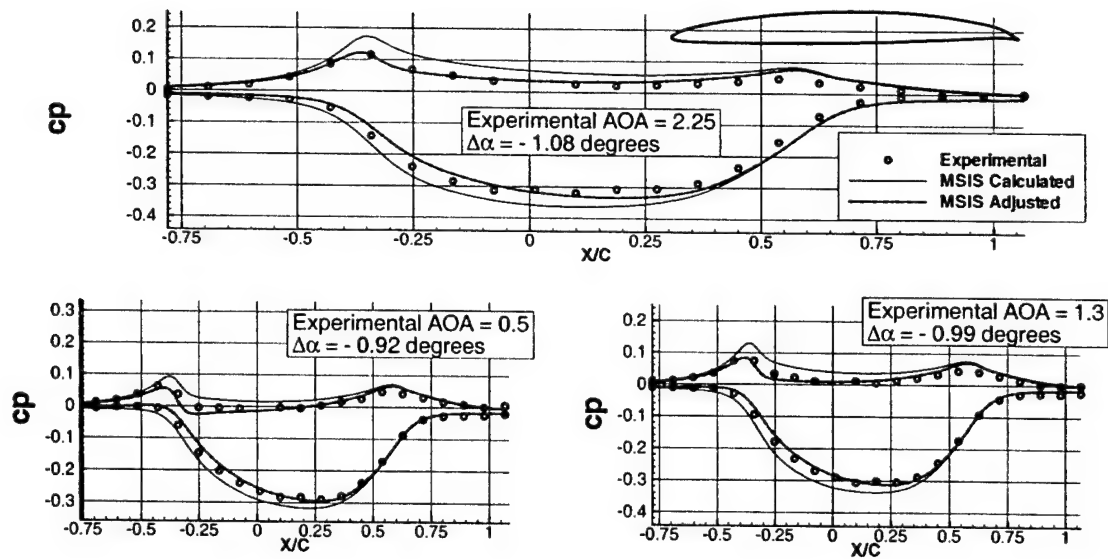


Figure 4-6: B1 Cupped Trailing Edge Foil

over prediction of pressure loading near the trailing edge when compared to the B1 Blunt foil.

4.5 Conclusions

4.5.1 It is demonstrated:

1. A modification to the infinite angle of attack suggested by Equation 3.1 provides not only improved predictions for the global lift coefficient, but also an improvement in local velocity predictions.
2. The presence of trailing edge thickness does not effect the ability of MSES to predict lift coefficient.
3. Equation 3.1 is equally effective at improving MSES predictions with or without trailing edge thickness.
4. In the presence of high trailing edge curvature there remains an over prediction in trailing edge loading and an under-prediction in leading edge loading that results in a good

estimation of global lift, but results in errors in predicting the moment coefficient for a wing section.

4.5.2 Questions for further exploration:

1. What is the physical cause of these errors?
2. Can a different form of turbulence modeling such as RANS produce superior results?

Chapter 5

Integral Boundary Layer Theory Compared to RANS

The coupled integral boundary layer code MSES is specifically designed for two dimensional fluid dynamics analyses associated with foils. The process of becoming an adequate user of this flow code required an investment of about a month to really understand the inputs, outputs, and steps necessary to verify convergence. After this initial investment a full convergence study for a given case from grid generation to a final solution takes about thirty minutes.

For this research the primary RANS code utilized is CFDSHIP. CFDSHIP is a fully implicit RANS code developed with the stated goal of modular code and ease of user modification for research. A full report on the details of the code development can be found in Reference [27]. I have personally used or attempted to use IFLOW, DTNS[13], UNCLE [3] and CFDSHIP. In my opinion, the CFDSHIP development team has accomplished the goal of code simplicity and has given the user the capability to freely add subroutines and modify boundary conditions without excessive danger of unknown effects. Within three months of starting to use the code the various modules and subroutines became intuitive. I spent significant time with each of the other codes as well but did not find the codes to be as organized or understandable.

The process of becoming an adequate RANS user is, for this author, at least a two year process. The complications of generating an adequate grid with high density in the appropriate locations and then determining run time parameters that will allow a RANS code to run to

convergence has been a tedious process at best. In the end, the result is a solution which is independent of grid geometry and topology. Having completed the initial investment, it now requires approximately two days to bring a single foil to convergence and verify that the solution is independent of grid density and topology.

As a note of interest, I did find that there were certain grid topologies combined with particular grid densities that would provide a solution that matched the experiment quite well. On each of these occasions careful grid refinement with proper convergence resulted in solutions which were again essentially identical to the MSES solutions.

It should be noted that although RANS is far more difficult to use, it is also far more general in its ability to handle arbitrary geometries. MSES is specifically designed to analyze a two dimensional foil like geometry. CFDSHIP is designed to be effective in a complex three dimensional environment associated with analyses of the types of flow that occur in a marine environment. The increased time and complexity associated with RANS described here is in part necessary because of the increased generality of the flow solutions.

5.1 Grid Topology

Figure 5-1 shows the overall grid geometry used and the leading edge details. A single zone was chosen for the entire inflow region in order to minimize the number of zone boundaries required. It was found that the presence of zone boundaries significantly increased the time to convergence and the potential for instability while marching toward a solution. With this geometry the tunnel walls and foil leading edge are all able to support a high grid density while using a structured grid.

The zones above and below the foil have increased density near the leading and trailing edges where the flow velocities have the highest gradients. These zones extend into the leading and trailing edge zones in order to maintain higher order accuracy across the zone boundaries. Experience indicates that if the upper and lower zones extend into the leading and trailing edge zones with an overlap of ten cells there is a significant improvement in stability and there is continuity of higher order terms across the boundary.

Figure 5-2 shows the details of the trailing edge grid topology. Here a single zone is again

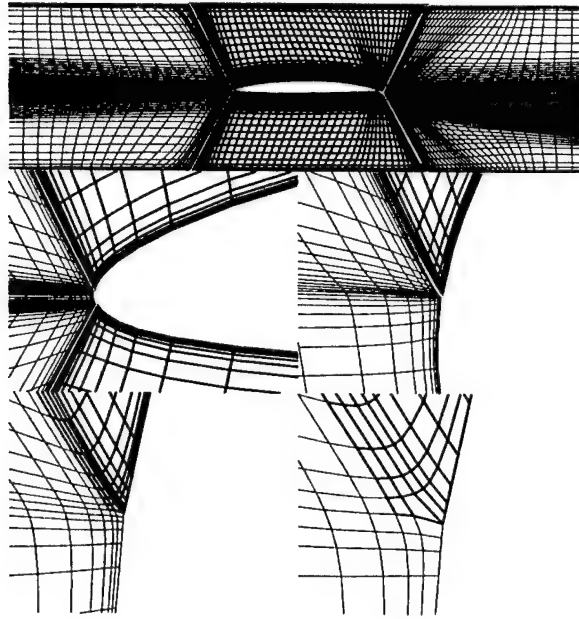


Figure 5-1: Leading Edge Grid Topology

used to enhance stability. A small aspect ratio (ten or less) is used at the trailing edge in order to ensure that the large flow gradients in this region can be captured.

5.2 Boundary Conditions

The tunnel walls can be modeled as slip or no-slip surfaces. MSES models the walls strictly as slip surfaces so the comparisons with MSES use slip surfaces. The experiment has a real wall so a no slip surface analysis is also required. It is found that the local flow conditions around the foil remain mostly unaffected by the wall boundary condition chosen. The pressure gradients at the walls are set to zero.

The inflow condition applies a horizontal velocity of unity and a zero gradient in the horizontal direction for vertical velocity and pressure. Other inflow possibilities such as constant pressure and zero vertical velocity were used for further evaluation. These other inflow conditions provide results consistent with those presented here.

The exit boundary condition is modeled as follows:

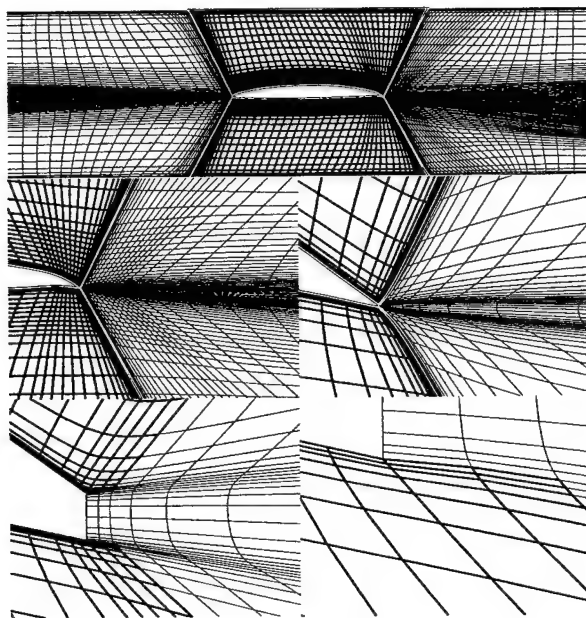


Figure 5-2: Trailing Edge Grid Topology

1. The pressure gradient in the horizontal direction is set to zero.
2. The velocity gradients in the horizontal direction are set to zero.
3. Mass flow out of the flow domain is calculated.
4. A "differential" horizontal velocity is uniformly applied to the outflow boundary in order to force global conservation of mass.

It has been our experience at the MIT water tunnel that RANS calculations for internal flow problems are quite often extremely unstable. There have been many attempts at exit boundary conditions. The set of exit boundary conditions used here have been applied to internal flow calculations including waterjets, propellers and foils with overall stable results. The RANS codes CFDSHIP and DTNS have both been exercised with these boundary conditions. The effect of the differential horizontal velocity is to maintain a reasonable solution during the convergence process and ultimately approach a zero differential horizontal velocity when convergence is achieved.

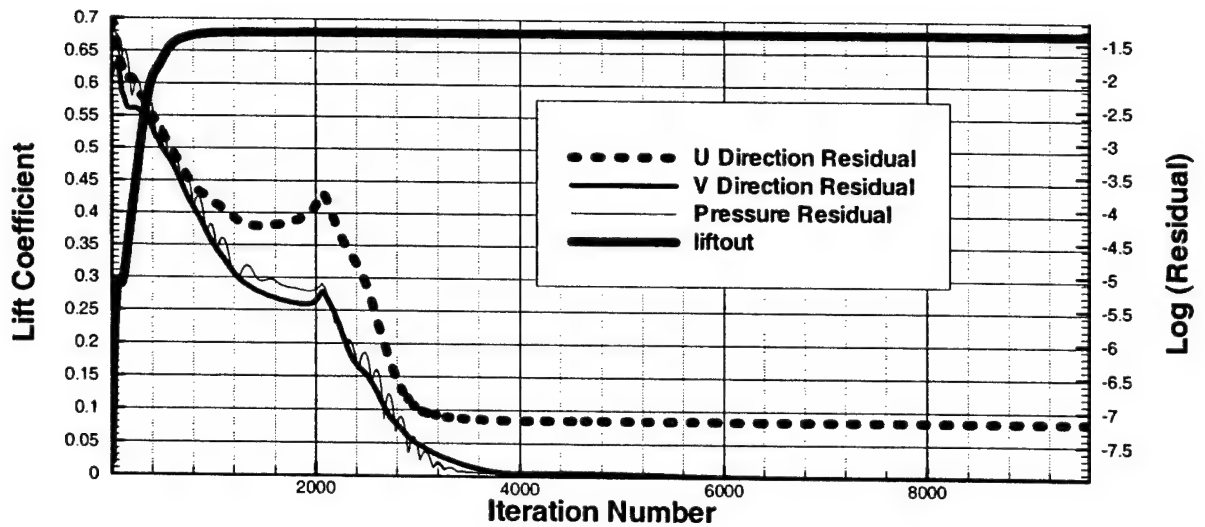


Figure 5-3: Iterative Convergence History

As mentioned above, pressure gradients are used as boundary conditions on all surfaces. This makes it necessary to fix the pressure at one location in the fluid domain. For these analyses the pressure at about the center of the upstream domain is set to zero.

5.3 Iterative Convergence

It is imperative to ensure that each case is fully converged with respect to the number of iterations. The most reliable method of verifying iterative convergence is to track the “residuals” and a relevant physical parameter. The residuals are expected to continue to decrease and the relevant physical parameter should become steady. For this study the fluid dynamic lift was measured each iteration by applying a numerical contour integration to a path in the fluid domain that surrounds the foil. When the predicted lift becomes constant and the residuals continue to decrease the problem is considered to be adequately converged. Figure 5-3 shows the convergence history for one of the B1 Blunt foil cases.

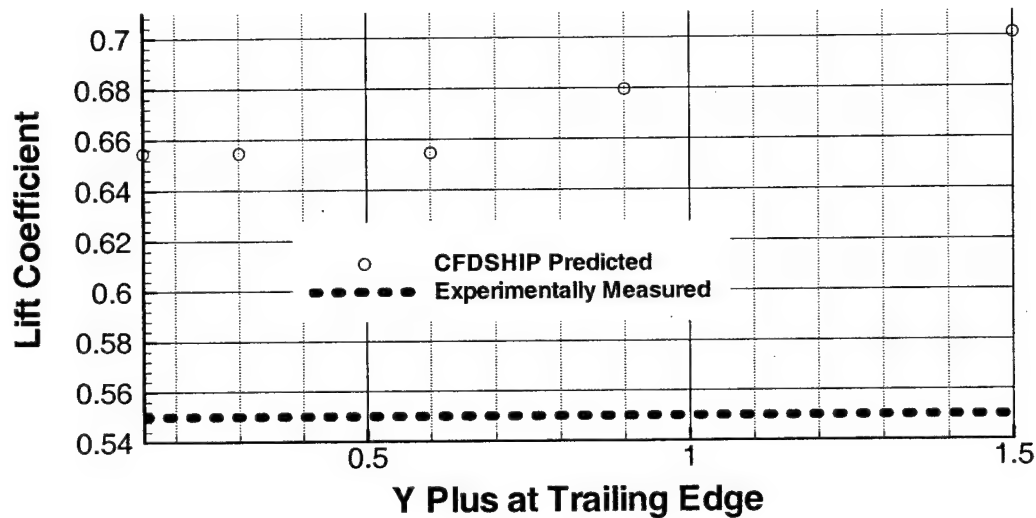


Figure 5-4: Y Plus Convergence for B1 Blunt Foil

5.4 Grid Density

5.4.1 Y Plus Convergence

The first issue explored is the height of the first grid node from the surface of the foil. The non-dimensional height above the foil surface is commonly referred to as the “Y⁺ value.” Most published results indicate that a Y⁺ value of one or less is needed to ensure the details of the boundary layer are captured. Equation 5.1 is the basis for calculating this parameter.

$$Y^+ = \frac{yV^*}{\nu} \quad (5.1)$$

y = distance to foil surface

ν = kinematic viscosity

$$V^* = \sqrt{\left(\frac{\tau_w}{\rho}\right)}$$

τ_w = wall shear stress

ρ = density

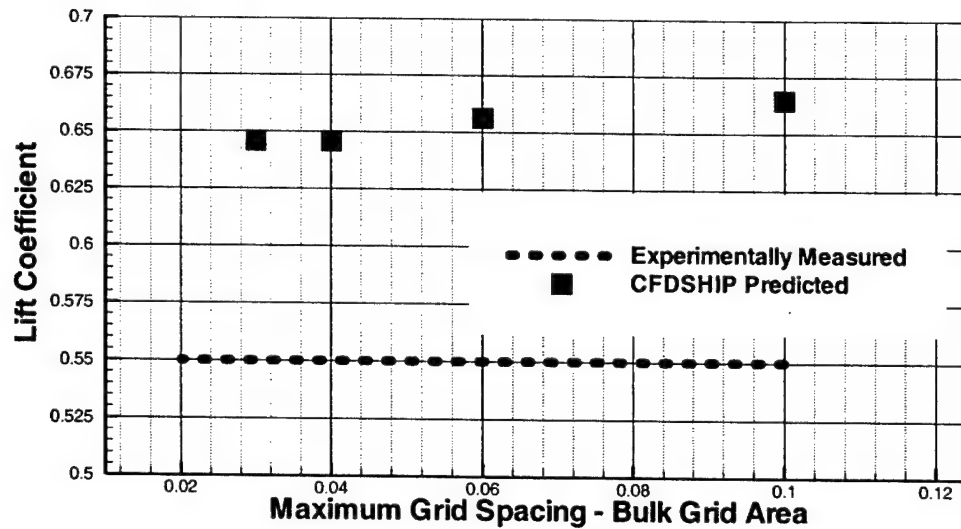


Figure 5-5: Bulk Grid Area Maximum Spacing

One of the practical problems in selecting a grid is that the wall shear stress is not known until after the solution is known. The experience of this process is that if the first node is too large it will give an inaccurate solution and if the first node is too close the solution will become unstable. The manner in which this dilemma is solved is to start off with a first node Y^+ value slightly too large and then reduce the first node height until no further changes in the solution occur. Figure 5-4 shows the lift coefficient changes as the Y^+ value is reduced to ensure convergence. It should be noted that each of the CFDShip Predicted values requires about two hours of computer time on a 1.8 GHz AMD Athlon Processor.

5.4.2 Grid Spacing

The upper and lower zones are separated into regions according to anticipated flow gradients. The leading edge region of the foil extends upstream and downstream of the leading edge by 5% of the chord length. The trailing edge region extends 5% upstream and downstream of the trailing edge region. The foil region extends 10% above and below the foil.

Figure 5-5 shows the lift coefficient versus maximum grid dimension in the bulk of the fluid. In each case this needs to be verified, but in cases analyzed for this research a bulk grid spacing



Figure 5-6: B1 Cupped Foil Geometry

of 4% of the chord length is adequate. A similar process must be conducted to verify that the grid spacing in the regions of higher flow gradients is also converged. The degree of refinement required in these regions varies depending on the details of the flow. Typical grid spacing in these regions is between 0.05% of the chord length for the B1 Cupped foil and 2% of the chord length for the HRA Fine Trailing Edge Foil.

5.4.3 Turbulence Models

CFDSHIP is programmed to support the $K-\epsilon$, $K-\omega$ and Baldwin/Lomax turbulence models. DTNS is programmed to support the $K-\epsilon$ and Baldwin/Lomax turbulence models. The foils under consideration here have been evaluated using the CFDSHIP $K-\omega$ turbulence model, the DTNS $K-\epsilon$ turbulence model, the DTNS Baldwin/Lomax turbulence model and the MSES integral boundary layer turbulence model. In each of these cases it is found that the details of the local boundary layers may vary, but the global lift coefficient as indicated by the flow velocities in the potential flow region where measurements were taken is almost identical.

5.5 Foil Comparisons

In Chapter 1 the results of a previous blind test on the B1-Cup foil were discussed as a part of the motivation for this research. In this blind test several authors of several codes (including those listed here) evaluated the B1 Cupped foil shown in Figure 5-6. The results reported were so varied that the conclusion was drawn that the details of the turbulence modeling or the software were inconsistent. The conclusion of this research is that the most likely reason for the previous variation in predictions is inadequate grid convergence study prior to drawing conclusions.

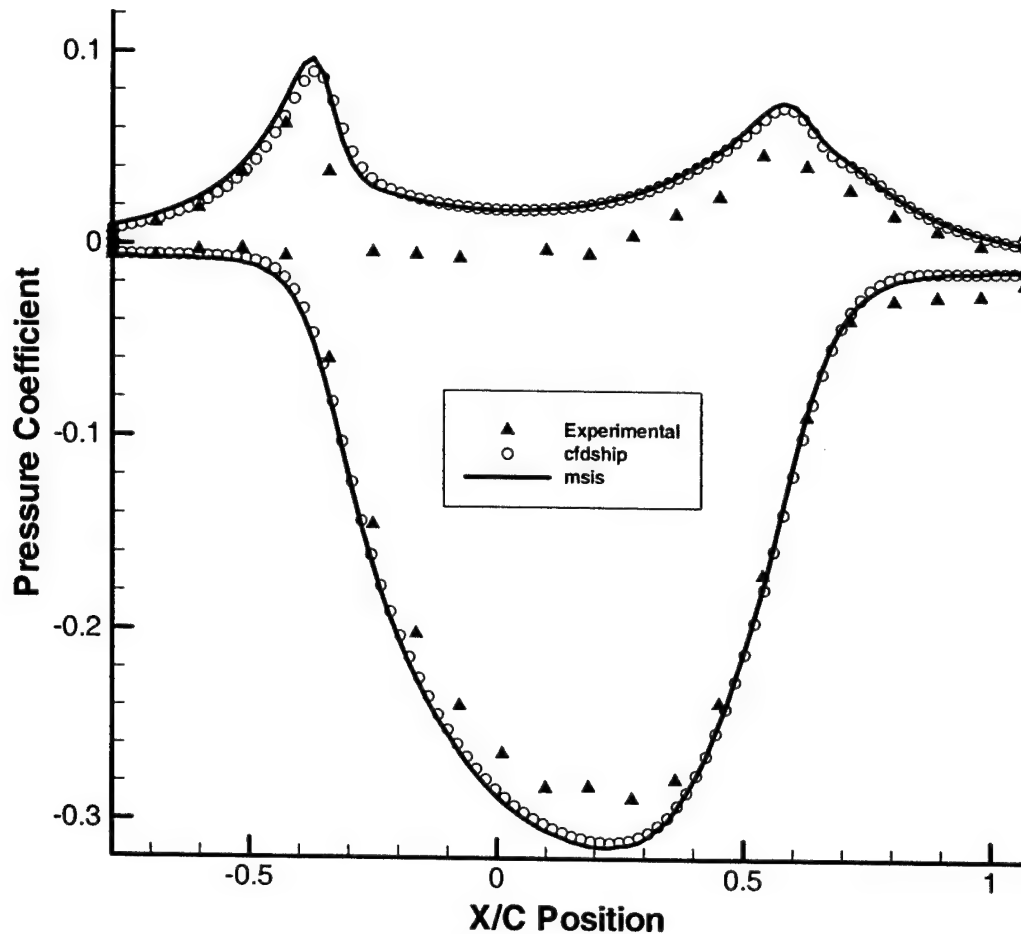


Figure 5-7: Solution Comparisons for the B1 Cupped Trailing Edge Foil

Figure 5-7 shows a fully converged solution from the CFDSHIP $K-\omega$ model, a fully converged solution from MSES and the experimentally measured datapoints. This foil experiences significant vortex shedding, significant separation prior to the trailing edge and has a very thick boundary layer. Shown here are the two most radically different turbulence models under consideration: IBLT and a two equation eddy viscosity model. The similarity in the results is striking.

The convergence procedure and comparisons similar to Figure 5-7 are conducted and the consistent result is that IBLT and RANS provide virtually identical results. The codes have been verified to give the same result for the HRA fine trailing edge foil, the HRA blunt trailing

edge foil, the B1 Blunt trailing edge foil and the B1 cupped trailing edge foil. In every case considered there is an over prediction of lift coefficient approximately consistent with Equation 3.1.

5.6 RANS Solution with Walls

One consideration is that the growth of a boundary layer on the upper and lower walls cause an overall acceleration of the fluid in the tunnel. In order to evaluate the magnitude of this concern, the water tunnel is modeled as a no-slip surface with a boundary layer. It is found that there is a slight increase in the velocity from the leading edge to the trailing edge. This is shown in Figure 5-8 by a slightly lower pressure coefficient in the back part of the foil. There is virtually no change in the overall pressure loading and it is certain that this phenomenon is not the source of the prediction errors with either RANS or IBLT.

5.7 Conclusions

This chapter demonstrates that RANS and coupled IBLT give essentially identical lift coefficient and pressure profile predictions when fully converged. With this established the following conclusions can be drawn:

1. These codes are developed completely independently, so it is certain that the differences between experiments and predictions are not caused by errors in the implementation of the underlying assumptions about the physics.
2. The differences between the codes and experiments can be predicted based on flow conditions which could be expected to effect the accuracy of the computational domain, not the experimental results. The differences between the codes and experiments are consistent across a spectrum of experimental facilities and geometries which make them unlikely to be caused by experimental error.
3. The codes use completely different methods to model the underlying assumptions about the physics and yet reach the same conclusion; thus, it is concluded that there is likely to be a common assumption which is in error.

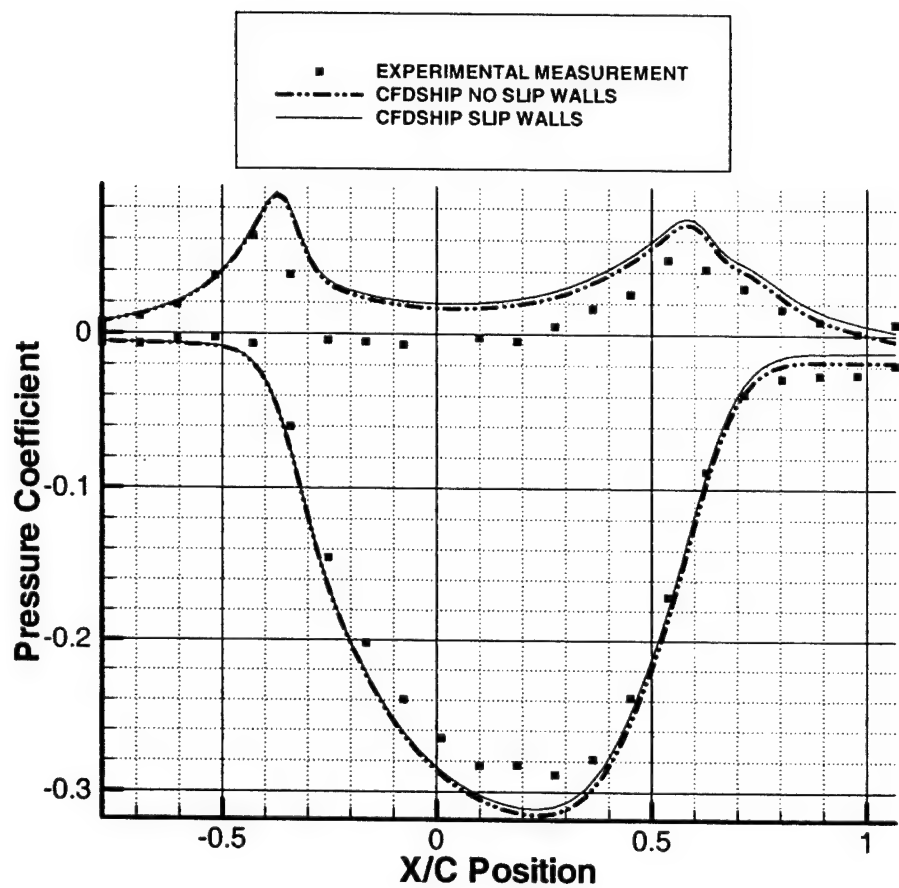


Figure 5-8: Comparison of Slip and No-Slip Solutions for Cupped Foil

The investigation into the underlying assumptions about the physics being modeled is explored in subsequent chapters.

Chapter 6

Analysis of Assumptions

In Chapter 5 the conclusion is drawn that the most probable explanation for the observed over prediction in lift is an inadequate assumption about the underlying physics which is common to both IBLT and steady RANS codes. In Chapter 2 an overview of these two approaches to solving the fluid dynamic problem is discussed. It is appropriate here to further consider the derivation of the underlying equations in order to highlight potential erroneous assumptions.

6.1 Navier-Stokes Equations

The Reynolds Averaged Navier Stokes (RANS) Equations are a time average of the Navier-Stokes Equations; therefore, the assumptions used in deriving the Navier-Stokes Equations are inherent in the RANS formulation. The Navier-Stokes Equations are derived as follows:

First, Newton's second law ($F = ma$) is applied to a fluid particle. Then both sides are divided by the volume and rearranged in accordance with tradition. This gives Equation 6.1.

$$\begin{aligned}
\rho \frac{DV}{Dt} &= f = f_{bodyg} + f_{bodymhd} + f_{surface} & (6.1) \\
\rho &= \text{density} \\
\frac{DV}{Dt} &= \text{particle derivative in Eulerian system} \\
f_{bodyg} &= \text{gravity forces} \\
f_{bodymhd} &= \text{magneto hydrodynamic forces} \\
f_{surface} &= \text{surface forces}
\end{aligned}$$

Assuming the magneto hydrodynamic forces are not relevant and applying a standard stress tensor notation gives the common form shown in Equation 6.2.

$$\rho \frac{DV}{Dt} = \rho g + \nabla \cdot \tau_{ij} \quad (6.2)$$

To this point in the derivation, the only assumption made is that the magneto hydrodynamic forces are not relevant, which seems safe. At this point in the derivation, assumptions about the fluid properties are required. Three basic assumptions about the fluid properties were made to obtain Stokes Hypothesis:

1. The fluid is continuous and the stress tensor (τ_{ij}) is a linear function of the strain rate.
2. The fluid is isotropic.
3. When strain rates are zero, deformation laws must reduce to the hydrostatic condition.

These assumptions have been shown to be accurate for all gases and most common fluids, including water. In this case the fluid under consideration is water, so the assumption of an incompressible fluid is made. The direct result of stokes hypothesis and an incompressible fluid is Equation 6.3 which gives the deformation law for incompressible Newtonian fluids.

$$\tau_{ij} = -p\delta_{ij} + \mu \left(\frac{\partial u_i}{\partial x_j} + \frac{\partial u_j}{\partial x_i} \right) \quad (6.3)$$

Combining Equation 6.1 and 6.3 gives the incompressible Navier Stokes Equations. Equation 6.4 is shown for the x direction instead of using indicial notation for clarity.

$$\rho \frac{Du}{Dt} = \rho g_x - \frac{\partial p}{\partial x} + \frac{\partial}{\partial x} \left(2\mu \frac{\partial u}{\partial x} \right) + \frac{\partial}{\partial y} \left[\mu \left(\frac{\partial u}{\partial y} + \frac{\partial v}{\partial x} \right) \right] + \frac{\partial}{\partial z} \left[\mu \left(\frac{\partial w}{\partial x} + \frac{\partial u}{\partial z} \right) \right] \quad (6.4)$$

6.2 Reynolds Averaged Navier-Stokes Equations

The Navier-Stokes equations are a direct result of Newton's Second Law and therefore apply equally in steady state or in a transient. To the extent that the assumptions made about the fluid properties are accurate, the Equations are accurate at any instant in time.

The concept employed by Reynolds is to model the fluid velocities and pressures with an average term and a fluctuating term. There are no further assumptions about the fluid or the physics. The result of time averaging is most easily seen by replacing the deformation law which was a result of Stokes hypothesis about the fluid properties (Equation 6.3) with a deformation law that includes the effect of unsteadiness, Equation 6.5.

$$\begin{aligned} \tau_{ij} &= -p\delta_{ij} + \mu \left(\frac{\partial u_i}{\partial x_j} + \frac{\partial u_j}{\partial x_i} \right) - \overline{\rho u'_i u'_j} \\ \mu \left(\frac{\partial u_i}{\partial x_j} + \frac{\partial u_j}{\partial x_i} \right) &= \text{steady (laminar) part of the stress} \\ \overline{\rho u'_i u'_j} &= \text{unsteady (turbulent) part of the stress} \end{aligned} \quad (6.5)$$

It is important to note that the time averaging of the Navier Stokes Equations has added no new assumptions. To this point, the only assumptions made concern the fluid properties in accordance with Stokes Hypothesis. These assumptions seem unlikely to be the source of observed errors.

While it is true that no new assumptions have been made, it is also true that nine new variables have been introduced. These nine new variables bring with them no real physical laws such that a great need for empirical modeling results. There have been extensive discussions among experts in the field concerning the possibility that these nine new variables sufficiently increase the difficulty in solving the physics that perhaps a totally new direction should be

taken. The following quote is from White, a noted expert in fluid dynamics:(Reference [29]):

Although statistical theory and numerical simulation are viable options, most of the research on turbulent-flow analysis in the past century has used the concept of time averaging. Applying time averaging to the basic equations of motion yields the Reynolds equations, which involve both mean and fluctuating quantities. One then attempts to model the fluctuation terms by relating them to mean properties or their gradients. This approach may now be yielding diminishing returns: Lumley (1989) gives a stimulating discussion of how time averaging might outlive its usefulness. The Reynolds equations are far from obsolete, however, and form the basis of most engineering analyses of turbulent flow.

6.3 Turbulence Modeling

The concept of turbulence modeling is, in its very essence, simply making an attempt to determine the nine unsteady terms in Equation 6.5. The difficulty lies in the fact that there are no further physical laws available. The following quote is from Reference [29] and highlights the difficulty associated with these terms:

Thus the mean momentum equation is complicated by a new term involving the turbulent inertia tensor $\overline{u'_i u'_j}$. This new term is never negligible in any turbulent flow and is the source of our analytic difficulties, because its analytic form is not known a priori. In essence, the time-averaging procedure has introduced nine new variables (the tensor components) which can be defined only through unavailable knowledge of the detailed turbulent structure. The components of $\overline{u'_i u'_j}$ are related not only to fluid physical properties but also to local flow conditions (velocity, geometry, surface roughness, and upstream history), and no further physical laws are available to resolve this dilemma. In a two dimensional turbulent boundary layer, the only significant term reduces to $\overline{u'v'}$, but even this single term requires extensive scratching about to achieve an analytic correlation which is semiempirical at best. Some of the empirical approaches have been quite successful, though rather thinly formulated from nonrigorous postulates.

Earlier in this chapter it is concluded that the RANS Equations in and of themselves contain few assumptions that can be questioned. The fact that the RANS and IBLT approaches provide virtually identical results gives the conclusion that it is very unlikely that the problem lies in the implementation. Given these observations it seems likely that source of the observed over-predictions must be in the turbulence modeling. This conclusion is buoyed by the fact that the quantity which best predicts the magnitude of the over-prediction is in its very essence a measure of the magnitude and assymetry of the local turbulence at the trailing edge of the foil. On the other hand, this research has implemented several different turbulence models that all provide consistent solutions.

6.4 Conclusions

There are a long list of experiments at multiple facilities that all demonstrate that lift is over-predicted by the flow codes. On the other hand, there are four different flow codes which use two radically different methods to model the fluid physics. There are four different methods used to model the turbulence. All of these flow solutions provide the same answer which is consistently higher than the experiments by a predictable amount. The dilemma forces us to stand back and ask the question:

Is there something about the flow around a foil which is unmodelled?

The answer to this question is yes!

1. All of the flow codes considered calculate only the time averaged behavior of the flow around the foil. The reality is that each time a discrete vortex is shed from the foil into the wake there is a surge in global lift coefficient. This surge in global lift coefficient results in another vortex of the opposite sign being shed and the process repeats. In a time averaged code, there are no discrete vortices shed and therefore there is no global response. The manner in which this phenomenon could manifest itself in a lift over-prediction would be through errors in wake trajectory caused by turbulence parameter inaccuracies.

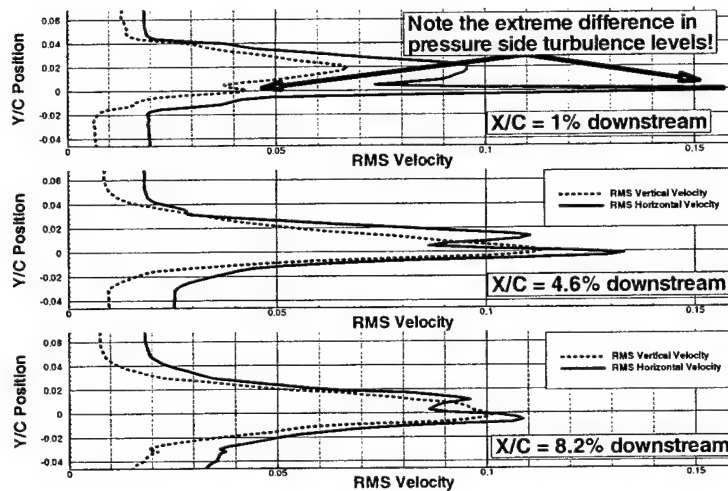


Figure 6-1: Cupped Foil Near Wake Turbulence Characteristics

2. All of the flow codes considered do not account for non-isotropic turbulence characteristics. Measurements using particle image velocimetry indicate that the flow around the trailing edge of the foils with large over prediction of lift experience highly non-isotropic turbulence characteristics. Figure 6-1 shows the measured horizontal and longitudinal turbulence characteristics for the B1 Cupped Foil at an angle of attack of about 0.5 degrees. Notice that at one percent of a chord length downstream of the foil the horizontally oriented turbulence intensity is about four times higher than the vertically oriented turbulence intensity!
3. It is likely that the former observation (unsteadiness) at least in part results in the latter observation (non-isotropic turbulence). In any case, both of these observations could explain how the flow codes could develop the same solution and still be different from the experiments. Other researchers have run into trouble predicting the characteristics of complicated flows like this. The following quote is from Henkes [14]:

An example of a complex flow is turbulent boundary-layer separation. The separation shows strong curvature and has strong velocity gradients. Such complex flow types can more accurately be predicted by differential Reynolds-stress models, which solve a partial differential equation for each component of the Reynolds-

stress tensor. For example, to calculate a 3D flow 6 equations are solved. (e.g. $\overline{u'^2}, \overline{v'^2}, \overline{w'^2}, \overline{u'v'}, \overline{v'w'}$ and $\overline{v'w'}$, respectively). In addition, the model also solves a differential equation for the dissipation rate. The reason that the differential Reynolds-stress models are most suited for complex flows is that the production of turbulence energy P does not have to be modelled. Therefore the production due to simple shear, curvature, 3D effects and rotation is represented exactly.

For flows that contain relatively large-scale spatial structures and low-frequency unsteadiness, like near wake flows, flow buffeting and dynamic stall, the use of a Large-Eddy Simulation seems to be a promising approach. In contrast to the earlier mentioned models, which all try to model the time-averaged equations, the LES only models the small-scale structures, whereas the large-scale structures are calculated from an unsteady time integration. As the small-scale turbulence is almost isotropic, the so-called subgrid models in LES are expected to be not very crucial. LES was originally developed for meteorological applications, like the earth's atmospheric boundary layer, which typically consists of large-scale structures. More recent research on LES is also devoted to aeronautical boundary layers.

Chapter 7

Unsteady Analysis

In the previous chapter it is concluded that the most likely improper assumption used in the steady flow codes considered is related to the fact that discrete vortices are shed at a discrete frequency related to the Strouhal Number at the foil trailing edge. These vortices yield a non-isotropic turbulence with a relatively low frequency variation that cannot be anticipated by a typical isotropic turbulence model.

7.1 Observed Vortex Shedding

In the introduction, reference was made to high speed photography which observed vortex shedding behind foils with blunt and beveled trailing edges (Reference [18]). These foils exhibited a highly organized vortex shedding pattern shown in Figure 7-1. The total trailing edge thickness in the case of the blunt foil is two percent, so the wavelength of the pattern observed is on the order of ten percent.

An experimental method called particle image velocimetry can be used to obtain an instantaneous velocity profile over a region of the fluid domain. This experimental method uses two pictures of the flow field very close together in time and then uses the distance the particles travel and the difference in time between pictures to obtain velocities. This experimental method is applied for the B1 Cupped foil (Section 4.4.3) and the HRA fine trailing edge foil (Section 4.3.1) in order to evaluate the characteristics of the vortex shedding.



Figure 7-1: Blunt and Beveled Foil Unsteadiness

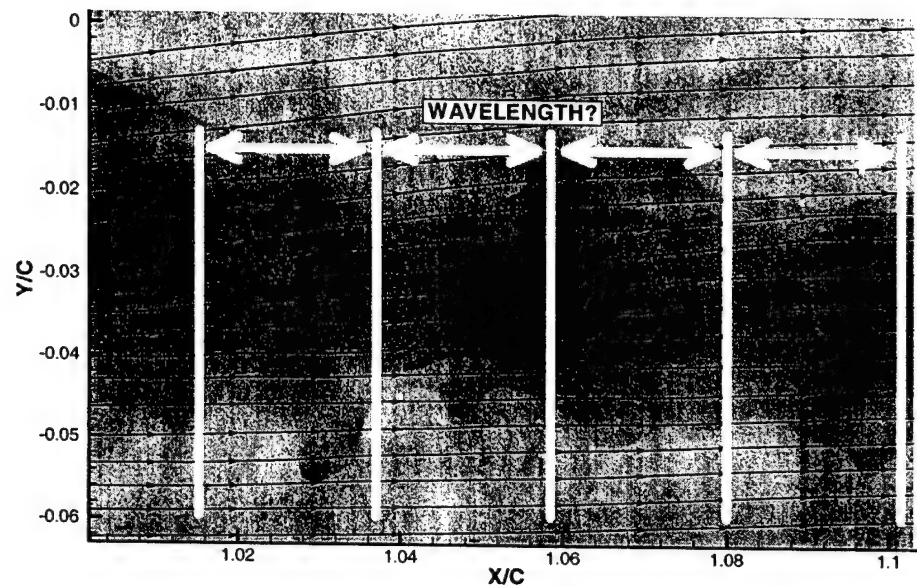


Figure 7-2: Wake Observation for the HRA Fine Trailing Edge Foil

7.1.1 HRA Fine Trailing Edge Foil Vortex Shedding

Figure 7-2 shows a single image of the wake from the particle image velocimetry. The contours are based on the magnitude of the horizontal velocity and the streamlines are integrated from the raw horizontal and vertical velocities. The estimate of wavelength indicated is based primarily on the contours of fluid velocity. There are fluctuations in the angle of the trailing edge streamlines of about ± 5 degrees depending on the phase at which the pictures are taken.

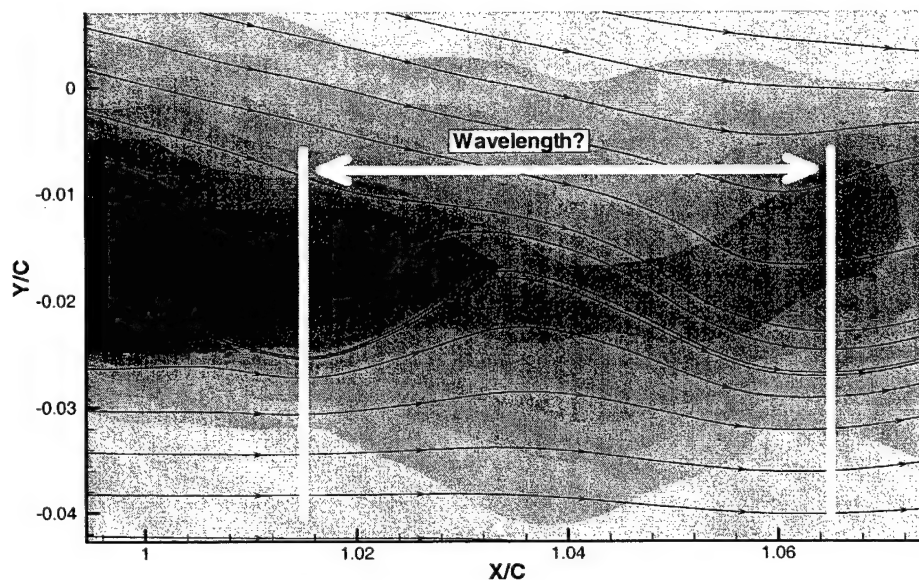


Figure 7-3: Wake Observation for the B1 Cupped Trailing Edge Foil

7.1.2 B1 Cupped Trailing Edge Foil Vortex Shedding

Figure 7-3 shows a single image of the wake of the cupped foil from the particle image velocimetry. The contours are based on the magnitude of the horizontal velocity and the streamlines are integrated from the raw horizontal and vertical velocities. It is noted that there is a significantly larger wavelength than for the HRA fine trailing edge foil and that the vortices continue impact the streamline direction much further downstream. There are very large fluctuations in the angle of the trailing edge streamlines. Based on observing several hundred pictures such as this it is noted that the pressure side vortices (counterclockwise revolution) have a strong tendency to have a very small core and a large local effect on velocity. The suction side vortices (clockwise revolution) have a tendency to have a much larger core and a much less distinct effect local velocities.

Kelvin's theorem indicates that the time averaged vorticity shed from the foil must be zero (neglecting the starting vortex). Figure 6-1 shows the result of time averaging 2,500 of the instantaneous particle image velocimetry data fields. In this Figure there is a strong anisotropic nature to the turbulence on the pressure side of the foil and somewhat less on the suction side.

It seems that the most likely explanation for the difference from the suction to pressure side anisotropic turbulence characteristics has to do with the effective core size of the vortices being shed. On the suction side of the foil there is a much larger boundary layer and greater formation time starting somewhat upstream of the trailing edge such that when the vortex leaves the foil it has a relatively large core. On the other hand, the pressure side boundary layer is very thin and the vortex is actually shown to form just downstream of the trailing edge of the foil and is very "tightly wound". The result is a highly asymmetric vortex shedding behavior.

7.2 Asymmetric Vortex Shedding Analysis

The particle image velocimetry observations make it appear that there is a clear distinction between the local turbulence and a larger low frequency turbulence associated with the vortex shedding. It is hoped that by gaining insight into the vortex shedding effects the problem can be better understood.

$$V_{\theta} = \frac{\Gamma_o}{2\pi r} \left[1 - \exp\left(-\frac{r^2}{4vt}\right) \right] \quad (7.1)$$

V_{θ} = tangential velocity due to vortex

Γ_o = vortex circulation

r = distance in space from vortex core

v = fluid viscosity

t = time since the vortex was a point vortex

Equation 7.1 is derived in Reference [29] and gives the velocity profile of a vortex which starts as a point vortex at time zero and then has a core growth and viscous dissipation over time. A small Fortran program is written to evaluate how a set of discrete vortices being shed from the trailing edge of a foil will effect the flow field. This program is provided in Appendix H.

First of all, it is interesting to see the essence of how the RANS Equations attempt to model a vortex field. Figure 7-4 shows a set of symmetric vortices in a typical time accurate format

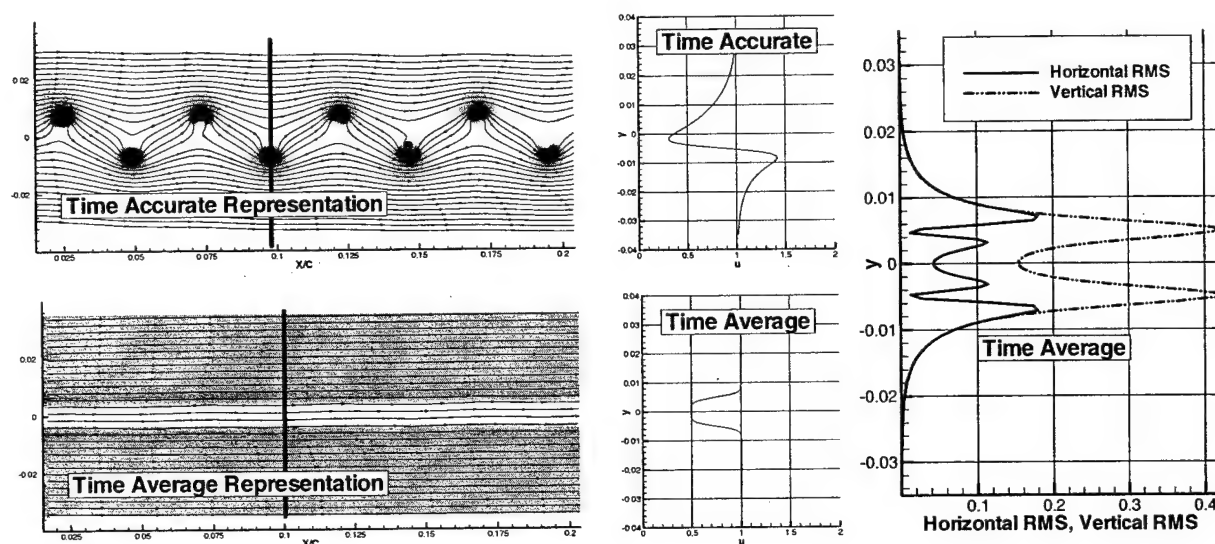


Figure 7-4: Time Averaged vs Time Accurate Representations of Symmetric Vortices

that you would see in a picture and also in a time averaged format. In the case shown in Figure 7-4 the vortices are symmetric and counter rotating such that the net effect on the outflow angle is zero. The vortices each have a vortex strength equal to one tenth of that of the B1 Cupped foil and the wavelength is based on the observed wavelength from PIV for the B1 Cupped foil.

The next question considered is how an asymmetry in core size effects the mean flow field. The reference starting time of the vortices is adjusted and then the calculations are performed again. The reference starting time is used to give the vortex an initial core size similar to the boundary layer thickness on the associated side of the foil. Figure 7-5 shows the time accurate and time averaged effects of asymmetry in the vortex core size. In this simulation the vortices are started at the same horizontal location, but with different reference formation times. It is interesting to note that the asymmetry in the RMS velocities shows the same character as the asymmetry in the experiment (Figure 6-1). It appears that the issue of vortex core size may account for the observed turbulence parameter asymmetry.

Now the question arises how the flow field would be effected if the vortices were released from slightly different horizontal positions. For example, on the cupped foil it appears that the pressure side vortex forms just barely beyond the trailing edge of the foil and the suction side

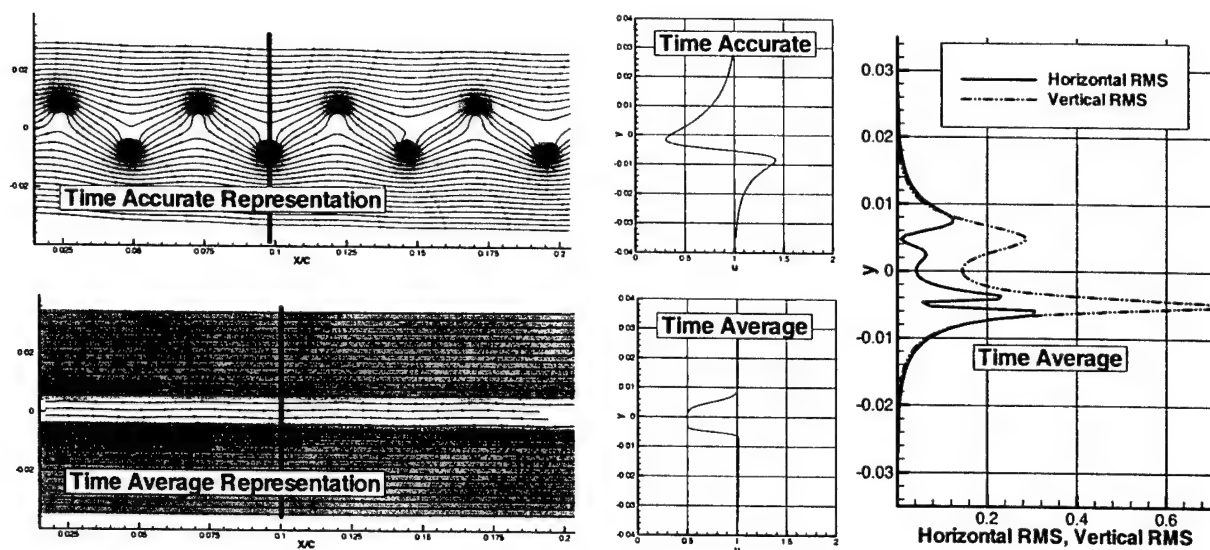


Figure 7-5: Time Accurate and Time Averaged Effects of Core Size Asymmetry

vortex forms about one to three percent upstream of the trailing edge. Figure 7-6 shows the time accurate and time averaged effect of releasing the pressure side vortex at the trailing edge and the suction side vortex two percent upstream. With this type of asymmetry the suction side vortex has a greater time that it effects the flow field and there is an obvious net change in the angle of attack. This type asymmetry explains why an adjustment in the foil angle of attack in accordance with Equation 3.1 results in improved velocity predictions throughout the flow domain.

In summary, these analyses indicate that asymmetric vortex shedding can effect the outflow angle and cause non-isotropic turbulence. These observations are consistent with experimental observations and could explain the offset in angle of attack since the errors in lift coefficient prediction are directly related to the asymmetry in the boundary layers and the size of the wake.

7.3 Unsteady RANS Analysis

Given these observations, a few computational strategies can be considered. The most general solution would be direct numerical simulation, but the best assessment to date is that a flow

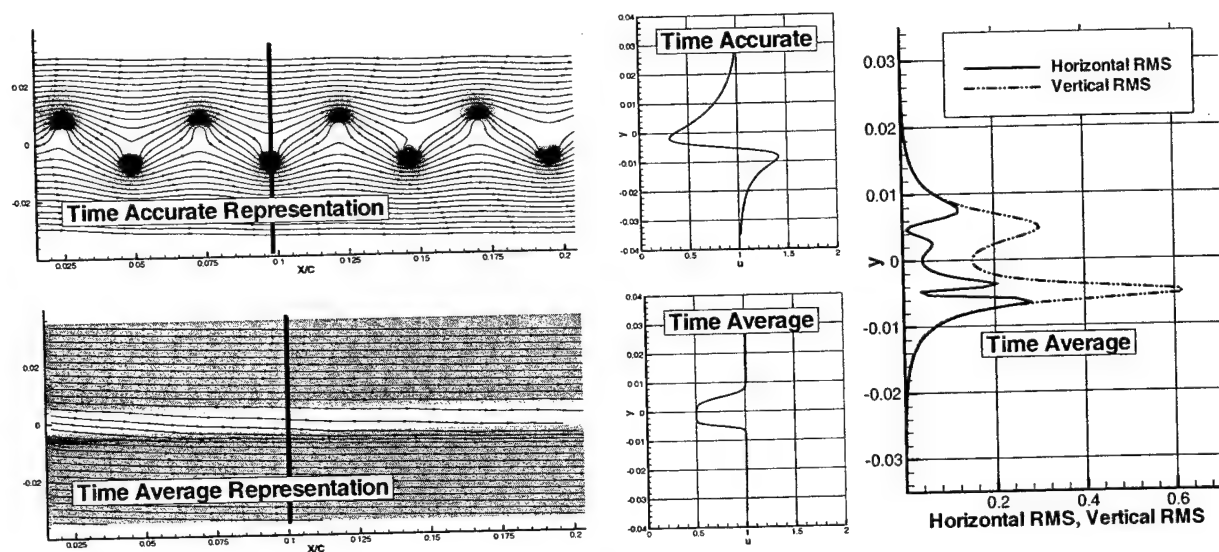


Figure 7-6: Time Accurate and Time Averaged Effects of Vortex Origination Point

field with this complexity could only be run at Reynolds Numbers in the thousands to tens of thousands. The next best choice would be a Large Eddy Simulation, but the best assessment to date is that a flow field with this complexity could only be reasonably run at Reynolds Numbers in the tens to hundreds of thousands. The final potential solution, which is exercised here is Unsteady Reynolds Averaged Navier Stokes (URANS). The following quote is a brief explanation of the URANS concept from Reference [12]:

It was noted that RANS models treat all of the unsteadiness in the flow as 'turbulence'. The concept of unsteady RANS modeling has been proposed; it is sometimes claimed that this type of calculation is a sort of very large eddy simulation (VLES). Let us discuss this seeming contradiction. Sometimes a RANS calculation fails to converge to a steady state solution; in its stead, an unsteady (usually time-periodic) solution is produced. Some authors claim that the results can be regarded as a VLES but this is hard to justify. If a flow has a separation between a large-scale unsteady field and small scale 'turbulence' and thus a spectrum with two peaks and a gap between them, VLES might make sense. Unfortunately, this kind of flow occurs very rarely, if at all. The atmosphere and ocean were thought to behave in this way

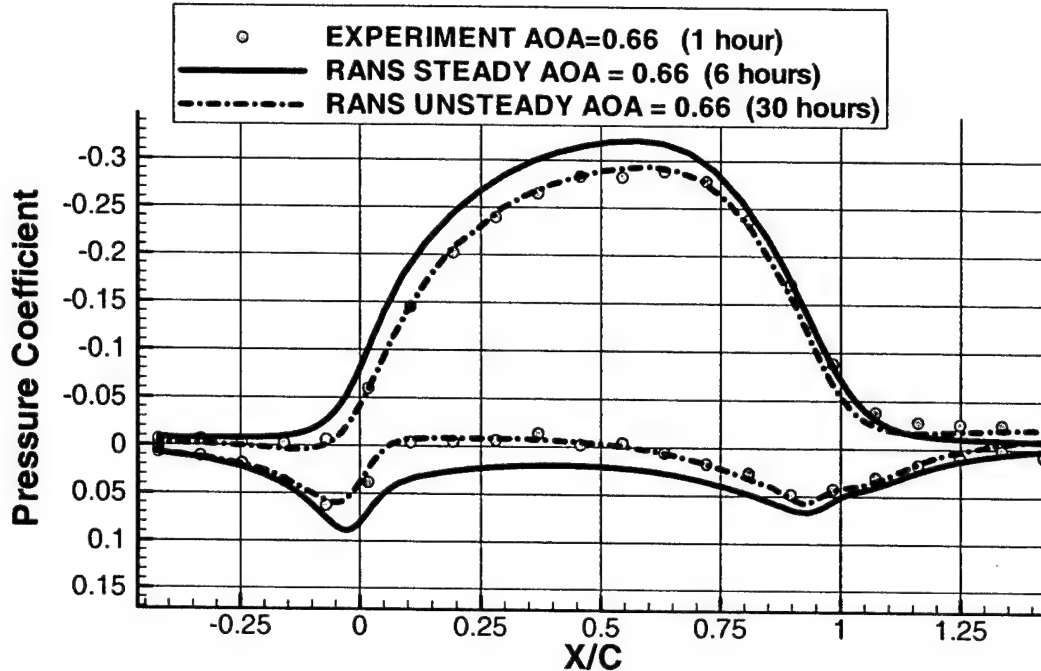


Figure 7-7: Steady and Unsteady RANS Analysis for B1 Cupped Foil

but recent evidence suggests that this is not the case. Without a spectral gap it is difficult to justify the idea that unsteady RANS calculations are a kind of VLES. Also, a model designed to represent only part of the unsteady motion should differ from one that models all of the unsteady motion.

CFDSHIP has a built in time accurate mode of operation that allows URANS calculations. The question arises whether or not the flow environment around a foil experiences the type of flow mentioned here. The lessons learned in the RANS grid convergence study were used to make a grid with higher density in the wake and adequate density on the foil. This grid is analyzed using the URANS formulation of CFDSHIP. The vortex shedding patterns observed in the calculations show a high degree of asymmetry and a frequency similar to that observed in the experiment. A time average of the fluid velocities around the foil is taken and the agreement with the experiment is remarkable. Figure 7-7 shows the results of URANS, RANS and the experiment.

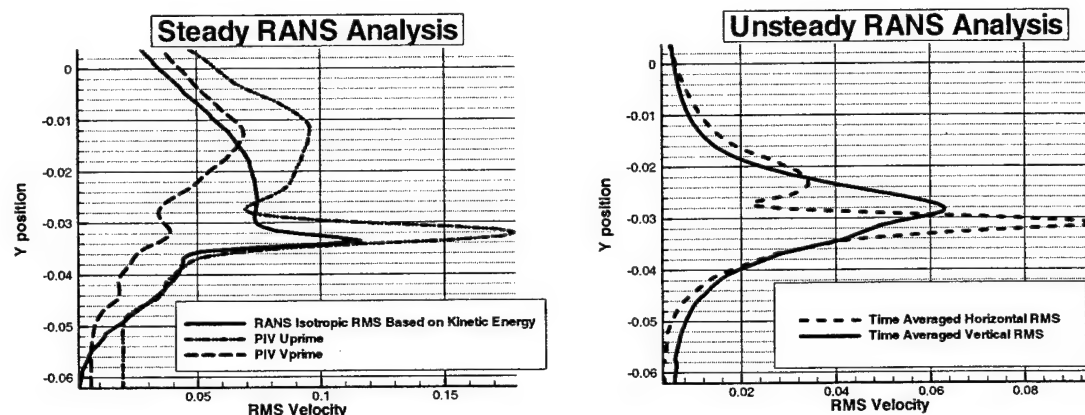


Figure 7-8: Unsteady Rans Non-Isotropic Turbulence

It should be noted here that the unsteady RANS formulation is very unstable. The actual run that is reported took thirty hours to run, but finding a set of run time parameters that would allow it to run took months. The horizontal pressure waves reported in Reference [23] were observed and seem to be the source of the unstable behavior.

7.4 Conclusions

This research indicates that a purely time averaged analysis of the flow field associated with a two dimensional foil fails to capture physics which are relevant to determining time average forces. The experimentally observed and computationally reproduced vortex shedding is demonstrated to result in an over-prediction of lift on foils with relevant geometries.

A series of new experiments and analysis of old experiments yields a correction which significantly improves the time average calculations, although it does not fully model the relevant physics. The improvement is shown to enhance not only the global lift coefficient predictions, but also the local velocity predictions. The experimental time average velocity measurements are tabulated to allow future comparisons with flow code improvements.

Chapter 8

Recommendations

8.1 Long Term Solution

The computational effort required to determine the effects of vortex shedding on a two dimensional foil is considerable. In this research it has been found that approximately 10,000 time steps per chord length are required to fully resolve the time accurate vortex shedding patterns. For most practical engineering solutions this option is clearly not practical.

This research indicates that it will be necessary to model anisotropic turbulence in order to fully capture the effects of vortex shedding on a two dimensional foil. A steady turbulence modeling technique such as second moment closure may be capable of predicting the time average flow field correctly since it explicitly solves a set of differential equations for each of the turbulence terms. Flow codes that use second moment closure for turbulence modeling are not widely available and currently are used primarily in research.

8.2 Short Term Solution

Many modern applications use integral boundary layer theory and panel methods to determine forces on surfaces that act as a two dimensional foil. For these types of applications Equation 3.1 can be used to estimate the difference between the steady state viscous calculation and the experiment or average time accurate calculation. The following example illustrates the manner in which this research can be used:

Example (Data from B1 Cupped Foil)

- A foil is evaluated using a fully viscous IBLT code (such as MSES) to have a lift coefficient of 0.64.
 - IBLT gives an upper side displacement thickness of 0.021 chord lengths.
 - IBLT gives a lower side displacement thickness of 0.005 chord lengths.
1. If the application lends itself to adjusting the computational angle of attack then the computational angle of attack is set 0.92 degrees less than the experimental angle of attack. This approach was used for all of the comparisons with water tunnel experiments reported in this thesis.

$$\Delta\alpha_{vortices} = -\frac{[\delta_{top}^* - \delta_{bottom}^*]}{chord} = -\frac{(.021 - .005)}{1.0} = -.016radians = -0.92deg$$

2. If the application does not lend itself easily to adjusting the foil angle of attack then thin foil theory can be used to estimate the change in lift associated with the angle error predicted by Equation 3.1. Equation 8.1 shows the approximate change in normal coefficient for this case.

$$\begin{aligned}\Delta C_{L\ vortices} &= -2\pi \frac{[\delta_{top}^* - \delta_{bottom}^*]}{chord} = -2\pi(.016) = -0.1 \\ 2\pi &= \text{lift slope from thin foil theory}\end{aligned}\tag{8.1}$$

Using this method, the lift coefficient (normal vector) is adjusted from 0.64 to 0.54.

Appendix A

Coupled Integral Boundary Layer Theory Convergence Study

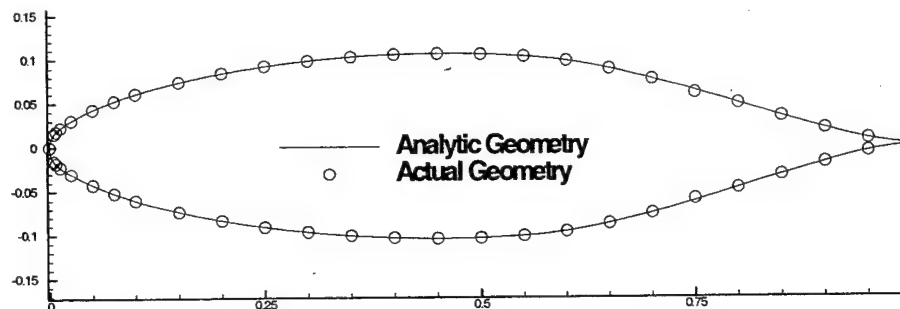


Figure A-1: NACA 66021 Foil Geometry

A.1 Foil Geometry

The foil used to demonstrate convergence is the NACA 66021 foil. The foil geometry is generated based on the mathematical equations in Reference [28]. The individual data points experimentally measured are listed in an appendix of the same reference and are shown along with the derived surface in Figure A-1. This foil is very thick (21%) and has maximum thickness relatively far back on the foil. These characteristics are similar to the shape of a propeller blade near the hub and have shown a tendency to result in larger discrepancies between experiments and predictions.

A.2 Grid Convergence

The domain used during the grid convergence study is eight chord lengths long and 3.75 chord lengths high. A base-line coarse mesh is created and then subdivided in streamwise and cross stream directions. Figure A-2 shows lift coefficient convergence versus total number of nodes. Table A.1 shows the final grid dimensions chosen. In reality, the grid chosen is far beyond what is required, but processor speeds are such that the excess gridding is of no consequence. Processing time for grid generation and analysis ranged from about two seconds to 60 seconds. The majority of the calculations require between 5 and 15 Newton iterations to reach convergence.

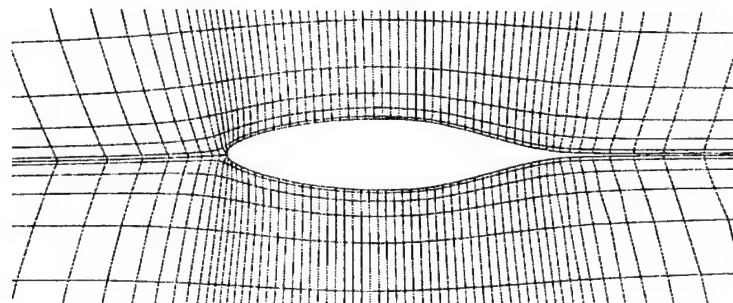
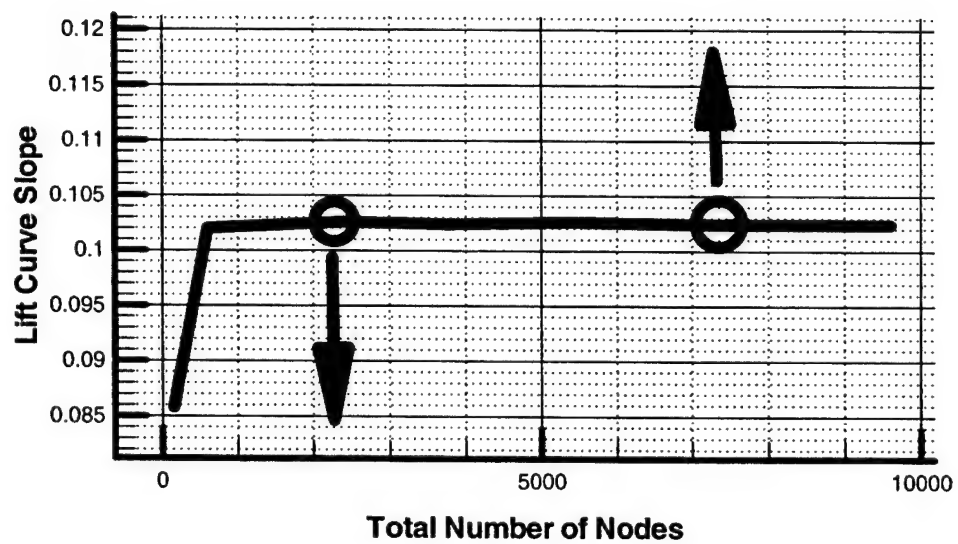
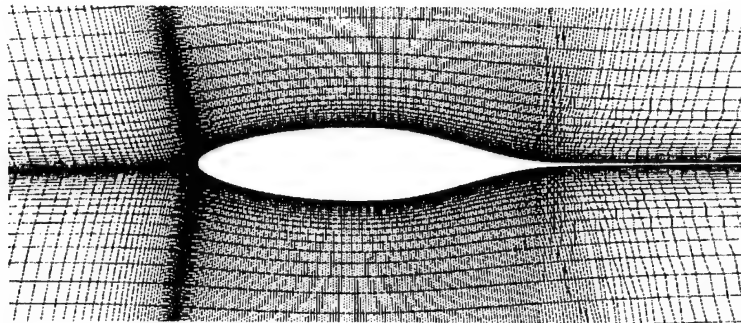


Figure A-2: MSIS Grid Convergence Summary

Description	Quantity
Foil Top and Bottom Nodes	150
Upstream Nodes	50
Downstream Nodes	50
Upper Half of Domain Streamlines	30
Lower Half of Domain Streamlines	30
Total Number of Nodes	15000

Table A.1: Converged Grid Characteristics

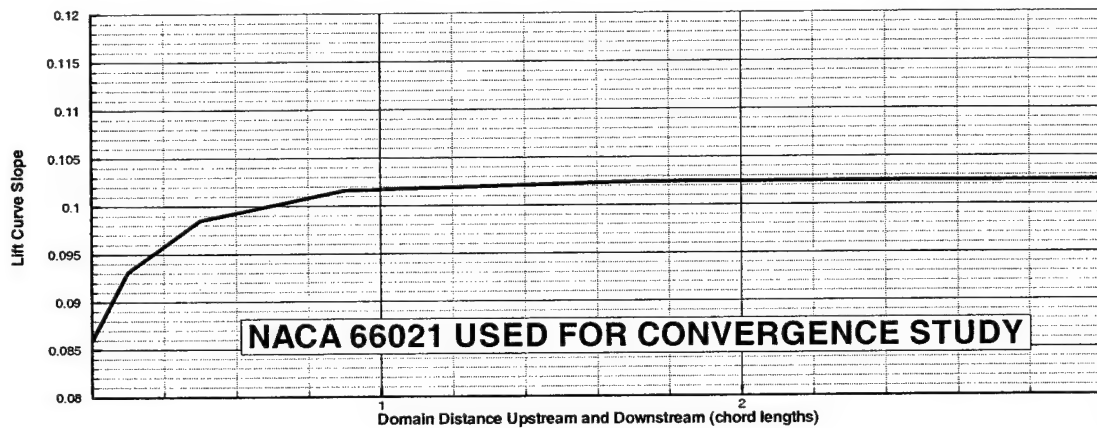


Figure A-3: Predicted Lift Coefficient vs MSIS Domain Length

A.3 Domain Size

The limits of the domain for this study are evaluated by changing the size of the domain and observing the effects on the predicted lift. Grid convergence is assured at each new domain length. Figures A-3 and A-4 show the variation in predicted lift coefficient based on the domain size. A domain height of 3.75 chord lengths is chosen based on the actual tunnel size and a distance upstream and downstream of 3.0 chord lengths is chosen based on Figure A-3.

A.4 Mach Number

Ultimately the goal of this research is in evaluating incompressible flows relevant to marine propellers. In general, incompressible flow is very similar to low Mach Number conditions in air, so the same tools and experiments will be useful. The experimental Mach Number for

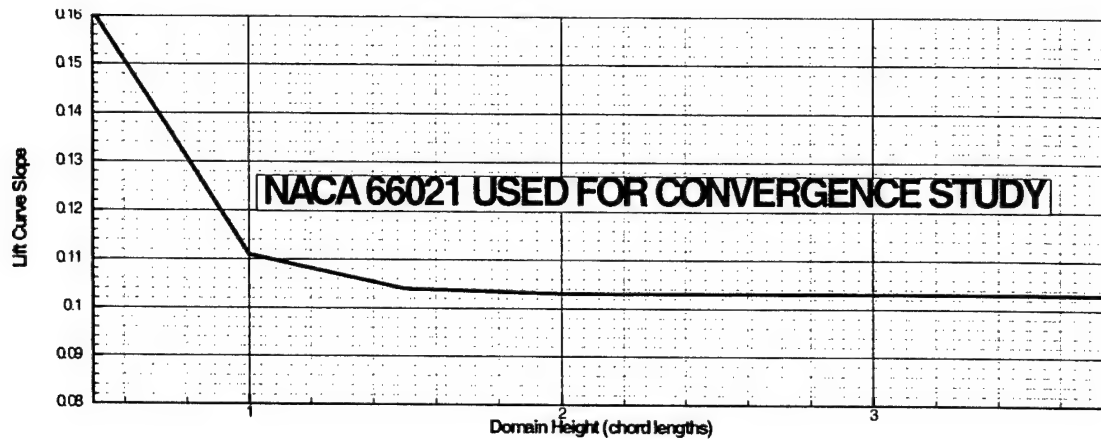


Figure A-4: Predicted Lift Coefficient vs MSIS Domain Height

the airfoils considered here is typically less than 0.1. Figure A-5 shows that lift coefficient predictions are insensitive to Mach Number over the region of interest. The Mach number chosen is 0.025 based on anticipated use with incompressible flow.

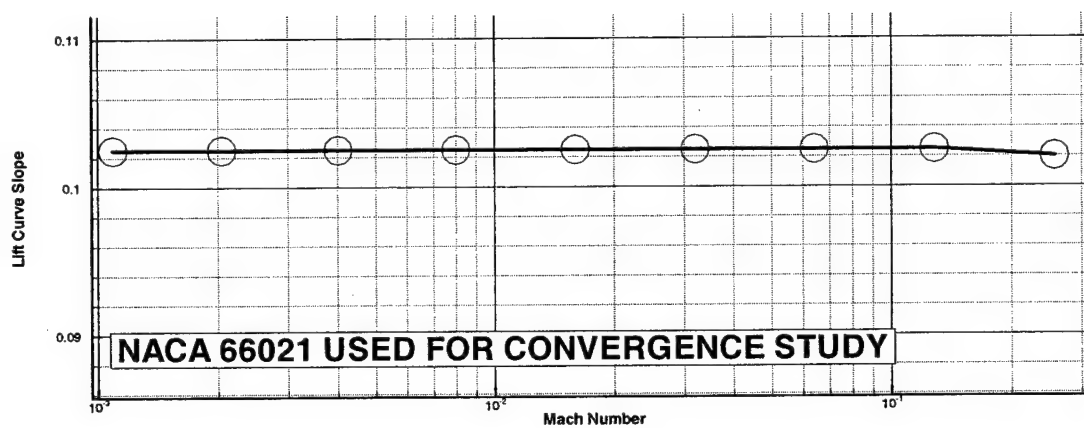
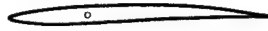


Figure A-5: Predicted Lift Coefficient vs Mach Number

Appendix B

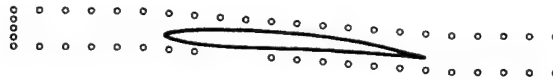
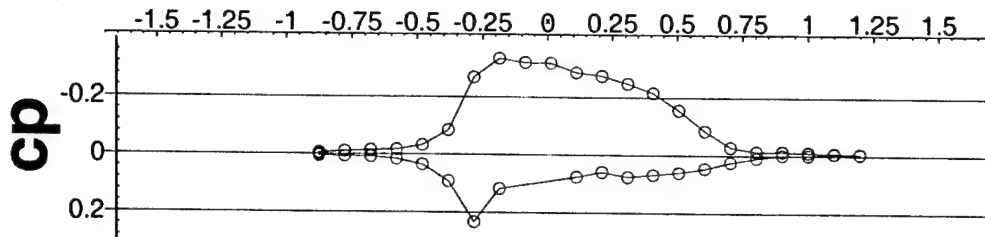
HRA Fine Trailing Edge Foil

Experimental Data



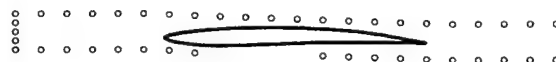
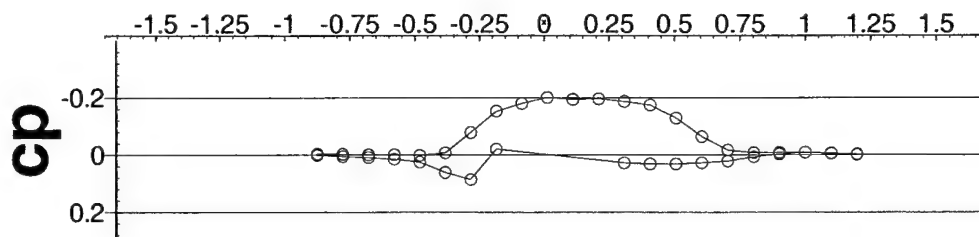
X/C	Y/C	X/C	Y/C	X/C	Y/C
0.7000	-0.0093	-0.1622	0.0208	0.0258	-0.0301
0.6949	-0.0082	-0.1873	0.0178	0.0759	-0.0274
0.6899	-0.0076	-0.2123	0.0143	0.1260	-0.0246
0.6824	-0.0064	-0.2374	0.0101	0.1761	-0.0218
0.6724	-0.0049	-0.2574	0.0062	0.2263	-0.0192
0.6598	-0.0029	-0.2700	0.0032	0.2764	-0.0170
0.6398	0.0003	-0.2800	0.0005	0.3265	-0.0151
0.6147	0.0043	-0.2875	-0.0020	0.3766	-0.0136
0.5897	0.0083	-0.2926	-0.0040	0.4142	-0.0126
0.5646	0.0122	-0.2963	-0.0060	0.4393	-0.0121
0.5395	0.0160	-0.2983	-0.0074	0.4643	-0.0117
0.5145	0.0195	-0.2997	-0.0091	0.4894	-0.0112
0.4894	0.0227	-0.2997	-0.0112	0.5145	-0.0109
0.4644	0.0256	-0.2983	-0.0129	0.5395	-0.0106
0.4393	0.0280	-0.2963	-0.0142	0.5646	-0.0104
0.4142	0.0301	-0.2926	-0.0160	0.5897	-0.0103
0.3766	0.0326	-0.2875	-0.0178	0.6147	-0.0103
0.3265	0.0349	-0.2800	-0.0200	0.6398	-0.0105
0.2764	0.0365	-0.2700	-0.0223	0.6598	-0.0107
0.2263	0.0374	-0.2574	-0.0247	0.6724	-0.0108
0.1761	0.0377	-0.2374	-0.0277	0.6824	-0.0110
0.1260	0.0373	-0.2123	-0.0305	0.6899	-0.0111
0.0759	0.0362	-0.1873	-0.0325	0.6949	-0.0113
0.0258	0.0346	-0.1622	-0.0339	0.7000	-0.0110
-0.0244	0.0321	-0.1371	-0.0346		
-0.0745	0.0289	-0.1121	-0.0348		
-0.1121	0.0259	-0.0745	-0.0342		
-0.1371	0.0235	-0.0244	-0.0325		

HRA Fine Trailing Edge Foil Geometry at AOA=0.0



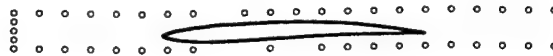
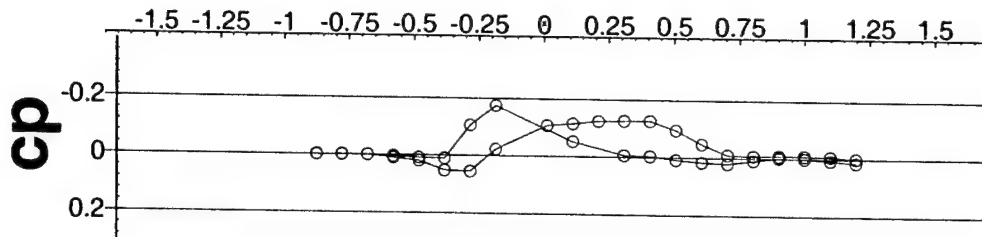
Chord = 405mm			Uinf= 5.312 m/sec		AOA= 4.3 degrees					
X/C	Y/C	U/Uinf	V/Uinf	Cp		X/C	Y/C	U/Uinf	V/Uinf	Cp
1.198	-0.117	1.003	-0.041	-0.004		-0.877	0.100	1.005	0.030	-0.006
1.099	-0.117	1.005	-0.049	-0.006		-0.778	0.100	1.009	0.041	-0.010
1.000	-0.117	1.000	-0.060	-0.001		-0.679	0.100	1.013	0.060	-0.015
0.901	-0.117	1.000	-0.062	-0.002		-0.580	0.100	1.013	0.085	-0.016
0.802	-0.117	0.988	-0.072	0.009		-0.481	0.100	1.024	0.126	-0.032
0.704	-0.110	0.973	-0.075	0.024		-0.383	0.100	1.064	0.194	-0.084
0.605	-0.103	0.951	-0.073	0.045		-0.284	0.094	1.218	0.228	-0.268
0.506	-0.096	0.936	-0.066	0.060		-0.185	0.087	1.288	0.098	-0.334
0.407	-0.090	0.928	-0.055	0.068		-0.086	0.080	1.280	0.040	-0.320
0.309	-0.083	0.921	-0.043	0.075		0.012	0.073	1.278	-0.049	-0.318
0.210	-0.076	0.938	-0.058	0.059		0.111	0.066	1.252	-0.064	-0.286
0.111	-0.069	0.921	-0.026	0.076		0.210	0.060	1.242	-0.058	-0.274
-0.185	-0.049	0.870	-0.094	0.117		0.309	0.053	1.216	-0.124	-0.247
-0.284	-0.042	0.730	0.006	0.233		0.407	0.046	1.186	-0.154	-0.215
-0.383	-0.036	0.889	0.162	0.092		0.506	0.039	1.131	-0.181	-0.156
-0.481	-0.036	0.958	0.111	0.035		0.605	0.033	1.067	-0.173	-0.085
-0.580	-0.036	0.981	0.077	0.016		0.704	0.026	1.018	-0.139	-0.028
-0.679	-0.036	0.990	0.056	0.008		0.802	0.019	1.009	-0.094	-0.014
-0.778	-0.036	0.992	0.041	0.007		0.901	0.019	1.011	-0.068	-0.013
-0.877	-0.036	0.994	0.030	0.006		1.000	0.019	1.009	-0.056	-0.011
-0.877	-0.002	0.998	0.030	0.002		1.099	0.019	1.007	-0.045	-0.008
-0.877	0.032	1.000	0.032	0.000		1.198	0.019	1.005	-0.036	-0.006
-0.877	0.066	1.003	0.028	-0.004		0.000	0.000	0.000	0.000	0.000
-0.877	0.100	1.005	0.030	-0.006		0.000	0.000	0.000	0.000	0.000

HRA Fine Foil Experimental Data at AOA=4.3 deg



Chord = 405mm			Uinf= 5.288 m/sec			AOA= 1.1 degrees				
X/C	Y/C	U/Uinf	V/Uinf	Cp		X/C	Y/C	U/Uinf	V/Uinf	Cp
1.198	-0.090	1.002	-0.025	-0.003		-0.679	0.087	1.000	0.026	-0.001
1.099	-0.090	1.004	-0.030	-0.005		-0.580	0.087	1.000	0.038	-0.001
1.000	-0.090	1.008	-0.036	-0.009		-0.481	0.087	0.997	0.059	0.002
0.901	-0.090	1.002	-0.038	-0.003		-0.383	0.087	1.002	0.098	-0.007
0.802	-0.090	0.993	-0.040	0.006		-0.284	0.084	1.065	0.151	-0.078
0.704	-0.086	0.978	-0.032	0.022		-0.185	0.081	1.137	0.117	-0.153
0.605	-0.083	0.972	-0.023	0.027		-0.086	0.077	1.163	0.085	-0.180
0.506	-0.079	0.968	-0.011	0.031		0.012	0.074	1.184	0.017	-0.201
0.407	-0.076	0.968	-0.002	0.031		0.111	0.070	1.178	0.002	-0.194
0.309	-0.072	0.972	0.011	0.028		0.210	0.067	1.180	-0.009	-0.196
-0.185	-0.062	1.017	-0.078	-0.021		0.309	0.063	1.171	-0.061	-0.187
-0.284	-0.052	0.906	-0.089	0.086		0.407	0.060	1.157	-0.096	-0.174
-0.383	-0.048	0.936	0.038	0.061		0.506	0.056	1.114	-0.132	-0.129
-0.481	-0.048	0.974	0.030	0.025		0.605	0.053	1.053	-0.136	-0.064
-0.580	-0.048	0.985	0.023	0.014		0.704	0.050	1.012	-0.100	-0.017
-0.679	-0.048	0.991	0.017	0.009		0.802	0.046	1.006	-0.061	-0.008
-0.778	-0.048	0.995	0.013	0.005		0.901	0.046	1.008	-0.042	-0.009
-0.877	-0.048	0.998	0.008	0.001		1.000	0.046	1.008	-0.032	-0.008
-0.877	-0.014	0.998	0.011	0.001		1.099	0.046	1.006	-0.026	-0.006
-0.877	0.020	0.998	0.011	0.001		1.198	0.046	1.000	-0.019	-0.001
-0.877	0.053	1.000	0.013	0.000						
-0.877	0.087	1.004	0.015	-0.004						
-0.778	0.087	1.002	0.021	-0.002						
-0.679	0.087	1.000	0.026	-0.001						

HRA Fine Foil Experimental Data at AOA=1.1 deg

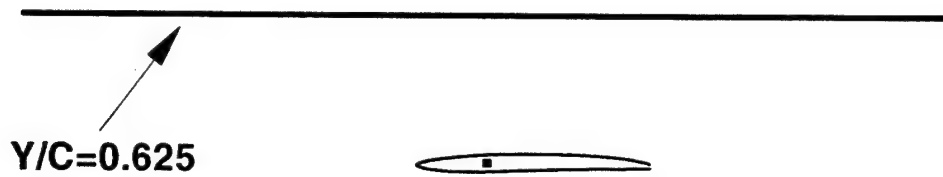


Chord = 405mm			Uinf= 5.284 m/sec			AOA= -1.7 degrees				
X/C	Y/C	U/Uinf	V/Uinf	Cp		X/C	Y/C	U/Uinf	V/Uinf	Cp
1.198	-0.034	0.986	-0.028	0.014		-0.778	0.061	0.999	-0.011	0.001
1.099	-0.034	0.994	-0.026	0.006		-0.679	0.061	0.999	-0.011	0.001
1.000	-0.034	0.999	-0.030	0.000		-0.580	0.061	0.990	-0.017	0.010
0.901	-0.034	1.001	-0.028	-0.002		-0.481	0.061	0.980	-0.013	0.019
0.802	-0.034	0.992	-0.025	0.008		-0.383	0.061	0.946	-0.002	0.052
0.704	-0.037	0.980	-0.013	0.019		-0.284	0.064	0.939	0.097	0.055
0.605	-0.041	0.984	0.011	0.016		-0.185	0.068	1.014	0.127	-0.023
0.506	-0.044	0.992	0.025	0.008		0.012	0.074	1.100	0.074	-0.107
0.407	-0.048	1.003	0.034	-0.004		0.111	0.078	1.107	0.053	-0.114
0.309	-0.051	1.005	0.051	-0.006		0.210	0.081	1.117	0.034	-0.124
0.309	-0.051	1.005	0.051	-0.006		0.309	0.085	1.118	-0.004	-0.125
0.111	-0.058	1.048	0.074	-0.052		0.407	0.088	1.118	-0.044	-0.126
-0.185	-0.068	1.160	-0.057	-0.175		0.506	0.092	1.088	-0.079	-0.095
-0.284	-0.072	1.086	-0.176	-0.106		0.605	0.095	1.043	-0.085	-0.047
-0.383	-0.075	0.984	-0.100	0.011		0.704	0.099	1.009	-0.057	-0.010
-0.481	-0.075	0.990	-0.049	0.009		0.802	0.102	1.007	-0.032	-0.007
-0.580	-0.075	0.995	-0.034	0.004		0.901	0.102	1.009	-0.015	-0.009
-0.679	-0.075	0.999	-0.036	0.000		1.000	0.102	1.009	-0.011	-0.009
-0.778	-0.075	1.001	-0.030	-0.002		1.099	0.102	1.007	-0.006	-0.007
-0.877	-0.075	0.999	-0.023	0.000		1.198	0.102	1.001	-0.008	-0.001
-0.877	-0.041	1.001	-0.025	-0.001						
-0.877	-0.007	1.001	-0.017	-0.001						
-0.877	0.027	0.999	-0.015	0.001						
-0.877	0.061	0.999	-0.011	0.001						

HRA Fine Foil Experimental Data at AOA=-1.7 deg

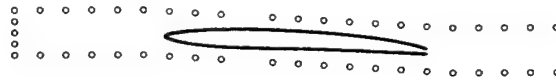
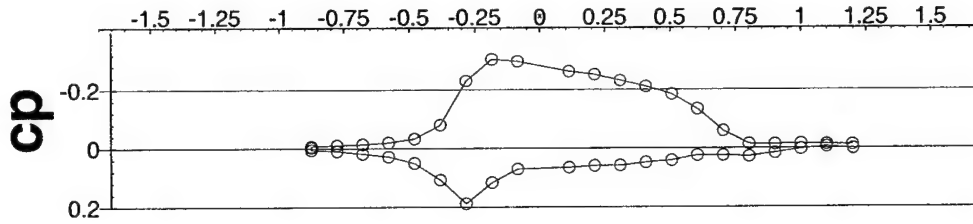
Appendix C

HRA Blunt Trailing Edge Foil Experimental Data



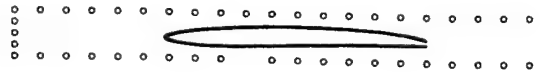
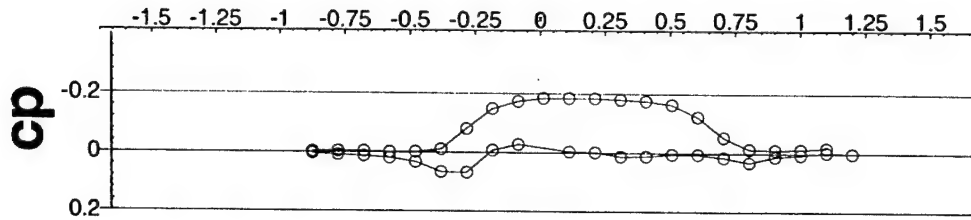
X/C	Y/C	X/C	Y/C	X/C	Y/C
0.7000	0.0001	-0.1250	0.0257	-0.1000	-0.0380
0.6950	0.0014	-0.1500	0.0231	-0.0500	-0.0378
0.6900	0.0026	-0.1750	0.0203	0.0000	-0.0368
0.6850	0.0038	-0.2000	0.0170	0.0500	-0.0352
0.6750	0.0061	-0.2250	0.0132	0.1000	-0.0334
0.6650	0.0083	-0.2500	0.0086	0.1500	-0.0314
0.6500	0.0114	-0.2650	0.0053	0.2000	-0.0295
0.6250	0.0160	-0.2750	0.0027	0.2500	-0.0278
0.6000	0.0198	-0.2850	-0.0004	0.3000	-0.0263
0.5750	0.0230	-0.2900	-0.0023	0.3500	-0.0250
0.5500	0.0258	-0.2950	-0.0047	0.4000	-0.0240
0.5250	0.0281	-0.2975	-0.0063	0.4250	-0.0236
0.5000	0.0301	-0.2990	-0.0076	0.4500	-0.0232
0.4750	0.0319	-0.3000	-0.0099	0.4750	-0.0229
0.4500	0.0335	-0.2990	-0.0121	0.5000	-0.0226
0.4250	0.0348	-0.2975	-0.0134	0.5250	-0.0223
0.4000	0.0360	-0.2950	-0.0149	0.5500	-0.0221
0.3500	0.0378	-0.2900	-0.0172	0.5750	-0.0218
0.3000	0.0389	-0.2850	-0.0189	0.6000	-0.0215
0.2500	0.0396	-0.2750	-0.0217	0.6250	-0.0212
0.2000	0.0397	-0.2650	-0.0240	0.6500	-0.0208
0.1500	0.0393	-0.2500	-0.0268	0.6650	-0.0205
0.1000	0.0383	-0.2250	-0.0305	0.6750	-0.0203
0.0500	0.0367	-0.2000	-0.0332	0.6850	-0.0201
0.0000	0.0345	-0.1750	-0.0353	0.6900	-0.0200
-0.0500	0.0316	-0.1500	-0.0367	0.6950	-0.0200
-0.1000	0.0279	-0.1250	-0.0376	0.7000	-0.0199

HRA Blunt Foil Geometry at AOA=0.0



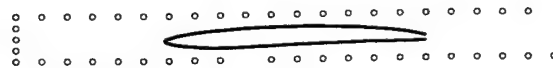
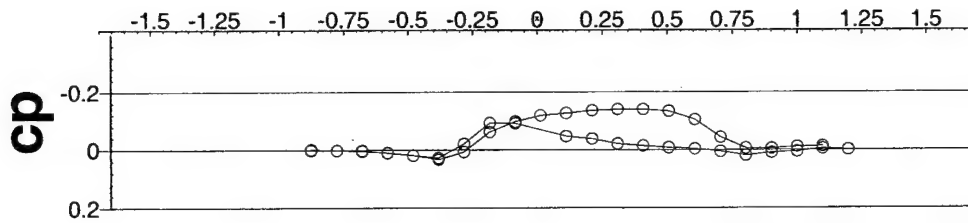
Chord = 405mm			Uinf= 5.13 m/sec		AOA= 3.6 degrees					
X/C	Y/C	U/Uinf	V/Uinf	Cp		X/C	Y/C	U/Uinf	V/Uinf	Cp
1.198	-0.138	0.998	-0.051	0.001		-0.877	0.025	1.002	0.037	-0.003
1.099	-0.138	1.004	-0.051	-0.005		-0.877	0.068	1.004	0.039	-0.005
1.000	-0.138	0.996	-0.053	0.003		-0.877	0.111	1.006	0.039	-0.007
0.901	-0.138	0.982	-0.057	0.016		-0.778	0.111	1.010	0.053	-0.011
0.802	-0.138	0.971	-0.049	0.028		-0.679	0.111	1.012	0.068	-0.014
0.704	-0.132	0.975	-0.039	0.024		-0.580	0.111	1.016	0.090	-0.020
0.605	-0.125	0.975	-0.051	0.024		-0.481	0.111	1.025	0.123	-0.033
0.506	-0.119	0.957	-0.053	0.041		-0.383	0.111	1.060	0.189	-0.080
0.407	-0.113	0.949	-0.053	0.048		-0.284	0.105	1.189	0.218	-0.231
0.309	-0.106	0.940	-0.047	0.058		-0.185	0.098	1.265	0.111	-0.306
0.210	-0.100	0.938	-0.045	0.059		-0.086	0.092	1.263	0.055	-0.299
0.111	-0.094	0.932	-0.039	0.065		0.111	0.079	1.236	-0.037	-0.264
-0.086	-0.081	0.924	-0.078	0.070		0.210	0.073	1.226	-0.051	-0.253
-0.185	-0.075	0.873	-0.078	0.116		0.309	0.067	1.207	-0.090	-0.232
-0.284	-0.068	0.789	0.006	0.188		0.407	0.060	1.187	-0.115	-0.211
-0.383	-0.062	0.879	0.117	0.107		0.506	0.054	1.162	-0.142	-0.185
-0.481	-0.062	0.943	0.097	0.050		0.605	0.048	1.113	-0.172	-0.134
-0.580	-0.062	0.969	0.074	0.028		0.704	0.041	1.045	-0.164	-0.059
-0.679	-0.062	0.981	0.055	0.018		0.802	0.035	1.008	-0.111	-0.014
-0.778	-0.062	0.990	0.041	0.009		0.901	0.035	1.010	-0.074	-0.013
-0.877	-0.062	0.994	0.031	0.005		1.000	0.035	1.014	-0.055	-0.015
-0.877	-0.019	0.994	0.035	0.005		1.099	0.035	1.012	-0.045	-0.013
-0.877	0.025	1.002	0.037	-0.003		1.198	0.035	1.012	-0.037	-0.012

HRA Blunt Foil Experimental Data at AOA=3.6 deg



Chord = 405mm			Uinf= 5.11 m/sec			AOA= 0.9 degrees				
X/C	Y/C	U/Uinf	V/Uinf	Cp		X/C	Y/C	U/Uinf	V/Uinf	Cp
1.198	-0.100	0.998	-0.041	0.001		-0.877	0.050	1.000	0.010	0.000
1.099	-0.100	1.002	-0.041	-0.003		-0.877	0.093	1.004	0.012	-0.004
1.000	-0.100	0.994	-0.039	0.005		-0.778	0.093	1.004	0.016	-0.004
0.901	-0.100	0.988	-0.039	0.011		-0.679	0.093	1.004	0.025	-0.004
0.802	-0.100	0.969	-0.022	0.031		-0.580	0.093	1.000	0.039	-0.001
0.704	-0.098	0.986	-0.008	0.014		-0.481	0.093	1.000	0.061	-0.002
0.605	-0.096	0.996	-0.022	0.004		-0.383	0.093	1.006	0.104	-0.011
0.506	-0.095	0.996	-0.022	0.004		-0.284	0.091	1.067	0.155	-0.081
0.407	-0.093	0.988	-0.022	0.011		-0.185	0.089	1.133	0.117	-0.149
0.309	-0.092	0.988	-0.012	0.012		-0.086	0.088	1.159	0.082	-0.174
0.210	-0.090	1.002	-0.023	-0.002		0.012	0.086	1.170	0.016	-0.185
0.111	-0.088	1.004	-0.002	-0.004		0.111	0.085	1.170	0.004	-0.185
-0.086	-0.085	1.025	-0.063	-0.028		0.210	0.083	1.170	-0.016	-0.185
-0.185	-0.083	1.004	-0.090	-0.008		0.309	0.081	1.166	-0.049	-0.181
-0.284	-0.082	0.926	-0.080	0.068		0.407	0.080	1.160	-0.076	-0.176
-0.383	-0.080	0.932	0.006	0.066		0.506	0.078	1.147	-0.114	-0.164
-0.481	-0.080	0.967	0.022	0.032		0.605	0.076	1.108	-0.141	-0.123
-0.580	-0.080	0.980	0.016	0.019		0.704	0.075	1.043	-0.141	-0.054
-0.679	-0.080	0.988	0.010	0.012		0.802	0.073	1.010	-0.094	-0.014
-0.778	-0.080	0.992	0.010	0.008		0.901	0.073	1.010	-0.061	-0.012
-0.877	-0.080	0.996	0.004	0.004		1.000	0.073	1.012	-0.045	-0.013
-0.877	-0.037	0.998	0.008	0.002		1.099	0.073	1.018	-0.037	-0.018
-0.877	0.006	1.002	0.008	-0.002						

HRA Blunt Foil Experimental Data at AOA=0.9



Chord = 405mm			Uinf= 5.13 m/sec		AOA= -0.9 degrees						
X/C	Y/C	U/Uinf	V/Uinf	Cp		X/C	Y/C	U/Uinf	V/Uinf	Cp	
1.198	-0.074	1.000	-0.021	-0.001		-0.877	0.037	1.000	-0.004	0.000	
1.099	-0.074	1.004	-0.023	-0.005		-0.877	0.081	1.002	-0.002	-0.002	
1.000	-0.074	0.995	-0.020	0.005		-0.778	0.081	0.998	0.000	0.002	
0.901	-0.074	0.991	-0.018	0.009		-0.679	0.081	0.998	0.000	0.002	
0.802	-0.074	0.981	0.000	0.019		-0.580	0.081	0.989	0.004	0.011	
0.704	-0.076	0.995	0.031	0.005		-0.481	0.081	0.981	0.016	0.019	
0.605	-0.077	1.004	0.018	-0.004		-0.383	0.081	0.965	0.045	0.033	
0.506	-0.079	1.008	0.016	-0.008		-0.284	0.082	0.987	0.113	0.007	
0.407	-0.080	1.014	0.021	-0.014		-0.185	0.084	1.053	0.123	-0.062	
0.309	-0.082	1.020	0.029	-0.021		-0.086	0.085	1.088	0.105	-0.098	
0.210	-0.083	1.037	0.008	-0.038		0.012	0.087	1.112	0.045	-0.119	
0.111	-0.085	1.045	0.033	-0.047		0.111	0.088	1.119	0.037	-0.127	
-0.086	-0.088	1.088	-0.029	-0.092		0.210	0.090	1.127	0.023	-0.136	
-0.185	-0.089	1.086	-0.080	-0.093		0.309	0.091	1.131	-0.010	-0.140	
-0.284	-0.091	1.014	-0.117	-0.021		0.407	0.093	1.131	-0.037	-0.140	
-0.383	-0.092	0.971	-0.053	0.027		0.506	0.094	1.123	-0.076	-0.134	
-0.481	-0.092	0.981	-0.023	0.019		0.605	0.095	1.094	-0.117	-0.105	
-0.580	-0.092	0.991	-0.012	0.009		0.704	0.097	1.035	-0.125	-0.044	
-0.679	-0.092	0.995	-0.012	0.005		0.802	0.098	1.002	-0.080	-0.006	
-0.778	-0.092	0.998	-0.012	0.001		0.901	0.098	1.004	-0.049	-0.005	
-0.877	-0.092	0.998	-0.010	0.002		1.000	0.098	1.010	-0.035	-0.011	
-0.877	-0.049	0.998	-0.002	0.002		1.099	0.098	1.012	-0.029	-0.013	
-0.877	-0.006	1.000	-0.004	0.000							

HRA Blunt Foil Experimental Data at AOA=-0.9

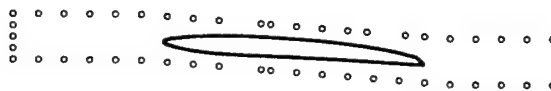
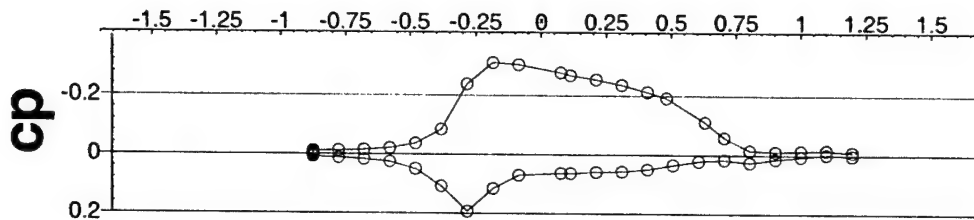
Appendix D

HRA Beveled Trailing Edge Foil Experimental Data



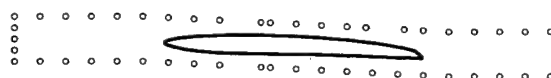
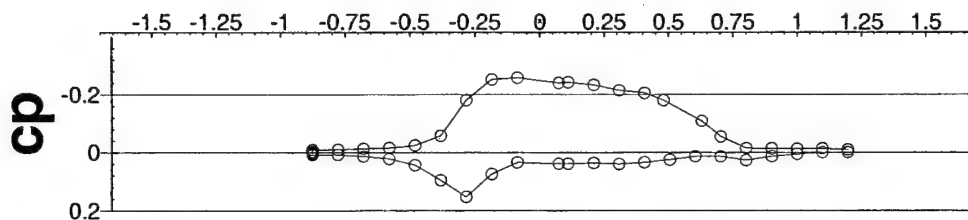
X/C	Y/C	X/C	Y/C	X/C	Y/C
0.7000	-0.0075	-0.1253	0.0270	-0.0498	-0.0359
0.6950	-0.0033	-0.1503	0.0243	0.0002	-0.0345
0.6899	0.0009	-0.1752	0.0212	0.0502	-0.0325
0.6849	0.0051	-0.2002	0.0178	0.1002	-0.0303
0.6748	0.0136	-0.2252	0.0138	0.1502	-0.0280
0.6748	0.0136	-0.2501	0.0090	0.2001	-0.0257
0.6648	0.0157	-0.2651	0.0056	0.2501	-0.0236
0.6498	0.0187	-0.2751	0.0029	0.3001	-0.0217
0.6248	0.0231	-0.2851	-0.0003	0.3501	-0.0200
0.5997	0.0267	-0.2901	-0.0022	0.4001	-0.0186
0.5747	0.0298	-0.2950	-0.0046	0.4251	-0.0180
0.5497	0.0323	-0.2975	-0.0063	0.4501	-0.0175
0.5247	0.0344	-0.2990	-0.0076	0.4751	-0.0169
0.4997	0.0363	-0.3000	-0.0099	0.5001	-0.0164
0.4747	0.0379	-0.2990	-0.0121	0.5251	-0.0160
0.4496	0.0392	-0.2975	-0.0134	0.5501	-0.0155
0.4246	0.0404	-0.2950	-0.0149	0.5751	-0.0151
0.3996	0.0414	-0.2899	-0.0171	0.6001	-0.0146
0.3496	0.0428	-0.2849	-0.0188	0.6251	-0.0141
0.2996	0.0436	-0.2749	-0.0215	0.6501	-0.0135
0.2496	0.0438	-0.2649	-0.0237	0.6651	-0.0131
0.1996	0.0435	-0.2499	-0.0264	0.6751	-0.0128
0.1496	0.0427	-0.2248	-0.0299	0.6851	-0.0126
0.0996	0.0414	-0.1998	-0.0325	0.6900	-0.0124
0.0496	0.0394	-0.1748	-0.0343	0.6950	-0.0123
-0.0003	0.0368	-0.1498	-0.0356	0.7000	-0.0122
-0.0503	0.0336	-0.1248	-0.0363		
-0.1003	0.0294	-0.0998	-0.0365		

HRA Bevel Foil Geometry at AOA=0.0



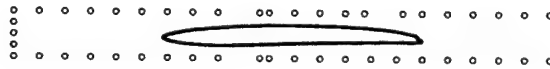
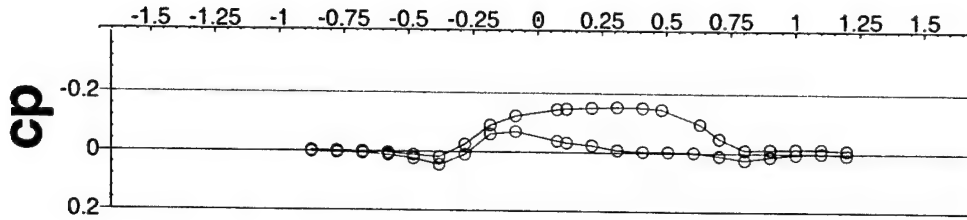
Chord = 405mm			Uinf= 5.094 m/sec		AOA= 4.4 degrees				
X/C	Y/C	U/Uinf	V/Uinf	Cp	X/C	Y/C	U/Uinf	V/Uinf	Cp
1.198	-0.142	0.997	-0.039	0.002	-0.877	0.027	0.999	0.035	0.000
1.099	-0.142	1.001	-0.047	-0.002	-0.877	0.070	1.005	0.033	-0.006
1.000	-0.142	0.993	-0.049	0.005	-0.877	0.113	1.011	0.035	-0.012
0.901	-0.142	0.985	-0.049	0.013	-0.778	0.113	1.011	0.047	-0.012
0.802	-0.142	0.974	-0.043	0.025	-0.679	0.113	1.013	0.065	-0.015
0.704	-0.135	0.984	-0.035	0.016	-0.580	0.113	1.017	0.088	-0.021
0.605	-0.128	0.978	-0.053	0.021	-0.481	0.113	1.029	0.124	-0.037
0.506	-0.122	0.964	-0.057	0.034	-0.383	0.113	1.066	0.183	-0.085
0.407	-0.115	0.948	-0.057	0.049	-0.284	0.106	1.197	0.206	-0.238
0.309	-0.108	0.940	-0.049	0.057	-0.185	0.099	1.270	0.100	-0.312
0.210	-0.101	0.938	-0.047	0.059	-0.086	0.092	1.268	0.043	-0.305
0.111	-0.094	0.934	-0.041	0.063	0.074	0.081	1.247	-0.049	-0.278
0.074	-0.092	0.934	-0.033	0.063	0.111	0.079	1.239	-0.051	-0.269
-0.086	-0.080	0.925	-0.079	0.069	0.210	0.072	1.227	-0.063	-0.255
-0.185	-0.074	0.874	-0.082	0.115	0.309	0.065	1.209	-0.102	-0.236
-0.284	-0.067	0.783	0.004	0.193	0.407	0.058	1.188	-0.124	-0.213
-0.383	-0.060	0.878	0.122	0.108	0.481	0.053	1.168	-0.145	-0.193
-0.481	-0.060	0.944	0.098	0.049	0.630	0.043	1.091	-0.179	-0.112
-0.580	-0.060	0.972	0.073	0.025	0.704	0.038	1.044	-0.165	-0.059
-0.679	-0.060	0.982	0.057	0.017	0.802	0.031	1.009	-0.116	-0.016
-0.778	-0.060	0.987	0.043	0.012	0.901	0.031	1.009	-0.077	-0.012
-0.877	-0.060	0.991	0.033	0.008	1.000	0.031	1.013	-0.057	-0.015
-0.877	-0.017	0.993	0.035	0.006	1.099	0.031	1.015	-0.045	-0.016
-0.877	0.027	0.999	0.035	0.000	1.198	0.031	1.009	-0.037	-0.010

HRA Beveled Foil Experimental Data at AOA=4.4 deg



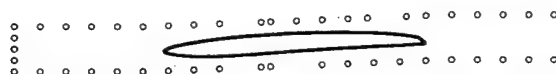
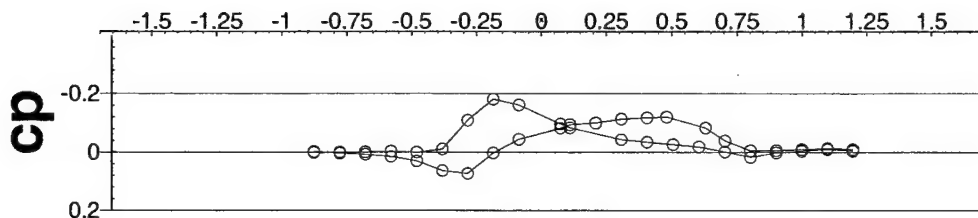
Chord = 405mm			Uinf= 5.112 m/sec		AOA= 3.35 degrees					
X/C	Y/C	U/Uinf	V/Uinf	Cp	X/C	Y/C	U/Uinf	V/Uinf	Cp	
1.198	-0.128	1.000	-0.043	-0.001	-0.877	0.020	1.000	0.027	0.000	
1.099	-0.128	1.000	-0.047	-0.001	-0.877	0.063	1.004	0.027	-0.004	
1.000	-0.128	0.994	-0.047	0.005	-0.877	0.106	1.009	0.029	-0.010	
0.901	-0.128	0.986	-0.047	0.013	-0.778	0.106	1.009	0.039	-0.010	
0.802	-0.128	0.972	-0.039	0.027	-0.679	0.106	1.011	0.055	-0.013	
0.704	-0.122	0.986	-0.031	0.013	-0.580	0.106	1.013	0.072	-0.016	
0.605	-0.117	0.986	-0.043	0.013	-0.481	0.106	1.019	0.102	-0.025	
0.506	-0.112	0.974	-0.045	0.024	-0.383	0.106	1.045	0.156	-0.058	
0.407	-0.107	0.964	-0.043	0.034	-0.284	0.101	1.152	0.186	-0.181	
0.309	-0.102	0.959	-0.037	0.040	-0.185	0.096	1.223	0.104	-0.253	
0.210	-0.097	0.962	-0.037	0.036	-0.086	0.091	1.230	0.057	-0.259	
0.111	-0.092	0.960	-0.027	0.038	0.074	0.083	1.217	-0.029	-0.241	
0.074	-0.090	0.960	-0.023	0.038	0.111	0.081	1.219	-0.029	-0.243	
-0.086	-0.082	0.962	-0.072	0.034	0.210	0.076	1.211	-0.045	-0.234	
-0.185	-0.077	0.919	-0.082	0.074	0.309	0.071	1.193	-0.080	-0.215	
-0.284	-0.072	0.833	-0.023	0.153	0.407	0.066	1.183	-0.104	-0.206	
-0.383	-0.067	0.896	0.084	0.095	0.481	0.062	1.160	-0.125	-0.181	
-0.481	-0.067	0.953	0.072	0.044	0.630	0.054	1.092	-0.164	-0.109	
-0.580	-0.067	0.976	0.055	0.022	0.704	0.050	1.043	-0.153	-0.055	
-0.679	-0.067	0.986	0.043	0.013	0.802	0.045	1.009	-0.106	-0.015	
-0.778	-0.067	0.992	0.031	0.008	0.901	0.045	1.011	-0.068	-0.014	
-0.877	-0.067	0.992	0.025	0.008	1.000	0.045	1.011	-0.051	-0.013	
-0.877	-0.024	0.996	0.029	0.004	1.099	0.045	1.013	-0.041	-0.014	
-0.877	0.020	1.000	0.027	0.000	1.198	0.045	1.009	-0.033	-0.010	

HRA Beveled Foil Experimental Data at AOA=3.35 deg



Chord = 405mm			Uinf= 5.08 m/sec		AOA= 0.4 degrees					
X/C	Y/C	U/Uinf	V/Uinf	Cp		X/C	Y/C	U/Uinf	V/Uinf	Cp
1.198	-0.085	0.994	-0.026	0.006		-0.877	-0.001	1.000	0.002	0.000
1.099	-0.085	1.000	-0.024	0.000		-0.877	0.043	1.000	0.004	0.000
1.000	-0.085	0.996	-0.026	0.004		-0.877	0.086	1.004	0.008	-0.004
0.901	-0.085	0.988	-0.024	0.011		-0.778	0.086	1.002	0.010	-0.002
0.802	-0.085	0.976	-0.006	0.023		-0.679	0.086	1.000	0.014	0.000
0.704	-0.085	0.990	0.016	0.010		-0.580	0.086	0.996	0.022	0.004
0.605	-0.086	1.002	0.010	-0.002		-0.481	0.086	0.988	0.035	0.011
0.506	-0.086	1.004	0.010	-0.004		-0.383	0.086	0.980	0.063	0.018
0.407	-0.086	1.004	0.014	-0.004		-0.284	0.086	1.018	0.124	-0.026
0.309	-0.086	1.008	0.022	-0.008		-0.185	0.086	1.081	0.116	-0.091
0.210	-0.086	1.024	0.006	-0.024		-0.086	0.086	1.112	0.094	-0.123
0.111	-0.086	1.031	0.026	-0.032		0.074	0.087	1.136	0.030	-0.145
0.074	-0.086	1.037	0.033	-0.039		0.111	0.087	1.138	0.028	-0.148
-0.086	-0.087	1.067	-0.026	-0.069		0.210	0.087	1.142	0.008	-0.152
-0.185	-0.087	1.057	-0.063	-0.061		0.309	0.087	1.144	-0.018	-0.154
-0.284	-0.087	0.986	-0.091	0.010		0.407	0.087	1.142	-0.043	-0.153
-0.383	-0.087	0.955	-0.022	0.044		0.481	0.087	1.136	-0.067	-0.147
-0.481	-0.087	0.976	-0.002	0.023		0.630	0.087	1.087	-0.120	-0.098
-0.580	-0.087	0.988	0.006	0.012		0.704	0.087	1.041	-0.116	-0.049
-0.679	-0.087	0.994	0.006	0.006		0.802	0.088	1.008	-0.071	-0.010
-0.778	-0.087	0.996	-0.002	0.004		0.901	0.088	1.012	-0.041	-0.013
-0.877	-0.087	0.998	-0.002	0.002		1.000	0.088	1.014	-0.026	-0.014
-0.877	-0.044	0.998	0.000	0.002		1.099	0.088	1.014	-0.020	-0.014
-0.877	-0.001	1.000	0.002	0.000		1.198	0.088	1.010	-0.014	-0.010

HRA Beveled Foil Experimental Data at AOA=0.4 deg

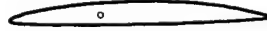


Chord = 405mm			Uinf= 5.208 m/sec			AOA= -1.9 degrees				
X/C	Y/C	U/Uinf	V/Uinf	Cp		X/C	Y/C	U/Uinf	V/Uinf	Cp
1.198	-0.053	1.004	-0.021	-0.004		-0.877	0.027	0.998	-0.010	0.001
1.099	-0.053	1.010	-0.019	-0.010		-0.877	0.071	0.998	-0.008	0.002
1.000	-0.053	1.004	-0.015	-0.004		-0.778	0.071	0.997	-0.008	0.003
0.901	-0.053	0.998	-0.015	0.001		-0.679	0.071	0.993	-0.013	0.007
0.802	-0.053	0.983	0.012	0.017		-0.580	0.071	0.985	-0.017	0.015
0.704	-0.057	1.000	0.044	-0.001		-0.481	0.071	0.970	-0.013	0.030
0.605	-0.061	1.018	0.042	-0.019		-0.383	0.071	0.935	-0.002	0.063
0.506	-0.065	1.025	0.044	-0.027		-0.284	0.075	0.922	0.079	0.072
0.407	-0.070	1.033	0.050	-0.035		-0.185	0.079	0.991	0.119	0.002
0.309	-0.074	1.041	0.060	-0.043		-0.086	0.083	1.037	0.119	-0.045
0.111	-0.082	1.079	0.063	-0.084		0.074	0.089	1.077	0.067	-0.082
0.074	-0.083	1.091	0.069	-0.097		0.111	0.091	1.089	0.065	-0.095
-0.086	-0.090	1.150	0.000	-0.161		0.210	0.095	1.094	0.048	-0.100
-0.185	-0.094	1.166	-0.061	-0.181		0.309	0.099	1.108	0.025	-0.114
-0.284	-0.098	1.094	-0.148	-0.110		0.407	0.103	1.112	-0.002	-0.118
-0.383	-0.102	1.006	-0.098	-0.011		0.481	0.106	1.114	-0.027	-0.120
-0.481	-0.102	0.998	-0.054	0.000		0.630	0.113	1.077	-0.084	-0.084
-0.580	-0.102	1.002	-0.040	-0.003		0.704	0.116	1.035	-0.086	-0.039
-0.679	-0.102	1.000	-0.027	-0.001		0.802	0.120	1.004	-0.050	-0.005
-0.778	-0.102	1.000	-0.017	-0.001		0.901	0.120	1.006	-0.023	-0.006
-0.877	-0.102	1.002	-0.019	-0.002		1.000	0.120	1.010	-0.013	-0.010
-0.877	-0.059	1.000	-0.015	-0.001		1.099	0.120	1.014	-0.006	-0.014
-0.877	-0.016	1.000	-0.012	0.000		1.198	0.120	1.010	-0.004	-0.010
-0.877	0.027	0.998	-0.010	0.001						

HRA Beveled Foil Experimental Data at AOA=-1.9 deg

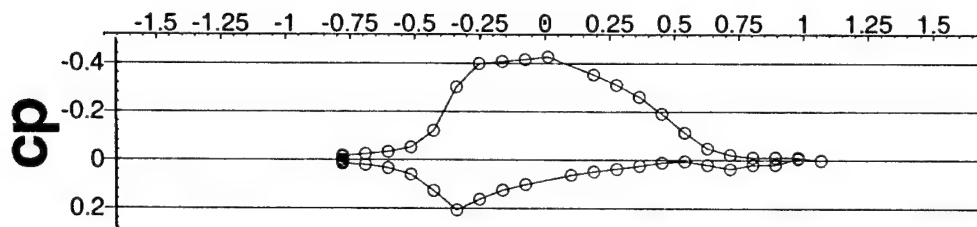
Appendix E

B1 Blunt Trailing Edge Foil Experimental Data



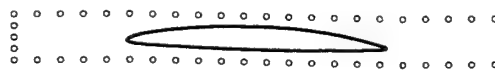
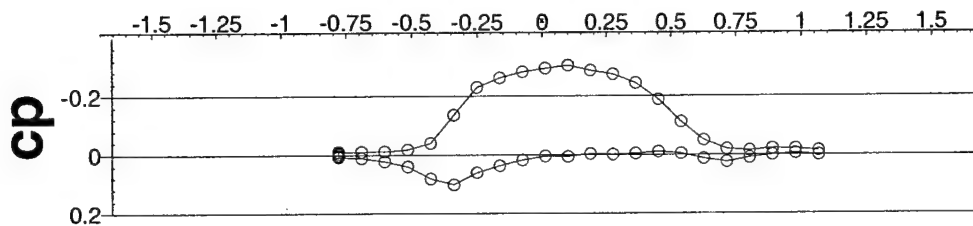
X/C	Y/C	X/C	Y/C	X/C	Y/C	X/C	Y/C
0.6499	-0.0212	-0.1046	-0.0364	-0.3233	-0.0002	0.4293	0.0332
0.6361	-0.0228	-0.1374	-0.0357	-0.3130	0.0032	0.4511	0.0299
0.6224	-0.0241	-0.1681	-0.0350	-0.3006	0.0068	0.4715	0.0265
0.6086	-0.0253	-0.1963	-0.0343	-0.2859	0.0105	0.4905	0.0231
0.5948	-0.0263	-0.2215	-0.0336	-0.2688	0.0143	0.5080	0.0198
0.5810	-0.0273	-0.2432	-0.0328	-0.2490	0.0182	0.5237	0.0166
0.5672	-0.0281	-0.2612	-0.0321	-0.2266	0.0221	0.5376	0.0137
0.5534	-0.0288	-0.2762	-0.0314	-0.2016	0.0260	0.5499	0.0111
0.5374	-0.0296	-0.2884	-0.0307	-0.1744	0.0298	0.5568	0.0095
0.5060	-0.0309	-0.2984	-0.0301	-0.1453	0.0335	0.5706	0.0063
0.4745	-0.0320	-0.3066	-0.0294	-0.1147	0.0369	0.5844	0.0030
0.4436	-0.0329	-0.3136	-0.0287	-0.0829	0.0400	0.5982	-0.0004
0.4140	-0.0338	-0.3197	-0.0281	-0.0502	0.0428	0.6120	-0.0040
0.3853	-0.0346	-0.3252	-0.0275	-0.0168	0.0451	0.6258	-0.0076
0.3571	-0.0353	-0.3303	-0.0268	0.0169	0.0470	0.6396	-0.0112
0.3292	-0.0360	-0.3348	-0.0260	0.0507	0.0484	0.6499	-0.0140
0.3010	-0.0365	-0.3387	-0.0252	0.0844	0.0495		
0.2721	-0.0370	-0.3422	-0.0242	0.1179	0.0501		
0.2421	-0.0374	-0.3450	-0.0231	0.1509	0.0503		
0.2107	-0.0378	-0.3473	-0.0218	0.1832	0.0501		
0.1778	-0.0380	-0.3490	-0.0203	0.2147	0.0496		
0.1437	-0.0382	-0.3499	-0.0185	0.2451	0.0487		
0.1088	-0.0382	-0.3499	-0.0165	0.2745	0.0475		
0.0731	-0.0382	-0.3489	-0.0144	0.3030	0.0459		
0.0372	-0.0381	-0.3468	-0.0120	0.3304	0.0440		
0.0011	-0.0378	-0.3433	-0.0093	0.3567	0.0418		
-0.0349	-0.0374	-0.3383	-0.0065	0.3820	0.0392		
-0.0703	-0.0369	-0.3317	-0.0034	0.4062	0.0363		

B1 Blunt Foil Geometry at AOA=0.0



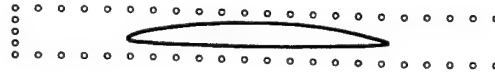
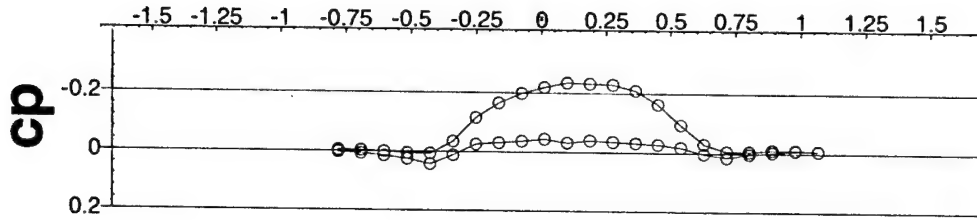
Chord = 455 mm			Uinf= 5.114 m/sec			AOA= 5.2 degrees					
X/C	Y/C	U/Uinf	V/Uinf	Cp		X/C	Y/C	U/Uinf	V/Uinf	Cp	
1.066	-0.136	0.997	-0.043	0.002		-0.780	0.111	1.015	0.065	-0.017	
0.978	-0.136	1.005	-0.045	-0.006		-0.692	0.111	1.021	0.084	-0.024	
0.890	-0.136	0.980	-0.055	0.019		-0.604	0.111	1.027	0.113	-0.033	
0.802	-0.136	0.980	-0.049	0.019		-0.516	0.111	1.038	0.162	-0.052	
0.714	-0.136	0.962	-0.037	0.037		-0.429	0.111	1.089	0.233	-0.120	
0.626	-0.131	0.980	-0.027	0.020		-0.341	0.111	1.240	0.258	-0.302	
0.538	-0.125	0.993	-0.049	0.005		-0.253	0.105	1.332	0.158	-0.399	
0.451	-0.119	0.987	-0.059	0.011		-0.165	0.099	1.345	0.078	-0.408	
0.363	-0.113	0.974	-0.063	0.024		-0.077	0.093	1.353	0.029	-0.416	
0.275	-0.107	0.960	-0.070	0.037		0.011	0.087	1.361	-0.051	-0.427	
0.187	-0.101	0.948	-0.072	0.048		0.187	0.075	1.302	-0.108	-0.354	
0.099	-0.095	0.933	-0.078	0.062		0.275	0.069	1.263	-0.160	-0.311	
-0.077	-0.083	0.888	-0.096	0.101		0.363	0.063	1.218	-0.196	-0.261	
-0.165	-0.077	0.862	-0.078	0.125		0.451	0.057	1.156	-0.215	-0.191	
-0.253	-0.071	0.819	-0.057	0.163		0.538	0.051	1.087	-0.209	-0.113	
-0.341	-0.065	0.765	0.041	0.207		0.626	0.045	1.032	-0.174	-0.048	
-0.429	-0.065	0.853	0.137	0.127		0.714	0.039	1.013	-0.131	-0.022	
-0.516	-0.065	0.931	0.117	0.060		0.802	0.039	1.007	-0.092	-0.011	
-0.604	-0.065	0.962	0.092	0.033		0.890	0.039	1.009	-0.070	-0.012	
-0.692	-0.065	0.978	0.065	0.020		0.978	0.039	1.009	-0.061	-0.011	
-0.780	-0.065	0.984	0.055	0.015		1.066	0.039	0.997	-0.049	0.002	
-0.780	-0.021	0.991	0.061	0.007							
-0.780	0.023	0.999	0.065	-0.001							
-0.780	0.067	1.011	0.061	-0.013							

B1 Blunt Foil Experimental Data at AOA=5.2 deg



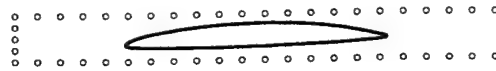
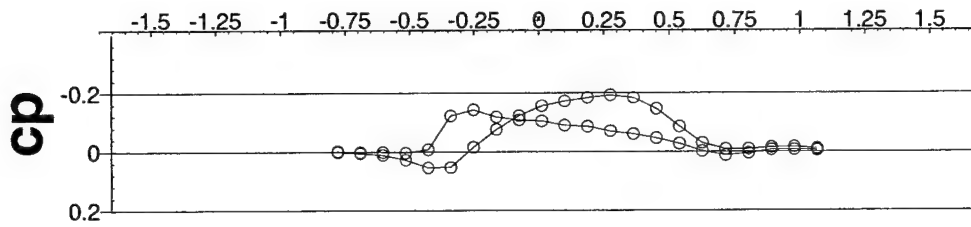
Chord = 455 mm			Uinf= 5.26 m/sec			AOA= 2.25 degrees				
X/C	Y/C	U/Uinf	V/Uinf	Cp		X/C	Y/C	U/Uinf	V/Uinf	Cp
1.066	-0.108	0.998	-0.051	0.001		-0.780	0.053	1.004	0.032	-0.004
0.978	-0.108	1.004	-0.053	-0.005		-0.780	0.097	1.010	0.036	-0.010
0.890	-0.108	0.998	-0.053	0.000		-0.692	0.097	1.010	0.048	-0.011
0.802	-0.108	0.989	-0.048	0.010		-0.604	0.097	1.010	0.065	-0.012
0.714	-0.108	0.975	-0.032	0.024		-0.516	0.097	1.013	0.097	-0.018
0.626	-0.105	0.987	-0.008	0.013		-0.429	0.097	1.029	0.148	-0.040
0.538	-0.103	1.004	-0.017	-0.004		-0.341	0.097	1.110	0.196	-0.136
0.451	-0.101	1.010	-0.023	-0.010		-0.253	0.095	1.198	0.158	-0.230
0.363	-0.098	1.004	-0.032	-0.004		-0.165	0.093	1.230	0.105	-0.262
0.275	-0.096	1.000	-0.040	-0.001		-0.077	0.090	1.249	0.068	-0.282
0.187	-0.093	1.002	-0.046	-0.003		0.011	0.088	1.260	0.002	-0.294
0.099	-0.091	0.992	-0.051	0.006		0.099	0.085	1.268	-0.021	-0.304
0.011	-0.088	0.994	-0.048	0.005		0.187	0.083	1.253	-0.061	-0.287
-0.077	-0.086	0.979	-0.074	0.018		0.275	0.080	1.240	-0.105	-0.274
-0.165	-0.083	0.960	-0.070	0.037		0.363	0.078	1.211	-0.148	-0.244
-0.253	-0.081	0.935	-0.070	0.060		0.451	0.075	1.160	-0.177	-0.188
-0.341	-0.078	0.892	-0.046	0.101		0.538	0.073	1.091	-0.181	-0.112
-0.429	-0.078	0.914	0.034	0.081		0.626	0.070	1.038	-0.148	-0.050
-0.516	-0.078	0.958	0.044	0.040		0.714	0.068	1.013	-0.106	-0.019
-0.604	-0.078	0.977	0.036	0.022		0.802	0.068	1.011	-0.074	-0.014
-0.692	-0.078	0.989	0.029	0.011		0.890	0.068	1.019	-0.053	-0.021
-0.780	-0.078	0.992	0.017	0.007		0.978	0.068	1.019	-0.046	-0.020
-0.780	-0.034	0.996	0.025	0.003		1.066	0.068	1.013	-0.040	-0.014
-0.780	0.010	0.998	0.034	0.001						

B1 Blunt Foil Experimental Data at AOA=2.25 deg



Chord = 455 mm					Uinf= 5.178 m/sec	AOA= 0.4 degrees				
X/C	Y/C	U/Uinf	V/Uinf	Cp		X/C	Y/C	U/Uinf	V/Uinf	Cp
1.066	-0.101	1.006	-0.041	-0.007		-0.780	0.050	1.000	0.012	0.000
0.978	-0.101	1.008	-0.037	-0.009		-0.780	0.094	1.004	0.017	-0.004
0.890	-0.101	1.002	-0.035	-0.003		-0.692	0.094	1.002	0.021	-0.003
0.802	-0.101	0.997	-0.027	0.003		-0.604	0.094	0.998	0.031	0.001
0.714	-0.101	0.985	-0.012	0.015		-0.516	0.094	0.993	0.048	0.006
0.626	-0.099	0.997	0.012	0.003		-0.429	0.094	0.989	0.087	0.007
0.538	-0.098	1.018	0.014	-0.018		-0.341	0.094	1.024	0.147	-0.035
0.451	-0.096	1.027	0.008	-0.028		-0.253	0.092	1.099	0.153	-0.115
0.363	-0.094	1.031	-0.002	-0.032		-0.165	0.091	1.147	0.126	-0.166
0.275	-0.093	1.035	-0.002	-0.036		-0.077	0.089	1.178	0.098	-0.199
0.187	-0.091	1.039	-0.014	-0.040		0.011	0.088	1.199	0.041	-0.220
0.099	-0.090	1.031	-0.015	-0.032		0.099	0.086	1.213	0.021	-0.236
0.011	-0.088	1.043	-0.017	-0.044		0.187	0.085	1.211	-0.015	-0.233
-0.077	-0.087	1.035	-0.042	-0.037		0.275	0.083	1.207	-0.060	-0.230
-0.165	-0.085	1.029	-0.042	-0.031		0.363	0.081	1.188	-0.100	-0.210
-0.253	-0.083	1.024	-0.056	-0.025		0.451	0.080	1.143	-0.145	-0.164
-0.341	-0.082	0.985	-0.079	0.012		0.538	0.078	1.080	-0.154	-0.095
-0.429	-0.082	0.956	-0.027	0.043		0.626	0.077	1.022	-0.129	-0.030
-0.516	-0.082	0.973	0.000	0.026		0.714	0.075	1.002	-0.081	-0.006
-0.604	-0.082	0.985	0.002	0.015		0.802	0.075	1.004	-0.050	-0.006
-0.692	-0.082	0.993	0.002	0.007		0.890	0.075	1.010	-0.037	-0.011
-0.780	-0.082	0.997	0.000	0.003		0.978	0.075	1.010	-0.029	-0.011
-0.780	-0.038	0.998	0.006	0.002		1.066	0.075	1.006	-0.025	-0.007
-0.780	0.006	1.000	0.012	0.000						

B1 Blunt Foil Experimental Data at AOA=0.4 deg

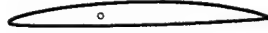


Chord = 455 mm			Uinf= 5.268 m/sec		AOA= -1.95 degrees					
X/C	Y/C	U/Uinf	V/Uinf	Cp		X/C	Y/C	U/Uinf	V/Uinf	Cp
1.066	-0.075	1.004	-0.023	-0.004		-0.780	0.038	0.998	-0.006	0.002
0.978	-0.075	1.006	-0.021	-0.006		-0.780	0.082	0.998	-0.002	0.002
0.890	-0.075	1.006	-0.013	-0.006		-0.692	0.082	0.995	-0.002	0.005
0.802	-0.075	0.995	-0.006	0.005		-0.604	0.082	0.989	-0.002	0.011
0.714	-0.075	0.987	0.013	0.013		-0.516	0.082	0.972	0.004	0.028
0.626	-0.077	1.000	0.051	-0.002		-0.429	0.082	0.943	0.028	0.055
0.538	-0.078	1.025	0.055	-0.027		-0.341	0.082	0.940	0.104	0.053
0.451	-0.080	1.044	0.049	-0.046		-0.253	0.083	1.004	0.150	-0.015
0.363	-0.081	1.057	0.049	-0.060		-0.165	0.085	1.063	0.148	-0.076
0.275	-0.083	1.067	0.042	-0.070		-0.077	0.087	1.109	0.129	-0.123
0.187	-0.085	1.082	0.028	-0.086		0.011	0.088	1.143	0.082	-0.156
0.099	-0.086	1.086	0.030	-0.090		0.099	0.090	1.158	0.063	-0.172
0.011	-0.088	1.099	0.032	-0.105		0.187	0.091	1.169	0.023	-0.184
-0.077	-0.089	1.103	-0.002	-0.108		0.275	0.093	1.177	-0.017	-0.193
-0.165	-0.091	1.112	-0.006	-0.119		0.363	0.094	1.167	-0.068	-0.184
-0.253	-0.093	1.133	-0.038	-0.143		0.451	0.096	1.131	-0.112	-0.146
-0.341	-0.094	1.109	-0.129	-0.123		0.538	0.098	1.074	-0.129	-0.086
-0.429	-0.094	1.002	-0.103	-0.008		0.626	0.099	1.023	-0.106	-0.029
-0.516	-0.094	0.995	-0.057	0.004		0.714	0.101	1.006	-0.063	-0.008
-0.604	-0.094	0.998	-0.032	0.001		0.802	0.101	1.008	-0.034	-0.009
-0.692	-0.094	0.998	-0.023	0.001		0.890	0.101	1.014	-0.025	-0.014
-0.780	-0.094	1.000	-0.017	-0.001		0.978	0.101	1.016	-0.017	-0.016
-0.780	-0.050	1.002	-0.015	-0.002		1.066	0.101	1.010	-0.015	-0.010
-0.780	-0.006	1.000	-0.008	0.000						

B1 Blunt Foil Experimental Data at AOA=-1.95 deg

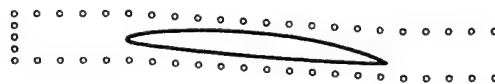
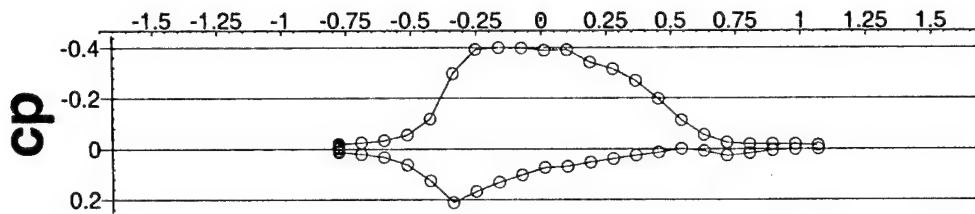
Appendix F

B1 Antisinging Trailing Edge Foil Experimental Data



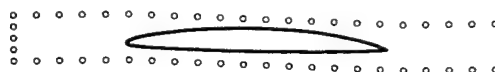
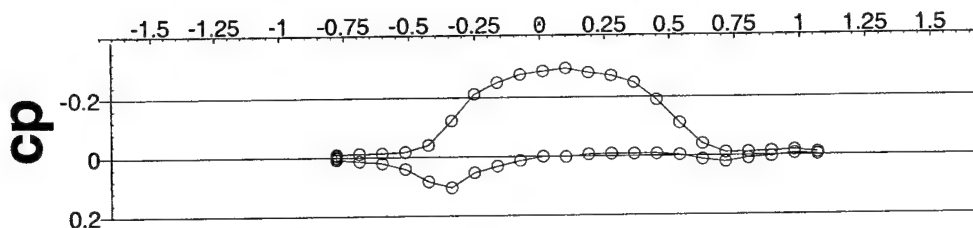
X/C	Y/C	X/C	Y/C	X/C	Y/C	X/C	Y/C
0.6500	-0.0193	0.2147	0.0500	-0.3490	-0.0216	0.1778	-0.0377
0.6435	-0.0164	0.1833	0.0505	-0.3473	-0.0231	0.2107	-0.0373
0.6367	-0.0135	0.1509	0.0505	-0.3450	-0.0244	0.2422	-0.0369
0.6297	-0.0107	0.1179	0.0502	-0.3422	-0.0256	0.2722	-0.0364
0.6226	-0.0079	0.0845	0.0495	-0.3387	-0.0265	0.3010	-0.0358
0.6153	-0.0053	0.0507	0.0484	-0.3348	-0.0273	0.3292	-0.0351
0.6080	-0.0028	0.0169	0.0468	-0.3303	-0.0281	0.3572	-0.0344
0.6007	-0.0004	-0.0168	0.0448	-0.3252	-0.0287	0.3853	-0.0336
0.5935	0.0018	-0.0501	0.0424	-0.3197	-0.0294	0.4140	-0.0327
0.5861	0.0039	-0.0829	0.0395	-0.3136	-0.0300	0.4437	-0.0317
0.5784	0.0060	-0.1147	0.0363	-0.3066	-0.0306	0.4745	-0.0307
0.5699	0.0081	-0.1453	0.0328	-0.2984	-0.0313	0.5060	-0.0295
0.5605	0.0103	-0.1744	0.0290	-0.2884	-0.0319	0.5375	-0.0281
0.5499	0.0126	-0.2016	0.0251	-0.2761	-0.0325	0.5682	-0.0264
0.5377	0.0152	-0.2265	0.0211	-0.2612	-0.0332	0.5977	-0.0245
0.5238	0.0181	-0.2490	0.0171	-0.2431	-0.0338	0.6252	-0.0221
0.5080	0.0212	-0.2688	0.0132	-0.2215	-0.0345	0.6500	-0.0193
0.4906	0.0244	-0.2859	0.0094	-0.1963	-0.0352		
0.4716	0.0278	-0.3006	0.0056	-0.1681	-0.0358		
0.4511	0.0311	-0.3130	0.0020	-0.1374	-0.0364		
0.4293	0.0344	-0.3233	-0.0015	-0.1046	-0.0369		
0.4062	0.0374	-0.3317	-0.0047	-0.0702	-0.0374		
0.3820	0.0402	-0.3383	-0.0078	-0.0349	-0.0378		
0.3568	0.0427	-0.3433	-0.0107	0.0011	-0.0380		
0.3304	0.0448	-0.3468	-0.0133	0.0372	-0.0382		
0.3030	0.0466	-0.3489	-0.0157	0.0732	-0.0382		
0.2746	0.0481	-0.3499	-0.0179	0.1088	-0.0381		
0.2451	0.0493	-0.3499	-0.0199	0.1438	-0.0380		

B1 Antisinging Foil Geometry at AOA=0.0



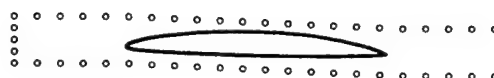
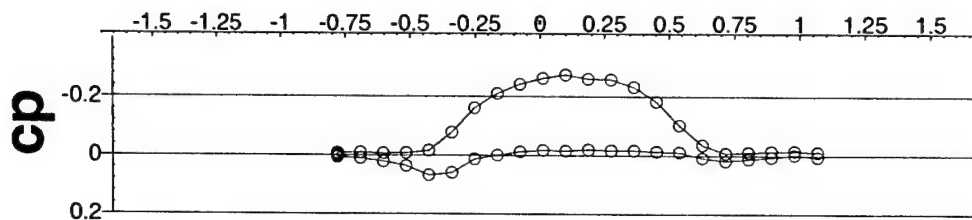
Chord = 455 mm			Uinf= 5.192 m/sec			AOA= 5.25 degrees				
X/C	Y/C	U/Uinf	V/Uinf	Cp		X/C	Y/C	U/Uinf	V/Uinf	Cp
1.066	-0.136	1.000	-0.050	-0.001		-0.780	0.067	1.007	0.060	-0.009
0.978	-0.136	0.998	-0.050	0.001		-0.780	0.111	1.017	0.060	-0.019
0.890	-0.136	0.994	-0.048	0.005		-0.692	0.111	1.021	0.083	-0.024
0.802	-0.136	0.982	-0.046	0.016		-0.604	0.111	1.027	0.112	-0.033
0.714	-0.136	0.973	-0.033	0.026		-0.516	0.111	1.042	0.158	-0.055
0.626	-0.131	0.992	-0.023	0.008		-0.429	0.111	1.088	0.227	-0.118
0.538	-0.125	1.000	-0.048	-0.001		-0.341	0.111	1.238	0.248	-0.298
0.451	-0.119	0.984	-0.064	0.014		-0.253	0.105	1.329	0.141	-0.393
0.363	-0.113	0.973	-0.064	0.025		-0.165	0.099	1.341	0.062	-0.400
0.275	-0.107	0.957	-0.075	0.039		-0.077	0.093	1.341	0.013	-0.399
0.187	-0.101	0.942	-0.083	0.053		0.011	0.087	1.333	-0.056	-0.390
0.099	-0.095	0.924	-0.081	0.069		0.099	0.081	1.333	-0.083	-0.392
0.011	-0.089	0.921	-0.075	0.073		0.187	0.075	1.292	-0.116	-0.342
-0.077	-0.083	0.886	-0.096	0.103		0.275	0.069	1.267	-0.160	-0.316
-0.165	-0.077	0.855	-0.079	0.131		0.363	0.063	1.225	-0.196	-0.270
-0.253	-0.071	0.813	-0.060	0.168		0.451	0.057	1.161	-0.218	-0.198
-0.341	-0.065	0.759	0.037	0.211		0.538	0.051	1.088	-0.208	-0.114
-0.429	-0.065	0.855	0.133	0.126		0.626	0.045	1.040	-0.171	-0.056
-0.516	-0.065	0.928	0.112	0.063		0.714	0.039	1.017	-0.127	-0.025
-0.604	-0.065	0.963	0.087	0.033		0.802	0.039	1.015	-0.091	-0.019
-0.692	-0.065	0.977	0.062	0.021		0.890	0.039	1.017	-0.069	-0.019
-0.780	-0.065	0.986	0.046	0.013		0.978	0.039	1.017	-0.058	-0.019
-0.780	-0.021	0.990	0.056	0.008		1.066	0.039	1.013	-0.050	-0.014
-0.780	0.023	1.000	0.056	-0.001						

B1 Antisinging Foil Experimental Data at AOA=5.2 deg



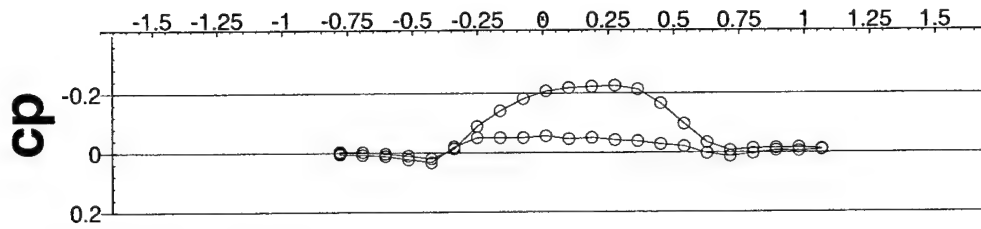
Chord = 455 mm					Uinf = 5.256 m/sec	AOA = 2.15 degrees				
X/C	Y/C	U/Uinf	V/Uinf	Cp		X/C	Y/C	U/Uinf	V/Uinf	Cp
1.066	-0.124	1.001	-0.049	-0.002		-0.780	0.061	1.005	0.032	-0.005
0.978	-0.124	1.005	-0.046	-0.006		-0.780	0.105	1.008	0.032	-0.009
0.890	-0.124	0.995	-0.046	0.004		-0.692	0.105	1.010	0.046	-0.011
0.802	-0.124	0.989	-0.042	0.010		-0.604	0.105	1.010	0.065	-0.012
0.714	-0.124	0.978	-0.029	0.021		-0.516	0.105	1.012	0.093	-0.017
0.626	-0.120	0.987	-0.008	0.012		-0.429	0.105	1.029	0.141	-0.040
0.538	-0.115	1.003	-0.011	-0.003		-0.341	0.105	1.100	0.185	-0.122
0.451	-0.111	1.006	-0.015	-0.007		-0.253	0.101	1.183	0.156	-0.212
0.363	-0.106	1.006	-0.025	-0.007		-0.165	0.096	1.221	0.108	-0.252
0.275	-0.102	1.006	-0.034	-0.007		-0.077	0.092	1.246	0.074	-0.279
0.187	-0.097	1.005	-0.042	-0.005		0.011	0.087	1.258	0.008	-0.291
0.099	-0.093	0.997	-0.044	0.002		0.099	0.083	1.265	-0.017	-0.301
0.011	-0.088	0.999	-0.036	0.000		0.187	0.078	1.252	-0.053	-0.285
-0.077	-0.084	0.984	-0.067	0.014		0.275	0.074	1.240	-0.101	-0.274
-0.165	-0.080	0.965	-0.063	0.033		0.363	0.069	1.216	-0.146	-0.250
-0.253	-0.075	0.942	-0.067	0.054		0.451	0.065	1.161	-0.183	-0.190
-0.341	-0.071	0.889	-0.042	0.104		0.538	0.060	1.088	-0.192	-0.111
-0.429	-0.071	0.911	0.044	0.084		0.626	0.056	1.027	-0.156	-0.040
-0.516	-0.071	0.957	0.048	0.041		0.714	0.052	1.005	-0.105	-0.010
-0.604	-0.071	0.978	0.042	0.021		0.802	0.052	1.008	-0.070	-0.011
-0.692	-0.071	0.986	0.032	0.014		0.890	0.052	1.012	-0.051	-0.014
-0.780	-0.071	0.991	0.023	0.008		0.978	0.052	1.016	-0.046	-0.017
-0.780	-0.027	0.997	0.029	0.003		1.066	0.052	1.008	-0.036	-0.009
-0.780	0.017	0.999	0.034	0.001						

B1 Antisinging Foil Experimental Data at AOA=2.15 deg



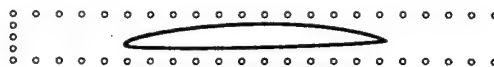
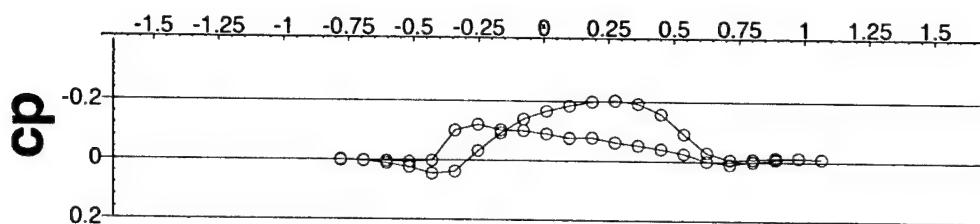
Chord = 455 mm					Uinf= 5.134 m/sec	AOA= 1.35 degrees				
X/C	Y/C	U/Uinf	V/Uinf	Cp		X/C	Y/C	U/Uinf	V/Uinf	Cp
1.066	-0.114	0.993	-0.049	0.005		-0.780	0.057	1.003	0.018	-0.003
0.978	-0.114	1.001	-0.043	-0.002		-0.780	0.101	1.007	0.027	-0.007
0.890	-0.114	0.993	-0.037	0.006		-0.692	0.101	1.009	0.033	-0.010
0.802	-0.114	0.988	-0.043	0.011		-0.604	0.101	1.005	0.047	-0.006
0.714	-0.114	0.982	-0.016	0.018		-0.516	0.101	1.005	0.070	-0.008
0.626	-0.111	0.991	0.012	0.008		-0.429	0.101	1.009	0.115	-0.016
0.538	-0.108	1.011	0.008	-0.011		-0.341	0.101	1.062	0.168	-0.077
0.451	-0.105	1.013	0.006	-0.013		-0.253	0.097	1.139	0.156	-0.161
0.363	-0.101	1.017	0.002	-0.017		-0.165	0.094	1.186	0.117	-0.210
0.275	-0.098	1.017	-0.006	-0.017		-0.077	0.091	1.215	0.086	-0.242
0.187	-0.095	1.019	-0.023	-0.019		0.011	0.087	1.235	0.027	-0.263
0.099	-0.092	1.015	-0.018	-0.015		0.099	0.084	1.245	0.002	-0.275
0.011	-0.088	1.017	-0.019	-0.017		0.187	0.081	1.233	-0.039	-0.261
-0.077	-0.085	1.011	-0.045	-0.012		0.275	0.078	1.229	-0.084	-0.259
-0.165	-0.082	0.999	-0.043	0.000		0.363	0.075	1.204	-0.132	-0.233
-0.253	-0.079	0.986	-0.051	0.013		0.451	0.071	1.157	-0.169	-0.184
-0.341	-0.075	0.937	-0.055	0.060		0.538	0.068	1.083	-0.181	-0.103
-0.429	-0.075	0.929	0.018	0.068		0.626	0.065	1.025	-0.150	-0.036
-0.516	-0.075	0.962	0.027	0.037		0.714	0.061	1.003	-0.097	-0.008
-0.604	-0.075	0.978	0.023	0.022		0.802	0.061	1.009	-0.062	-0.011
-0.692	-0.075	0.989	0.014	0.010		0.890	0.061	1.013	-0.049	-0.014
-0.780	-0.075	0.993	0.010	0.007		0.978	0.061	1.015	-0.039	-0.016
-0.780	-0.031	0.997	0.018	0.003		1.066	0.061	1.011	-0.037	-0.012
-0.780	0.013	0.999	0.019	0.001						

B1 Antisinging Foil Experimental Data at AOA=1.35 deg



Chord = 455 mm			Uinf= 5.15 m/sec			AOA= -0.1 degrees				
X/C	Y/C	U/Uinf	V/Uinf	Cp		X/C	Y/C	U/Uinf	V/Uinf	Cp
1.066	-0.095	1.008	-0.033	-0.008		-0.780	0.048	1.002	0.006	-0.002
0.978	-0.095	1.004	-0.035	-0.005		-0.780	0.091	1.004	0.010	-0.004
0.890	-0.095	1.006	-0.029	-0.006		-0.692	0.091	1.002	0.014	-0.002
0.802	-0.095	0.996	-0.027	0.004		-0.604	0.091	0.996	0.021	0.004
0.714	-0.095	0.986	0.002	0.013		-0.516	0.091	0.988	0.039	0.011
0.626	-0.095	0.996	0.031	0.003		-0.429	0.091	0.977	0.072	0.020
0.538	-0.094	1.019	0.033	-0.020		-0.341	0.091	1.004	0.136	-0.013
0.451	-0.093	1.027	0.025	-0.028		-0.253	0.091	1.074	0.153	-0.088
0.363	-0.092	1.037	0.021	-0.038		-0.165	0.090	1.124	0.132	-0.141
0.275	-0.091	1.041	0.016	-0.042		-0.077	0.089	1.163	0.107	-0.182
0.187	-0.090	1.049	0.006	-0.050		0.011	0.088	1.188	0.054	-0.208
0.099	-0.089	1.045	0.004	-0.046		0.099	0.087	1.198	0.033	-0.218
0.011	-0.088	1.054	0.006	-0.056		0.187	0.086	1.202	-0.004	-0.222
-0.077	-0.087	1.049	-0.025	-0.050		0.275	0.085	1.204	-0.047	-0.226
-0.165	-0.086	1.049	-0.025	-0.050		0.363	0.084	1.190	-0.095	-0.213
-0.253	-0.085	1.049	-0.045	-0.051		0.451	0.083	1.146	-0.138	-0.166
-0.341	-0.084	1.016	-0.087	-0.019		0.538	0.082	1.082	-0.151	-0.096
-0.429	-0.084	0.965	-0.037	0.034		0.626	0.081	1.025	-0.124	-0.033
-0.516	-0.084	0.977	-0.008	0.023		0.714	0.080	1.004	-0.074	-0.007
-0.604	-0.084	0.988	0.000	0.012		0.802	0.080	1.012	-0.045	-0.013
-0.692	-0.084	0.992	0.002	0.008		0.890	0.080	1.014	-0.029	-0.014
-0.780	-0.084	0.994	0.002	0.006		0.978	0.080	1.016	-0.025	-0.016
-0.780	-0.040	0.998	0.006	0.002		1.066	0.080	1.012	-0.021	-0.012
-0.780	0.004	1.002	0.006	-0.002						

B1 Antisinging Foil Experimental Data at AOA=-0.1 deg

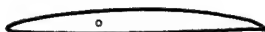


Chord = 455 mm					Uinf= 5.302 m/sec	AOA= -1.5 degrees				
X/C	Y/C	U/Uinf	V/Uinf	Cp		X/C	Y/C	U/Uinf	V/Uinf	Cp
1.066	-0.079	1.009	-0.023	-0.009		-0.780	0.040	0.998	-0.011	0.002
0.978	-0.079	1.013	-0.025	-0.013		-0.780	0.084	1.000	-0.009	0.000
0.890	-0.079	1.007	-0.023	-0.007		-0.692	0.084	0.996	-0.008	0.004
0.802	-0.079	1.000	-0.015	0.000		-0.604	0.084	0.988	-0.006	0.012
0.714	-0.079	0.990	0.006	0.010		-0.516	0.084	0.975	0.004	0.025
0.626	-0.080	1.000	0.041	0.000		-0.429	0.084	0.952	0.034	0.046
0.538	-0.081	1.024	0.049	-0.026		-0.341	0.084	0.954	0.111	0.038
0.451	-0.082	1.039	0.043	-0.041		-0.253	0.085	1.020	0.149	-0.032
0.363	-0.083	1.051	0.041	-0.053		-0.165	0.086	1.079	0.143	-0.092
0.275	-0.084	1.060	0.038	-0.062		-0.077	0.087	1.124	0.124	-0.140
0.187	-0.086	1.075	0.023	-0.078		0.011	0.088	1.152	0.074	-0.167
0.099	-0.087	1.073	0.021	-0.076		0.099	0.089	1.169	0.057	-0.185
0.011	-0.088	1.086	0.025	-0.090		0.187	0.090	1.183	0.017	-0.199
-0.077	-0.089	1.096	-0.011	-0.100		0.275	0.091	1.186	-0.025	-0.204
-0.165	-0.090	1.098	-0.013	-0.103		0.363	0.092	1.175	-0.075	-0.193
-0.253	-0.091	1.113	-0.045	-0.120		0.451	0.094	1.141	-0.121	-0.158
-0.341	-0.092	1.088	-0.126	-0.100		0.538	0.095	1.079	-0.141	-0.092
-0.429	-0.092	0.994	-0.094	0.002		0.626	0.096	1.022	-0.117	-0.029
-0.516	-0.092	0.992	-0.051	0.007		0.714	0.097	1.003	-0.070	-0.006
-0.604	-0.092	0.996	-0.030	0.004		0.802	0.097	1.007	-0.043	-0.008
-0.692	-0.092	0.998	-0.021	0.002		0.890	0.097	1.013	-0.030	-0.013
-0.780	-0.092	1.000	-0.017	0.000		0.978	0.097	1.013	-0.021	-0.013
-0.780	-0.048	1.002	-0.013	-0.002		1.066	0.097	1.009	-0.021	-0.009
-0.780	-0.004	1.002	-0.011	-0.002						

B1 Antisinging Foil Experimental Data at AOA=-1.5 deg

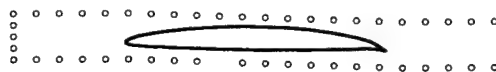
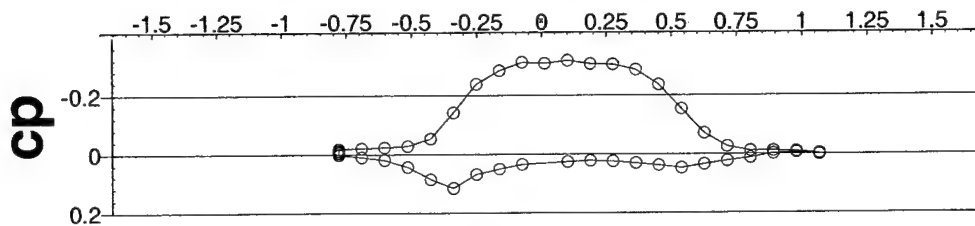
Appendix G

B1 Cupped Trailing Edge Foil Experimental Data



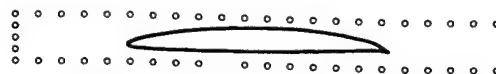
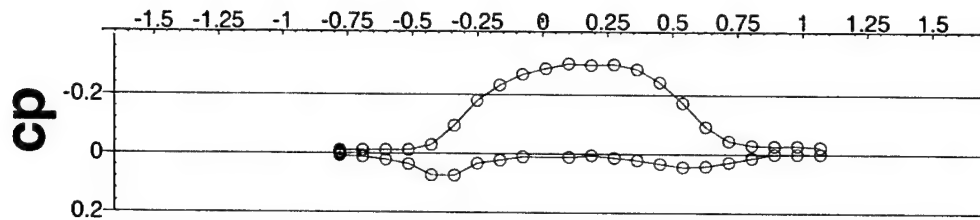
X/C	Y/C	X/C	Y/C	X/C	Y/C
0.6502	-0.0235	-0.1816	0.0256	-0.0211	-0.0382
0.6309	-0.0098	-0.2129	0.0205	0.0329	-0.0377
0.6127	0.0004	-0.2408	0.0154	0.0867	-0.0370
0.5952	0.0080	-0.2651	0.0104	0.1394	-0.0361
0.5778	0.0137	-0.2856	0.0056	0.1901	-0.0350
0.5599	0.0180	-0.3028	0.0009	0.2381	-0.0337
0.5412	0.0218	-0.3168	-0.0035	0.2824	-0.0323
0.5210	0.0256	-0.3279	-0.0077	0.3230	-0.0309
0.4994	0.0295	-0.3364	-0.0115	0.3596	-0.0294
0.4762	0.0333	-0.3426	-0.0150	0.3922	-0.0280
0.4516	0.0371	-0.3468	-0.0182	0.4207	-0.0267
0.4254	0.0406	-0.3491	-0.0210	0.4452	-0.0256
0.3977	0.0438	-0.3498	-0.0235	0.4660	-0.0247
0.3685	0.0465	-0.3488	-0.0263	0.4837	-0.0238
0.3378	0.0488	-0.3461	-0.0284	0.4987	-0.0230
0.3057	0.0506	-0.3421	-0.0301	0.5114	-0.0223
0.2721	0.0519	-0.3368	-0.0315	0.5226	-0.0217
0.2371	0.0527	-0.3303	-0.0325	0.5334	-0.0210
0.2007	0.0530	-0.3227	-0.0334	0.5446	-0.0203
0.1630	0.0528	-0.3138	-0.0342	0.5574	-0.0195
0.1242	0.0520	-0.3031	-0.0350	0.5725	-0.0187
0.0847	0.0507	-0.2891	-0.0358	0.5899	-0.0181
0.0448	0.0488	-0.2702	-0.0365	0.6090	-0.0184
0.0049	0.0463	-0.2449	-0.0371	0.6293	-0.0200
-0.0347	0.0431	-0.2117	-0.0377	0.6502	-0.0235
-0.0737	0.0394	-0.1711	-0.0381		
-0.1115	0.0352	-0.1247	-0.0383		
-0.1477	0.0305	-0.0741	-0.0384		

B1 Cupped Foil Geometry at AOA=0.0



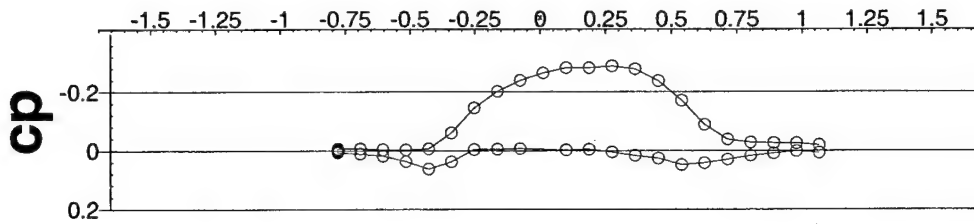
Chord = 455 mm			Uinf= 5.086 m/sec			AOA= 2.25 degrees				
X/C	Y/C	U/Uinf	V/Uinf	Cp		X/C	Y/C	U/Uinf	V/Uinf	Cp
1.066	-0.116	0.997	-0.057	0.002		-0.780	0.101	1.017	0.041	-0.018
0.978	-0.116	1.003	-0.061	-0.005		-0.692	0.101	1.018	0.055	-0.020
0.890	-0.116	0.999	-0.063	-0.001		-0.604	0.101	1.020	0.075	-0.023
0.802	-0.116	0.985	-0.061	0.013		-0.516	0.101	1.022	0.106	-0.028
0.714	-0.116	0.975	-0.049	0.023		-0.429	0.101	1.040	0.157	-0.053
0.626	-0.112	0.963	-0.051	0.035		-0.341	0.101	1.115	0.203	-0.142
0.538	-0.109	0.952	-0.026	0.047		-0.253	0.098	1.203	0.173	-0.239
0.451	-0.106	0.961	-0.016	0.038		-0.165	0.094	1.247	0.126	-0.285
0.363	-0.102	0.969	-0.008	0.030		-0.077	0.091	1.272	0.090	-0.313
0.275	-0.099	0.975	-0.012	0.024		0.011	0.087	1.272	0.028	-0.310
0.187	-0.095	0.977	-0.020	0.022		0.099	0.084	1.280	0.002	-0.319
0.099	-0.092	0.973	-0.022	0.026		0.187	0.081	1.270	-0.043	-0.308
-0.077	-0.085	0.963	-0.041	0.035		0.275	0.077	1.266	-0.090	-0.306
-0.165	-0.081	0.948	-0.039	0.050		0.363	0.074	1.247	-0.144	-0.287
-0.253	-0.078	0.928	-0.041	0.069		0.451	0.070	1.199	-0.185	-0.236
-0.341	-0.075	0.877	-0.016	0.115		0.538	0.067	1.125	-0.208	-0.154
-0.429	-0.075	0.908	0.067	0.085		0.626	0.063	1.052	-0.191	-0.071
-0.516	-0.075	0.954	0.069	0.043		0.714	0.060	1.015	-0.149	-0.026
-0.604	-0.075	0.979	0.053	0.019		0.802	0.060	1.005	-0.106	-0.010
-0.692	-0.075	0.989	0.043	0.010		0.890	0.060	1.007	-0.083	-0.010
-0.780	-0.075	0.997	0.033	0.003		0.978	0.060	1.007	-0.067	-0.009
-0.780	-0.031	0.999	0.037	0.000		1.066	0.060	1.001	-0.059	-0.003
-0.780	0.013	1.005	0.041	-0.006						
-0.780	0.057	1.011	0.041	-0.012						

B1 Cupped Foil Experimental Data at AOA=2.25 deg



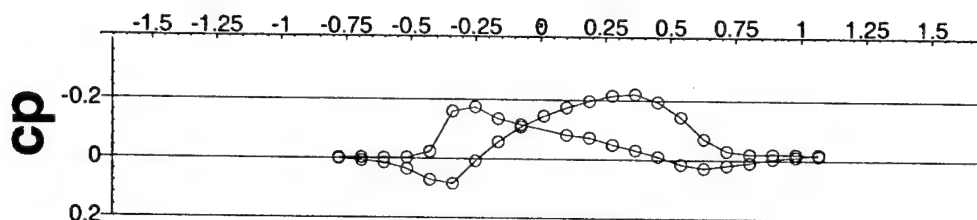
Chord = 455 mm					Uinf= 5.08 m/sec	AOA= 1.3 degrees				
X/C	Y/C	U/Uinf	V/Uinf	Cp		X/C	Y/C	U/Uinf	V/Uinf	Cp
1.066	-0.105	0.998	-0.063	0.000		-0.780	0.096	1.010	0.031	-0.010
0.978	-0.105	0.998	-0.067	0.000		-0.692	0.096	1.010	0.041	-0.011
0.890	-0.105	0.998	-0.063	0.000		-0.604	0.096	1.010	0.059	-0.012
0.802	-0.105	0.984	-0.067	0.013		-0.516	0.096	1.008	0.085	-0.011
0.714	-0.105	0.970	-0.055	0.028		-0.429	0.096	1.020	0.132	-0.029
0.626	-0.103	0.957	-0.045	0.041		-0.341	0.096	1.075	0.183	-0.094
0.538	-0.101	0.955	-0.020	0.044		-0.253	0.094	1.154	0.169	-0.180
0.451	-0.099	0.967	-0.008	0.033		-0.165	0.092	1.203	0.134	-0.232
0.363	-0.097	0.978	-0.010	0.021		-0.077	0.090	1.236	0.104	-0.270
0.275	-0.095	0.986	-0.012	0.014		0.011	0.088	1.256	0.037	-0.289
0.187	-0.092	0.994	-0.022	0.006		0.099	0.086	1.270	0.014	-0.306
0.099	-0.090	0.988	-0.024	0.011		0.187	0.083	1.266	-0.030	-0.301
-0.077	-0.086	0.988	-0.045	0.011		0.275	0.081	1.266	-0.079	-0.304
-0.165	-0.084	0.976	-0.043	0.022		0.363	0.079	1.248	-0.134	-0.288
-0.253	-0.082	0.965	-0.053	0.033		0.451	0.077	1.207	-0.175	-0.243
-0.341	-0.080	0.921	-0.045	0.075		0.538	0.075	1.144	-0.199	-0.174
-0.429	-0.080	0.923	0.022	0.074		0.626	0.073	1.073	-0.187	-0.093
-0.516	-0.080	0.963	0.035	0.036		0.714	0.071	1.033	-0.146	-0.045
-0.604	-0.080	0.978	0.030	0.021		0.802	0.071	1.024	-0.108	-0.030
-0.692	-0.080	0.988	0.024	0.011		0.890	0.071	1.024	-0.083	-0.027
-0.780	-0.080	0.992	0.014	0.008		0.978	0.071	1.026	-0.067	-0.028
-0.780	-0.036	0.994	0.026	0.006		1.066	0.071	1.022	-0.061	-0.024
-0.780	0.008	1.000	0.026	0.000						
-0.780	0.052	1.004	0.028	-0.004						

B1 Cupped Foil Experimental Data at AOA=1.3 deg



Chord = 455 mm			Uinf= 5.228 m/sec			AOA= 0.5 degrees				
X/C	Y/C	U/Uinf	V/Uinf	Cp		X/C	Y/C	U/Uinf	V/Uinf	Cp
1.066	-0.095	0.991	-0.055	0.008		-0.780	0.091	1.006	0.023	-0.006
0.978	-0.095	0.997	-0.063	0.001		-0.692	0.091	1.006	0.031	-0.007
0.890	-0.095	0.989	-0.065	0.009		-0.604	0.091	1.002	0.044	-0.003
0.802	-0.095	0.981	-0.061	0.017		-0.516	0.091	1.000	0.065	-0.002
0.714	-0.095	0.968	-0.057	0.030		-0.429	0.091	1.000	0.109	-0.006
0.626	-0.094	0.956	-0.033	0.042		-0.341	0.091	1.044	0.170	-0.060
0.538	-0.093	0.951	-0.019	0.048		-0.253	0.090	1.123	0.172	-0.145
0.451	-0.092	0.974	0.002	0.026		-0.165	0.090	1.176	0.142	-0.202
0.363	-0.091	0.983	0.010	0.017		-0.077	0.089	1.211	0.115	-0.240
0.275	-0.091	0.995	0.000	0.005		0.011	0.088	1.236	0.055	-0.265
0.187	-0.090	1.004	-0.019	-0.004		0.099	0.087	1.251	0.034	-0.283
0.099	-0.089	1.002	-0.010	-0.002		0.187	0.086	1.251	-0.006	-0.282
-0.077	-0.087	1.006	-0.033	-0.007		0.275	0.085	1.255	-0.054	-0.289
-0.165	-0.086	1.004	-0.036	-0.005		0.363	0.084	1.243	-0.107	-0.279
-0.253	-0.085	1.002	-0.057	-0.004		0.451	0.083	1.205	-0.155	-0.238
-0.341	-0.085	0.958	-0.075	0.038		0.538	0.083	1.144	-0.182	-0.171
-0.429	-0.085	0.935	-0.002	0.063		0.626	0.082	1.071	-0.172	-0.089
-0.516	-0.085	0.962	-0.004	0.037		0.714	0.081	1.029	-0.132	-0.038
-0.604	-0.085	0.981	0.011	0.019		0.802	0.081	1.023	-0.094	-0.028
-0.692	-0.085	0.989	0.015	0.011		0.890	0.081	1.023	-0.069	-0.026
-0.780	-0.085	0.993	0.015	0.007		0.978	0.081	1.023	-0.057	-0.025
-0.780	-0.041	0.997	0.011	0.003		1.066	0.081	1.018	-0.050	-0.019
-0.780	0.003	1.000	0.021	-0.001						
-0.780	0.047	1.004	0.021	-0.004						

B1 Cupped Foil Experimental Data at AOA=0.5 deg



Chord = 455 mm					Uinf= 5.198 m/sec	AOA= -2.75 degrees				
X/C	Y/C	U/Uinf	V/Uinf	Cp		X/C	Y/C	U/Uinf	V/Uinf	Cp
1.066	-0.054	1.020	-0.037	-0.020		-0.780	0.072	0.998	-0.012	0.001
0.978	-0.054	1.010	-0.033	-0.011		-0.692	0.072	0.993	-0.015	0.007
0.890	-0.054	1.004	-0.037	-0.005		-0.604	0.072	0.985	-0.017	0.015
0.802	-0.054	0.991	-0.029	0.009		-0.516	0.072	0.964	-0.013	0.035
0.714	-0.054	0.981	-0.013	0.019		-0.429	0.072	0.925	0.010	0.072
0.626	-0.058	0.972	0.012	0.028		-0.341	0.072	0.906	0.096	0.085
0.538	-0.063	0.983	0.050	0.016		-0.253	0.076	0.979	0.160	0.008
0.451	-0.067	1.008	0.065	-0.010		-0.165	0.080	1.043	0.165	-0.057
0.363	-0.071	1.029	0.067	-0.032		-0.077	0.084	1.093	0.154	-0.109
0.275	-0.075	1.047	0.069	-0.050		0.011	0.088	1.131	0.112	-0.146
0.187	-0.079	1.070	0.044	-0.073		0.099	0.093	1.158	0.096	-0.175
0.099	-0.083	1.077	0.058	-0.082		0.187	0.097	1.179	0.058	-0.197
-0.077	-0.092	1.110	0.031	-0.117		0.275	0.101	1.197	0.013	-0.216
-0.165	-0.096	1.127	0.019	-0.136		0.363	0.105	1.200	-0.040	-0.221
-0.253	-0.100	1.162	-0.019	-0.175		0.451	0.109	1.175	-0.096	-0.195
-0.341	-0.104	1.141	-0.140	-0.161		0.538	0.113	1.127	-0.137	-0.145
-0.429	-0.104	1.016	-0.121	-0.023		0.626	0.117	1.060	-0.135	-0.071
-0.516	-0.104	1.000	-0.069	-0.003		0.714	0.122	1.025	-0.094	-0.030
-0.604	-0.104	1.000	-0.046	-0.001		0.802	0.122	1.018	-0.062	-0.020
-0.692	-0.104	1.002	-0.029	-0.003		0.890	0.122	1.020	-0.042	-0.021
-0.780	-0.104	1.002	-0.023	-0.003		0.978	0.122	1.020	-0.035	-0.020
-0.780	-0.060	1.000	-0.019	-0.001		1.066	0.122	1.014	-0.031	-0.014
-0.780	-0.016	1.000	-0.015	-0.001						
-0.780	0.028	0.998	-0.017	0.001						

B1 Cupped Foil Experimental Data at AOA=-2.75 deg

Appendix H

Decaying Vortex Tracking Program

Bibliography

- [1] I. H. Abbott and A. E. Von Doenhoff. *Theory of Wing Sections*. Dover, New York, 1959.
- [2] Ira H. Abbott and Albert E. VON Doenhoff. Summary of airfoil data. Technical Report NACA Report No. 824, NACA, Fort Eustis, VA, 1945.
- [3] Taylor L. K. Arabshahi, A. and D. L. Whitfield. Uncle: Toward a comprehensive time-accurate incompressible navier-stokes flow solver,. In *AIAA 33rd Aerospace Sciences Meeting and Exhibit*, Reno, Nevada, January 1995. AIAA.
- [4] J.P.A.J. Van Beeck and C. Benocci. Introduction to the modeling of turbulence. In *Lecture Series 2000-04*, 2000.
- [5] H. V. Borst and S. F. Hoerner. *Fluid-Dynamic Lift*. Liselotte A. Hoerner Fluid Dynamics, Brick Town, NJ, 1975.
- [6] T. E. Brockett. Minimum Pressure Envelopes for Modified NACA-66 Sections with NACA $a=0.8$ Camber and Buships Type I and Type II Sections. Report 1780, DTNSRDC, Teddington, England, Feb 1966.
- [7] J. D. Dannecker. A Numerical Study of Fluid Flow Around Two-Dimensional Lifting Surfaces. Master's thesis, Massachusetts Institute of Technology, June 1997. also Naval Engineer's thesis.
- [8] M. Drela. XFOIL: An Analysis and Design System for Low Reynolds Number Aerofoils. *Lecture Notes in Engineering: Low Reynolds Number Aerodynamics*, (54), 1989.
- [9] M. Drela. XFOIL: An Analysis and Design System for Low Reynolds Number Airfoils. In *Proceedings of the Conference on Low Reynolds Number Aerodynamics*, 1989.

- [10] M. Drela. Newton solution of coupled viscous/inviscid multielement airfoil flows. *AIAA Journal*, (1470), 1990.
- [11] R.S. Fairman. A Comparison of Experimental and Computational Analyses of Two Dimensional Foil Sections. Master's thesis, MIT Department of Ocean Engineering, June 2000.
- [12] J.H. Ferziger. The Physics and Simulation of Turbulence State of the Art 1998. *Introduction to the Modelling of Turbulence*, (2000-04), 2000.
- [13] J. J. Gorski. Multiple Block Calculations of the Navier-Stokes Equations for Incompressible Flows. In *Proceedings of the 12th U.S.-Federal Republic of Germany Data Exchange Meeting*, Bethesda, MD USA, 1988.
- [14] R.A.W.M. Henkes. *Overview of Turbulence Models for External Aerodynamics*. Deft University Press, Netherlands, 1998.
- [15] J. Jorde. A Study of Two Cambered Trailing Edge Geometries. Technical report, Dept. of Ocean Engineering, Massachusetts Institute of Technology, December 1995.
- [16] J. E. Kerwin. New facilities for research in naval architecture and marine engineering at mit: Variable pressure water tunnel. Technical report, New England Section, SNAME, October 1967.
- [17] J. E. Kerwin. A Vortex Lattice Method for Propeller Blade Design: MIT-PBD-10 User's Manual. Technical Report Report 84-2, MIT Department of Ocean Engineering, January 1984.
- [18] R. W. Kimball. A Study on the Performance of Hydrofoils with Thick Trailing Edges. Master's thesis, Department of Ocean Engineering, Massachusetts Institute of Technology, September 1997.
- [19] R.W. Kimball, J.O. Scherer, and T.E. Taylor. Enhancements to the Design and Analysis of Waterjet Propulsors Using a Coupled Lifting-Surface/RANS Technique and Comparison with Experiment. In *Waterjet Propulsion III*, Gothenburg, Sweden, February 2001. Royal Institution of Naval Architects.

- [20] Sir Horace Lamb. *Hydrodynamics*. Dover, sixth edition, 1932.
- [21] E. H. Lurie. A Note on the Error Analysis of Velocity Measurements of the Flapping Foil Experiment. Technical Report Rep. 95-3, Department of Ocean Engineering, Massachusetts Institute of Technology, November 1995.
- [22] E.A. Lurie. *Investigation of High Reduced Frequency, Separated Trailing Edge Flows*. PhD thesis, MIT Department of Ocean Engineering, September 1996.
- [23] E.G. Paterson and F. Stern. Computation of unsteady marine-propulsor blade flows - part 1: Validation and analysis. *Journal of Fluids Engineering*, 119:145-147, 1997.
- [24] James Q. Rice. Investigation of a Two Dimensional Hydrofoil in Steady and Unsteady Flows. Master's thesis, MIT Department of Ocean Engineering, June 1991.
- [25] F.W. Riegels. *Aerofoil Sections*. Butterworths, London, 1961.
- [26] John Stack. Tests of airfoils designed to delay the compressibility burble. Technical Report NACA Technical Note 976, NACA, 1944.
- [27] Paterson E.G. Stern, F. and Tahara. Cfdship-iowa: Computational fluid dynamics method for surface-ship boundary layers, wakes, and wave fields. Technical Report 381, IIHR Report, July 1996.
- [28] Albert E. Von Doenhoff and JR Abbott, Frank T. The langley two-dimensional low-turbulence pressure tunnel. tn 1283. Technical report, NACA, 1947.
- [29] F. M. White. *Viscous Fluid Flow*. McGraw-Hill, second edition, 1991.